Natural and Mixed Convection from PCBs with Flushed and Protruding Heat Sources

A Thesis Submitted
In Partial Fulfillment of the Requirements
For the Degree of

Master of Technology
by

Rajeev Kumar Pandit

to the

DEPARTMENT OF MECHANICAL ENGINEERING

INDIAN INSTITUTE OF TECHNOLOGY KANPUR

August 2003

CERTIFICATE

It is certified that the work contained in the thesis entitled "**Natural and Mixed Convection from PCBs with Flushed and Protruding Heat Sources**" by **Mr. Rajeev Kumar Pandit (Y110533)**, has been carried out under my supervision and this work has not been submitted elsewhere for a degree.

Keshav Kant
01.08.2003

(Dr. Keshav Kant)
Professor,
Department of Mechanical Engineering,
Indian Institute of Technology,
Kanpur,
August, 2003

ACKNOWLEDGEMENTS

I take this opportunity to express my deep sense of gratitude to my supervisor Professor Keshav Kant, to whom I owe more than I can possibly express, for his warm guidance that led to the completion of this work. It was a great pleasure to work under him as a lot of care and affection was available throughout. I shall ever remain grateful to him.

I would like to dedicate this work to my parents, elder brother, bhabhiji, sister and brother-in-law for their enduring love, support and inspiration.

I express my appreciation and indebtedness to Mr. Vipin Yadav, who apart from motivating me throughout my stay at IIT Kanpur, helped me professionally.

I would like to thank Mr. D.S. Murthy, Mr. Ashok Pise, my friends Atanu, Arvind, Abhay, Mukesh, and Ankur for their warm affections and help to make my stay at IIT Kanpur a pleasant one.

Last but not the least I would like to thank Sushil Mishra, and Wahab who helped in my work from time to time.

Rajeev Kumar Pandit

IIT Kanpur (Rajeev Kumar Pandit)

Date: 01/08/2003

Abstract

Printed circuit boards (PCBs) are one of the basic constituents of any modern electronic assembly. A single PCB may hold large variety of electronic components including different types of ICs, high power transistors, resistors, capacitors, diodes etc. & etc. Now a days, designing any PCB for a particular application does not merely mean deciding the electrical and electronic parametric values of components to be mounted with suitable circuitry, but it also includes the incorporation of thermal design based upon thermal parameters like safe operating temperature, associated heat flux value, cooling technique, coolant properties, coolant flow path etc. In fact, in many of the high-tech electronic appliances and gadgets, it is the thermal design that draws the first attention rather than the electronic or electrical considerations.

Present work deals with the study of various thermal parameters necessary for the design of PCBs and the associated electronic machinery. PCBs have been thermally modeled using various types of models available in literature. These include uniform wall temperature and uniform surface heat flux models; and also some more realistic models s like a plane surface with projecting heat sources similar to commercial ICs. Natural convection and mixed convection cooling of vertically oriented PCBs using air as coolant has been taken as the very basis of entire numerical and experimental study. Numerical modeling and simulation of PCBs are done using a ready to use software 'FLUENT' version 6.0. Experimental modeling and simulation has been achieved by upgrading already existing test rig and using state-of-the-art National Instruments data acquisition instrumentation.

In the study presented here for various plate spacings, heat transfer characteristics have been observed for natural convection as well as for mixed convection. In the latter, two different values of externally imposed pressure were considered for numerical simulation. In this part, the entire PCB was considered

Here multiple protruding heat generation sources were considered over the PCB surface. Variation of temperature, heat flux and Nusselt number has been studied for different values of plate spacings and different coolant (air) velocities. Finally, numerical and experimental data has been compared and suitable empirical relations are suggested in a manner useful in thermal design of an electronic system. Using the information presented in the work, it is possible to tentatively suggest a cooling technique for given type of PCBs in an electronic system and further to effectively design the appropriate cooling mechanism.

CONTENTS

NOMENCLATURE

b	Plate Spacing
g	Gravitational Acceleration, $m.s^{-2}$
H	Plate Height, mm
UHF	Uniform Heat Flux, $W.cm^{-2}$
UWT	Uniform Wall Temperature, K
$Gr_{L.}$	Grashoff number measured along the plate
$Re_{L.}$	Reyonld number measured along the plate
Pr	Prandtl number
T_0	Fluid inlet temperature.
T_h	Plate surface temperature
$C^{''}$	Constant whose value depends on overall thermal conductivity of oxide layers deposited on aluminium heat sink.
ΔT	Difference in front face and back face temperatures of heat sink.
T_R	Room temperature.
u	Fluid velocity in X-direction
v	Fluid velocity in Y-direction
P	Pressure difference
β	Coefficient of thermal expansion
α	Thermal diffusivity
q	Heat flux
ν	Kinematics viscosity

List of Figures

LIST of TABLES

Chapter 1

GENERAL BACKGROUND

1.1 Introduction

The thermal state of the microelectronic units has always been a question of great importance. The continuous increase of the component density raises more and more serious heat sinking problems. Some VLSI chips dissipate 20-50 Watts, recent multi-chip module packages are designed up to 2000 Watts dissipation. Moreover we are in the advent of 3 dimensional (cubic) packaging of IC's with stacked silicon chips - the severity of overheating problems can be foreseen. Few arrangements of the electronic components on the PCB's are shown in figures 1.1 and 1.2.

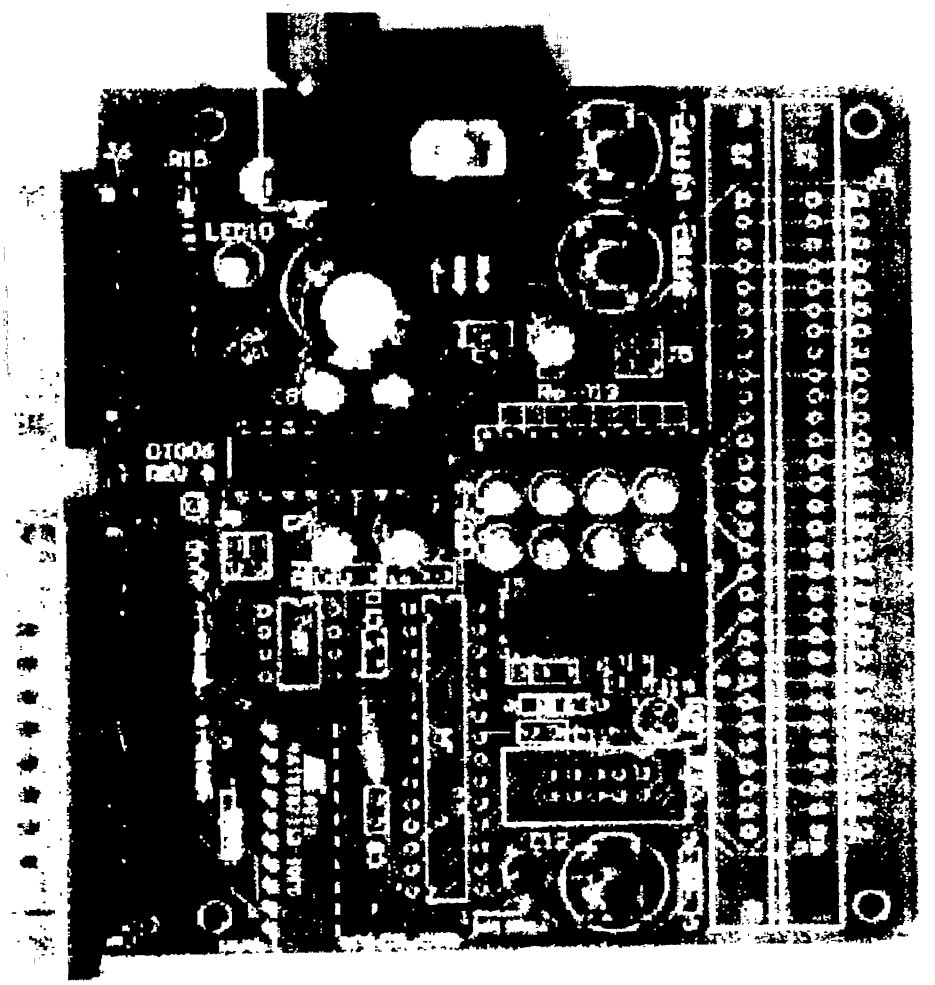

Figure 1.1: IC's, Capacitors and Resistors placed on a PCB.

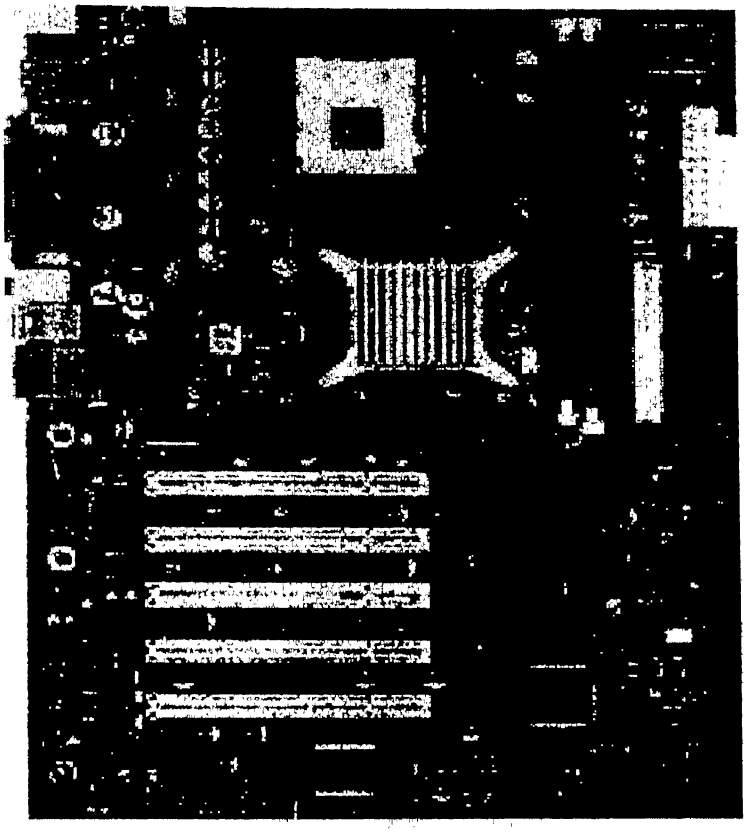

Figure 1.2: Mother Board of Central Processing Unit

Cooling the latest electronic devices such as video game chips, power transistors, central processing units (CPUs), cellular, mobiles, programmable logic controllers (PLCs), adjustable speed drives etc. is not an easy task. Packing the components more densely effectively reduces the dimensions of the circuit and increases processing speed, but leaves little room for heat dissipation. Tightly packed cabinets restrict airflow, resulting in rapidly rising internal temperatures and increasing control failures. Some equipment with these drawbacks are shown in figures 1.3, 1.4 and 1.5.

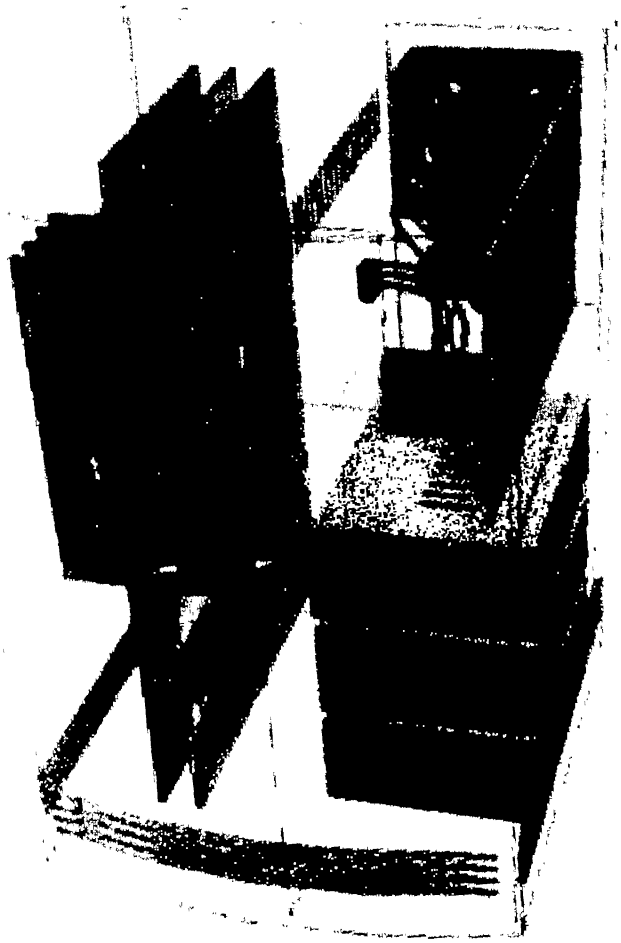

Figure 1.3: Central Processing Unit

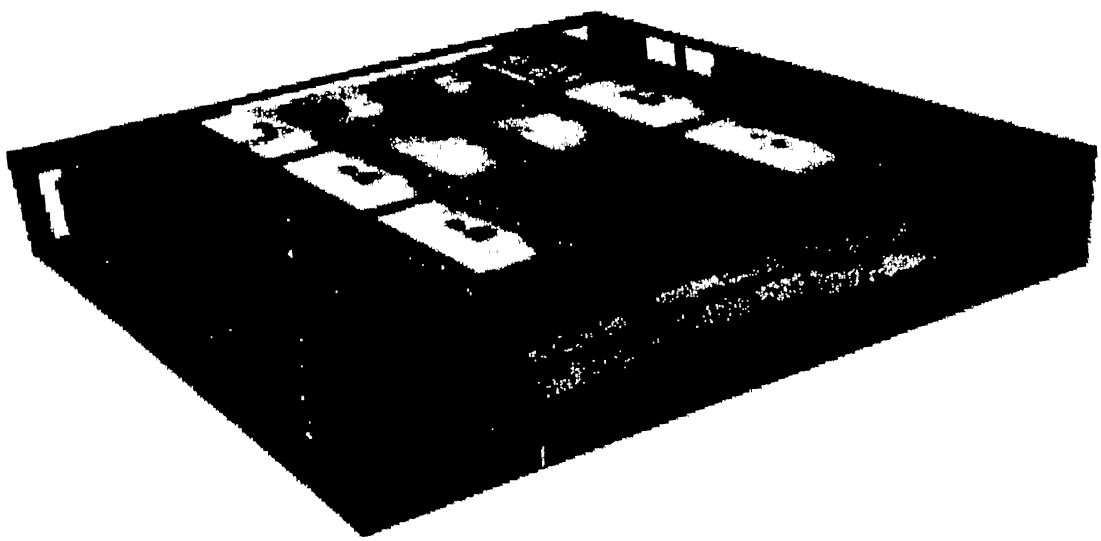

Figure 1.4: Schematic arrangement of more than one PCB inside an electronic chassis.

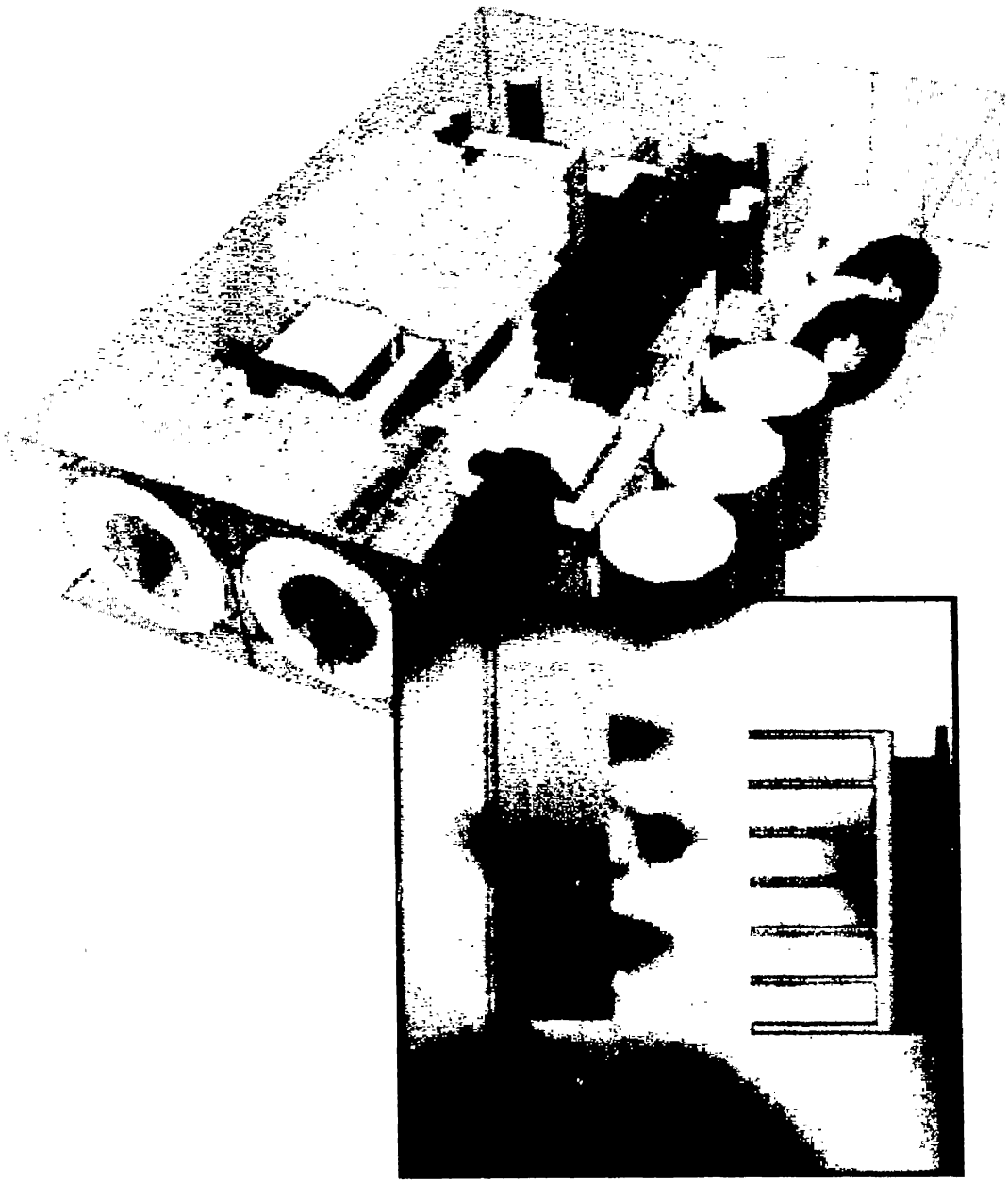

Figure 1.5: Application of Heat Sinks inside an electronic system.

In such a difficult situation demand for adequate efforts for better thermal design purpose and effective thermal control has increased considerably. In fact, the need for proper heat dissipation from many of the modern high-tech electronic equipments and devices has become critical and crucial. Figure1.6 shows an arrangement for the heat dissipation by conduction mechanism from heat source to cooling medium.

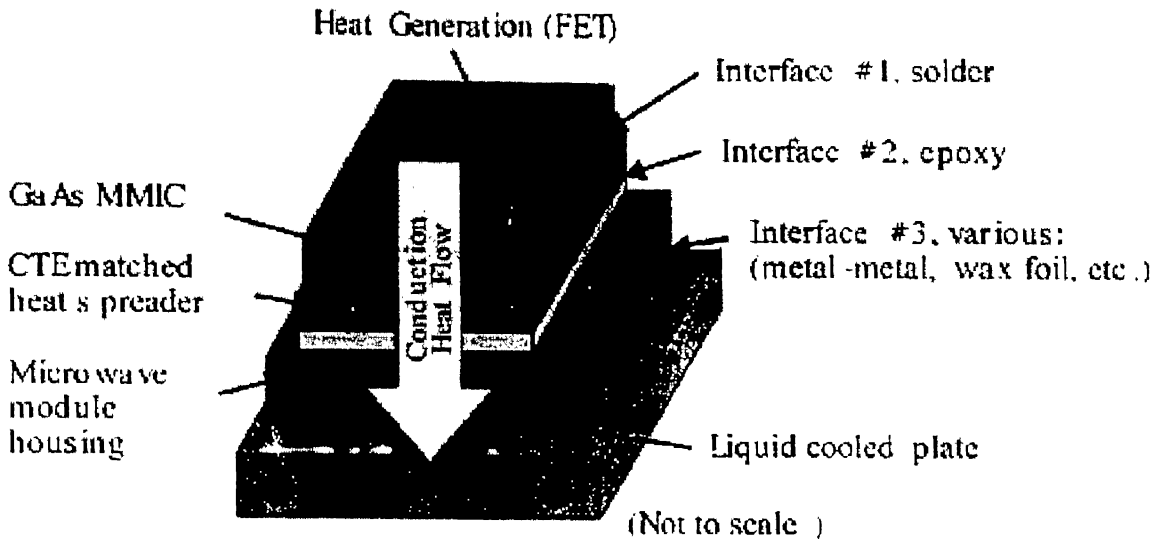

Figure 1.6: Flow path of heat through various components inside a typical electronic Package.

As far as the contribution of design and mounting part is concerned, significant benefits can be achieved through the use of surface mounted devices (SMDs) and using general surface-mount technology. Thus, the major benefits include the reduction in size and weight resulting in higher probability of efficient thermal management and increased ability to withstand mechanical shocks and vibrations resulting from employment of dynamic cooling devices like fans.

The cooling need and constraints vary with the specific product application. The application areas have been broadened into device-level, including PCB and IC packages and sub-level including space, size environment constraints. The space and size constrained devices have been categorised into handheld communication devices and portable computing devices. The environmentally constrained devices include outdoor telecommunication enclosure and high-altitude electronics.

Reliability in electronics is obtained by decreasing the operating temperatures. It is possible to double the reliability if the working temperature is lowered just by 10°C. In order to achieve lower operating temperatures, an integrated circuit is

attached with a heat sink that takes away the heat at the primary level. Practically this chip-sink assembly is mounted on a printed circuit board (PCB) which is generally a multi-layered composite consisting of copper foil and glass-reinforced polymer.

It is convenient to treat any PCB as a homogeneous material with two different effective thermal conductivities viz. in-plane thermal conductivity and through thermal conductivity. The heat generated by the electronic components is transferred first by conduction through the board and then by convection to the air which is the preferred mechanism. External skin temperature of most of the electronic equipments is designed to be safe to human touch. This along with other mentioned temperature limitations imposes severe restriction on the arrangement of PCBs inside the equipment chassis. For passively cooled systems, a number of arrangements is possible for mounting the PCBs

Failure Modes:

Important types of problems related with heat generation in electronic components are tabulated in Table 1.1. The design process is generally first directed at the cooling parameters, keeping the geometry of the electronic circuitry unchanged. Therefore different fluids, flow rates, inlet fluid temperature and flow configurations are considered to determine if an acceptable design is obtained. If not the dimensions, number and locations may be varied; within the given constraints. If even this doesn't lead to an acceptable design, the mode of cooling may be varied; for instance, going from natural to forced convection in air, to liquid immersion or to phase change heat transfer.

Table 1.1: Failure Mode Characteristic

Failure Mode	Characteristic
Soft Failure	Circuit continues to operate, but doesn't meet specifications when the temperature is elevated beyond the maximum operating temperature. Circuit returns to normal operation when temperature is lowered. Failure occurs due to change in component parameters with temperature.
Hard Failure (Short term)	Circuit does not operate. Circuit may or may not return to normal operation when temperature is lowered. Failure is likely due to component or interconnection breakdown, but may also be due to change in component parameters with temperature.
Hard Failure (Long term)	Circuit does not operate at any temperature. Failure is irreversible. Failure may be caused by corrosion, inter-metallic formation or similar phenomenon. Failures may also be caused by mechanical stresses due to difference in temperature coefficient of expansion (TCE) between a component and the substrate.

1.2 Methods of Cooling Electronic Components

Advancement in circuit integration technology with cooling need has invented time to time many cooling techniques.

In earlier days when the components were not closely packed, Natural Convection was sufficient to transfer heat. But as the technology developed, densely packed components produced higher heat flux, and so Forced as well as Mixed Convection mode of heat transfer came into existence. Now-a-days due to very advanced technology, jet impingement and micro channel cooling techniques are also used frequently. In the following subsections some of these techniques are discussed.

1.2.1 Electronic Cooling by Natural Convection:

This mode of heat transfer comes into play when there is difference of densities of cold and hot fluids. The fluid in contact with the heat source gets heated, so its density decreases relatively than that of cold fluid farther away from the heat

source. So the lighter fluid goes upward and the hotter one comes downward, thus these driving forces form circular type currents known as convection currents.

Though natural convection has very low heat transfer coefficient, it is preferred for low-end applications because of its reliability and simplicity. Normally heat transfer coefficient achievable in natural convection is of the order of 5 to 25 $W/m^2.k$. This limits the heat flux to a value of 0.1 to 1.0 W/cm^2 and allowable temperature to less than 100°C despite significantly low end equipment, compared to forced convection or immersion boiling because of its inherent reliability and simplicity. Communication switching devices, avionics packages, electronic test equipment, consumer electronics and low-end computer packages are often cooled by natural convection in air.

1.2.2 Electronic Cooling by Forced Convection:

In this mode of heat transfer the concerned fluid is moved using fan, blower or a pump to provide high fluid (air or liquid) velocity so to get less thermal resistance across the boundary layer of the fluid on the heated surface. This results in higher heat transfer rates. Forced air system can provide heat transfer rates in electronic systems that are 10 times greater than those available with natural convection and radiation; so this method is particularly used where the rate of heat generated is very high. Application of forced convection cooling method results in size reduction of electronic systems and increase in component density. This also reduces the formation of a hot spot and increases the component reliability, but requires design complexity due to arrangement of fan or pump. All these increase cost, power, noise, complexity and maintenance of fans or pumps. For liquid cooled system, the size and weight may also increase. Both laminar as well as turbulent flow conditions can exist with forced convection in liquid and in air. For more heat removal turbulent flow condition is much more desirable. However, turbulent flow results in a greater pressure drop.

1.2.3 Electronic Cooling by Mixed Convection:

In this mode of heat transfer, the effect of buoyancy is also considered in addition to that of the forced convection flow in computational domain. Heat transfer in

mixed convection can be significantly different from its value in both natural and pure forced convection. The heat transfer in case of mixed convection depends on the duct geometry, orientation of the duct, and whether the flow is fully developed or developing.

1.3 Cooling Efficiency Concept:

The cooling efficiency [29] is defined as the ratio of the heat that can be dissipated from a PCB and a reference case. The reference case is defined as an ideal smooth isothermal parallel plate case with a temperature level equal to the maximum temperature of the PCB plate.

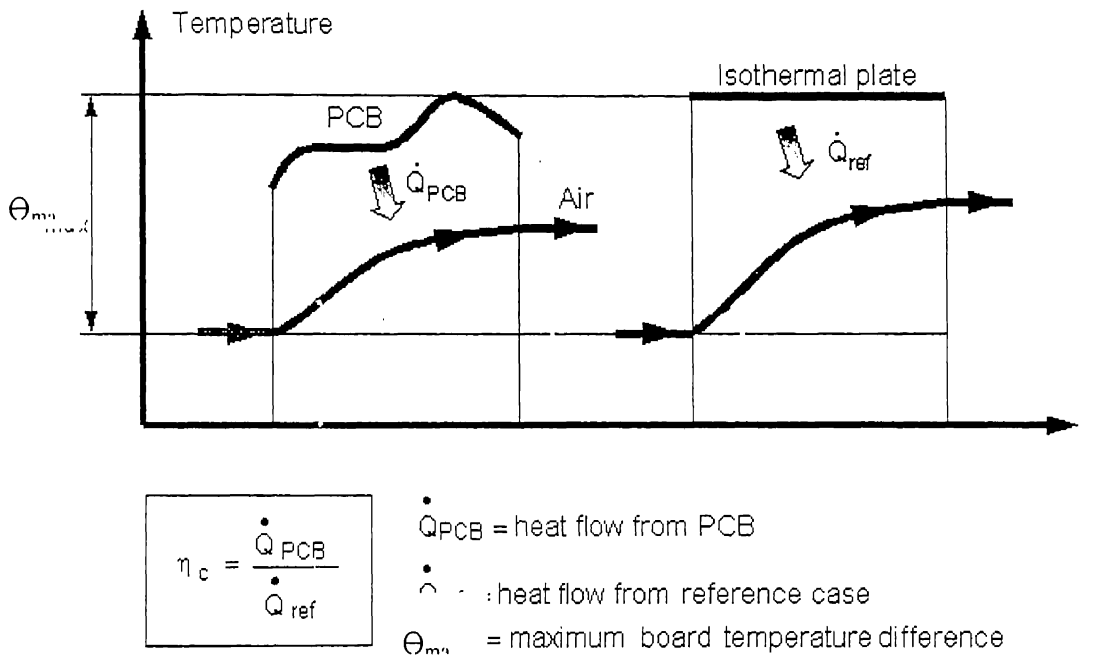

Figure 1.7: Graphical representation of Cooling Efficiency

Quite apparent other requirement for the reference case is that the plates must have the same size, thickness, surface-to-surface distance and air flow as for the PCB. What might be less apparent is that it must not include radiation. The cooling efficiency always must be based on the inlet temperature difference. Serial cooling is a term that is often used for cases where the same airflow cools several PCBs

placed consecutively. The cooling efficiency concept is more important for single rather than for serially cooled PCBs.

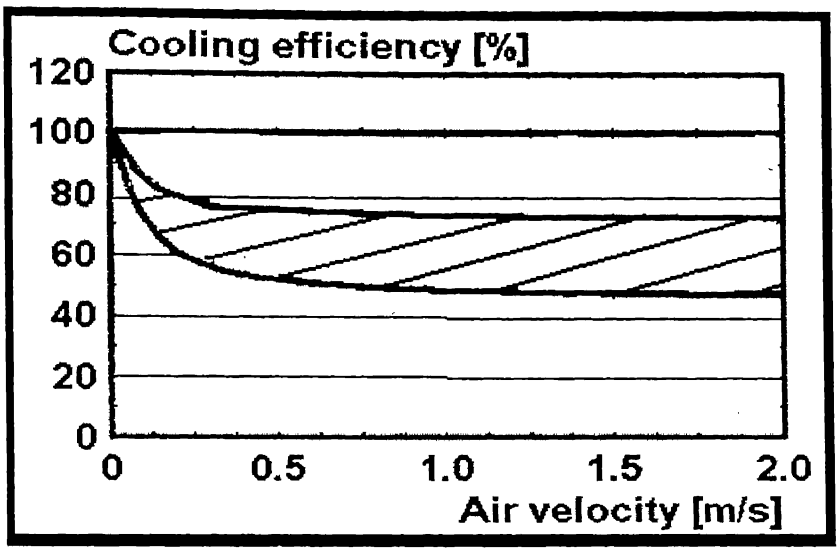

Figure -1.8: Effect of air velocity upon the cooling efficiency

Figure 1.8 shows range of cooling efficiency at different air velocities. Everything that makes a PCB deviates from the isothermal reference case and has an impact on the cooling efficiency, positively or negatively. There are many factors that can have an impact in this respect. The two most obvious ones are the thermal conductivity of the PCB plate and the distribution of the heat sources.

It could be tempting to assume that 100% is the maximum limit for the cooling efficiency. This is however not quite the case. Heat sinks can push the value above the 100% limit. Even a plain PCB can, at least in theory, also surpass this limit. The reason for this is that the cooling efficiency is based on the maximum board temperature. The surface temperatures of the components are however frequently higher. The components on a high density PCB can therefore boost the heat dissipation to such an extent that they act more like counterbalancing the low

board temperatures found between the components. The highest cooling efficiency value that has been observed for a PCB without heat sinks is 102%.

1.4 Present Requirements

All these efforts are made to maintain constant component temperature between 65°C and 85°C. Electronic cooling can also be classified as direct cooling and indirect cooling. In the former, direct cooling the cooling fluid is in direct contact with the heat generating source. By this high heat flux can be removed, but getting rid of the contamination problem is extremely expensive. In indirect cooling, heat is removed first by a primary coolant and then this heat is transferred to secondary coolant like air.

An efficient thermal design strategy requires a balanced combination of both experimental and numerical efforts, with an awareness of the latest developments in thermal cooling technologies. Such expertise is a pre-requisite to permit high-quality, cost-effective thermal design solutions to be implemented in the shortest possible turnaround time. Over the last decade, thermal design practices have progressed from basic analytical and semi-empirical calculations, applicable to simple electronic systems, in tandem with extensive physical prototype characterization, to a high reliance on virtual prototyping using numerical predictive techniques, such as Computational Fluids Dynamics (CFD)-based methods. This practice is the only realistic design approach to permit the analysis of today's complex equipment, while also contributing to significantly reduce both prototyping costs and development cycle times. While accurate and efficient analysis requires highly trained engineers, numerically-produced thermal designs still require experimental verification due to both inherent limitations in the codes used and uncertainties in the physical boundary conditions. In this regard, high level of heat dissipation requires more accurate experimental characterization of thermal performance than in the past, where vendor supplied component junction-to-reference thermal resistances were used to calculate component operating temperature. This approach is now recognized to lead to significant

underestimation of operating temperature, hence catastrophic product field failures. Instead, electrical sensing methods and infrared thermography are the only reliable methods to quantify component and board operating temperature respectively.

1.5 Scope of the Present Work:

Component modeling is one of the most difficult issues in the thermal design. It has been vividly discussed for more than a decade. It has been the subject for several research projects, but there does not seem to be any consensus yet. Often at first glance, a model seems to be working well, but once all its intricate details are unfolded, its appearance changes drastically.

In the present work efforts are made to model two important constituents of electronic equipments, both belonging to different hierarchy levels. First, the heat generation from IC package and the second, the printed circuit board (PCB) mounted with limited number of heat generating sources. Ideal cases of uniform wall temperature and uniform wall heat flux have also given due consideration. Mounted heat generating sources are flushed and protruded. Heat fluxes dealt with belong to the natural and mixed convection air cooling regimes. Experiments are conducted for an array of four protruding heat sources over vertically mounted PCB. Numerical investigation is made for ideal cases of uniform temperature and uniform heat flux condition over vertically oriented model PCB.

The results obtained from the study are compared with the ideal cases available in the literature and with the results of the present ongoing research project in the area. Magnitude and trends in the heat flux values obtained are discussed with acceptable ranges for the above mentioned convection regimes. Some useful empirical relations to compute Mean Nusselt No. with Plate Spacings are also proposed at the end. This empirical relation is valid over the Nusselt No. range of 200 to 600 for the air velocity up to 3.5 m/s.

Chapter- 2

LITERATURE SURVEY

2.1 Introduction:

In order to improve the existing techniques for the cooling of individual electronic devices, containing arrays of electronic elements such as multichip modules, in-depth knowledge of the fundamental limitations and capabilities of each method is very essential. The present chapter gives a, review including the summary of the analytical, numerical and experimental works reported in the literature.

Work done in this field can be put under following main categories---

1. Natural convection cooling,
2. Forced convection cooling,
3. Mixed convection cooling,
4. Miscellaneous works.

2.2. Natural Convection Cooling:

Anand et al. [1] proposed a technique for determining the optimum plate spacing between arrays of parallel plates. Considerations were given to channels subjected to both uniform wall temperature (UWT) and uniform heat flux (UHF) conditions including both symmetric and asymmetric heating. For free convection heat transfer in parallel plate channels, the heat transfer coefficient for fully developed flow between two plates was the lower bound, and the heat transfer coefficient for a single plate was the upper bound. An optimization function was obtained by developing a lumped system energy balance, and the heat transfer coefficient was represented by composite relations for both the UWT and UHF cases. Optimum plate spacing for different thermal configurations was obtained by maximizing the heat dissipation. Although they considered an array of plates, the composite relations for the heat transfer coefficients actually were based on a single channel analysis. They declared the ratio B/L (B-channel width, L-Channel height) corresponding to the maximum channel average Nusselt number to be the maximum plate spacing for single channels. Composite expressions involving the

single plate limit and the fully developed limit for single-channel Nusselt numbers were used, and the maximum B/L was determined by inspection. Laminar flow of air with constant thermophysical properties between vertical parallel plates was considered. The Boussinesq approximation was used to confine the variation of air density to the buoyancy term in the axial momentum equation. Two dimensional flow equations used for air were based on the boundary layer approximation. Based on the aforementioned simplifying assumptions, suitable model equations in nondimensional form were used.

Levy [2] studied the optimum spacing between parallel vertical Isothermal flat plates dissipating heat by natural convection to the environment. The aim of this study was to determine the minimum optimum plate spacing for a given heat flux value to minimize the temperature difference between the plates and the fluid. He found the minimum temperature difference when the plate spacing was made so large that the wall boundary layers didn't merge.

Naylor et al. [3] studied 2D laminar free convection between isothermal vertical plates including entrance flow effects. They used fully elliptic forms of Navier - Stokes and energy equations considering novel inlet flow boundary conditions. Comparison of the results with approximate boundary layer results showed that full elliptic solution was necessary to get accurate local quantities near the channel entrance. Though, the trends of the local heat transfer distributions were same, the numerical predictions were much lower than the experimental data particularly at the channel exit. This could be due to the experimental error. Also, the experimental data available in the literature for the symmetrically heated isothermal channel are limited so nothing could be said with certainty. At low values of Rayleigh number, the parabolic and elliptic solutions were almost same throughout the channel. However, at higher Rayleigh number, there existed a large difference near the channel entrance, which was due to the entrance flow effects. At a high Rayleigh number, the fluid separation at the entrance had a 'venturi' effect on the main stream flow resulting in local reduction of pressure. It is important to mention that the flow separation at the entrance had a profound effect on local heat transfer.

Mendez et al. [4] studied the steady state heat transfer characteristics of a thin vertical strip with internal heat generation. The non-dimensional temperature distribution in the strip was obtained as a function of the following parameters--

1. The intensity and distribution of the internal heat sources
2. The aspect ratio of the strip
3. The longitudinal heat conductance of the strip
4. The Prandtl number of the fluid. Both, thermally thin and thick wall approximations were considered. The total thermal energy at averaged temperature of the strip was found to decrease as the influence of the longitudinal heat conduction effects in the strip decreased in the thermally wall regime. After reaching a minimum, it increased again in the thermally thick wall regime.

Wang et al. [5] multigrid technique for the laminar natural convection air cooling of a vertical plate having wall-attached protruding, discretely heated integrated circuit (IC) packages. This study has great practical importance because it demonstrated the influence of blockage (IC package) dimensions, and their power distribution on the buoyancy induced flow and thermal field in such a configuration. A 2-D, steady state model was used to describe the conjugate natural convection/conduction heat transfer. The fluid physical properties were assumed to be uniform except for the buoyancy terms, which were computed using the Boussinesq approximation of Navier-Stokes equations. The influence of the geometrical parameters (B and L_G), and of the dissipated power (Q) on the velocity and temperature fields was discussed. Due to the effect of B and L_G , it was observed that when the ICs were distributed uniformly along the electronic board, the temperatures produced were lower as compared to the situation of assembling all the ICs in the inlet zone. However, the maximum temperature was found to be insensitive to the position of a bigger component along the electronic board. In general, there was a large interval in the chips temperature between the first and second ICs and this effect was dominant in downstream. For the buoyancy-induced flow, the perturbation of the boundary layer flow due to different distribution of the heated ICs, remained very localized, and didn't propagate far away. Moreover, the buoyancy induced mass flow rate was

practically insensitive to the variation of the geometrical parameters. The sensitivity study indicated that the uniform power distribution was the best case, and produced the lowest maximum temperature and also indicated the best location of the highly dissipating ICs in the inlet region of the board. The study showed that in all cases, the buoyancy-induced flow was starting as a purely natural convection in the bottom of the board, but developed to a mixed convection at the top, where a small recirculation zone appeared behind the last IC.

Yao [6] gave an analytical solution for the fluid flow and heat transfer in the entry region of a heated vertical channel considering the conditions of constant wall temperature and constant wall heat flux. In this study, the hydrodynamically and thermally developing laminar flow (entry flow) in a heated vertical channel was presented. At inlet to maintain a uniformly distributed velocity profile, the entrance of the channel was connected to a chamber, and this was possible due to the rapid contraction of the fluid passage between the chamber and the channel. Analytical solution gave different axial length scales. These scales distinguished the regions of different convective mechanisms that a developing flow had to pass through before reaching its fully developed state. Analytical solution indicated that natural convection eventually becomes the dominant heat transfer mode if $Gr > Re$ for constant wall temperature, and $Gr^2 > Re$ for constant wall heat flux. This study also indicated the reason of reverse flow for $Re < 5000$.

Manca et al. [7] investigated experimentally natural convection between horizontal, heated, parallel plates in air by visualizing the flow and measuring the air temperature. Based on the plate spacing, Gr varied in the range of 1.22×10^5 to 1.06×10^6. Flow patterns and probable onset of secondary motions were observed for three heating modes: (1) both plates heated, (2) upper plate heated and lower one unheated, and (3) upper plate unheated and lower one heated. The main flow pattern resembled a *C* shape (C loop) for all modes. The flow visualization showed that the main C loop flow extended as far as half the length of the plate. In fact, the flow penetrated inside cavity close to the leading edge of the lower plate and exited from the upper part, by reversing its motion between the plates. Secondary flows were absent when only the upper plate was heated, whereas for the other

heating modes, thermals started in the inflow side of the C loop over the lower heated plate, and then they changed into longitudinal vortices. These vortices then broke out in the reversal region of the flow, and a chaotic motion originated in the outflow branch of the C loop, adjacent to the upper plate. The chaotic flow extended as far as to the exit section of the open-ended cavity. The existence of these structures was confirmed by measurements of instantaneous temperature values. When the lower plate was heated and upper one was not, the flow became more chaotic in the outflow branch of the *C* loop as Gr was increased.

Jang [8] investigated experimentally the free convective heat transfer in a composed rectangular parallelogrammic enclosure with a guide vane. Experimental variables were guide vane thickness, the various inclination angles of parallelogrammic enclosure part and the various lengths of rectangular enclosure part. The experiment covered a range of Rayleigh numbers between 2.4 $\times 10^8$ and 9.8 $\times 10^8$ for Prandtl number of 0.71. The variables also covered the inclination angles of the parallelogrammic enclosure part w.r.t the horizontal, ϕ ,of 15, 30, 45, and 60 degree considering an aspect ratio of L_p/H = 0.75. Air was used as the working fluid. It was found that the heat transfer coefficient for ϕ= 60 deg, d^* = 0.6 and L_r/H = 0.5 was increased by about 30% than that for ϕ =15 deg, d^* =1.0 and L_r/H =0.0. The results obtained were as follows:

(1) The present experimental data for d* = 1.0 and L_r/H =0.0 were proved in good agreement with those of the previous study.

(2) For ϕ = 60 deg and L_r/H=0.5, the Nusselt number showed a maximum value.

(3) The optimum thickness of guide vane was found as d^* = 0.6 for ϕ =60 deg and L_r/H=0.5.

(4) The parametric correlation for the ranges of the parameters investigated was found to be

$$Nu = 0.0037\,(Ra)^{0.429\,(d)\,0.050}\,(Lr/H)\,0.0415$$

For ϕ = 60 deg, $2.4\times 10^8 < Ra < 9.8\times 10^8$, Pr = 0.71 and L_p/H = 0.75.

2.3 Forced Convection Cooling:

Young et al. [9] studied the numerical simulation of forced convective, incompressible flow in a channel with a two dimensional array of multiple heated obstacles attached to one wall. The emphasis was given on three levels of Nusselt numbers: local distributaions along the obstacle exposed faces, mean values for individual faces, and overall obstacles mean values. This study incorporated the effects of variations in the obstacle height, width, spacing, and number, along with obstacle thermal conductivity, fluid flow rate and heating method, to illustrate important fundamental and practical results. The periodic behavior of the mean Nusselt number along with the velocity components and temperature distributions for the array were explicitly demonstrated. The solid thermal conductivity was varied between values typical of electronic component materials. Smaller, widely spaced obstacles transferred thermal energy into the fluid more effectively. Narrow gaps between tall obstacles allowed the upstream thermal transport by cavity vor ices through reduced cavity-core flow interaction and in some cases heated the upstream obstacles. In the isotherms within the obstacles, the effect of surface heat flux and volumetric heating produced small changes in Nusselt numbers. Large values of the solid thermal conductivity effectively isothermalized the obstacles regardless of heating method or geometry. The periodic behaviors were explicitly demonstrated by doubling the number of obstacles.

Young et al. [10] investigated the forced convective cooling of a heated obstacle mounted upon a channel wall. The Navier-Stokes equations were used to characterize the the flow field surrounding the conductive obstacle. Special emphasis was given in the systematic analysis of local Nusselt number distributions and mean Nusselt numbers for the individual exposed obstacle faces. The study employed parametric numerical simulation considering variations in the obstacle height and width, as well as the thermal conductivity ratio k_{solid} /k_{fluid}, flow rate and, heating method to capture the fundamental and practical results. The rectangular obstacle changed the parabolic velocity field significantly, resulting in recirculation zones both up- and downstream and a thermal boundary layer along the top face. The effect of flow and temperature fields on parametric changes in

the governing parameters, Reynolds number, solid thermal conductivity, heating method, and two geometric parameters were shown. This investigation showed the significant effect of the shape and material of the obstacle on the fluid flow and heat transfer. An analytical solution provided a reasonable estimate for the Nusselt number on the top face of the obstacle if the bypass height was utilized to characterize the flow. When the thermal energy was introduced through volumetric generation or surface heat flux, a little difference in Nusselt numbers was found. Correlation's, developed for the obstacle mean Nusselt numbers as functions of the parametric variables described the numerical results with mean errors less than 6%.

Tso et al. [11] experimentally investigated the single-phase forced convection heat transfer using water as fluid from in-line four simulated electronic chips, which were flush, mounted to one wall of a vertical rectangular channel. The effects of the most influential geometric parameters on heat transfer including chip number, and channel height were tested. The channel height was varied over values of 0.5, 0.7, and 1.0 times the heat source length. Three values used for heat flux were 5 w/cm^2, 10 w/cm^2, and 20 w/cm^2 and Reynolds number was varied in the range of 6 $\times 10^2$ to 8 $\times 10^4$. The experimental results indicated that heat transfer coefficient was affected strongly by the number of chips and the Reynolds number and weakly by the channel height. Following were the conclusions of the experimental study-

(1) There were three distinct heat transfer regions including laminar, transition from laminar to turbulent, and turbulent associated with the Reynolds number range of the experiments. The Reynolds number based on the hydraulic diameter was considered as better approach to determine the existence of laminar or turbulent flow rather than the Reynolds number based on heat source length.

(2) Results from this experiment agreed well with results for air-cooling of heat sources of similar geometry when Peclet numbers were used to correlate data in laminar flow and Nusselt numbers were normalized against the Prandtl number in turbulent flow. This suggested that data for air-cooling might be used to predict the

heat transfer characteristic of liquid-cooling for similar geometry if the Prandtl number scaling was considered.

Hollworth and Durbis [12] conducted experiments to evaluate the performance of a low velocity air jet system used to cool a simulated electronic package. Their test model consisted of an uniform array of rectangular elements mounted on a board. Each element was cooled by a cluster of four jets and spent fluid was vented at one end through the channel formed between the two boards. Cross flow of air appeared to enhance heat transfer from the exit end of the channel.

Roeller et al.[13] identified the fundamental factors influencing the convective transfer of heat from an isolated protrusion of varying dimension in a channel. This was actually a configurational prototype of many fan cooled electronic systems. Flow structure and average heat transfer characteristics were also experimentally investigated. A Nusselt number correlation was developed as a function of channel Reynolds number, the extent of protrusion and various channel geometric parameters.

Anderson and Moffat [14] studied forced convection heat transfer in a channel populated with discrete components similar to those found in electronic cooling situations. They demonstrated that the thermal-mixing enhancement aimed at decreasing temperature nonuniformities in the channel could significantly reduce the component temperatures. Typically up to 19% reduction in overall temperature rise could be achieved by this method.

2.4 Mixed Convection Cooling:

Barletta et al. [15] analyzed combined free and forced convection flow in a parallel-plate vertical channel in the fully developed region considering the effect of viscous dissipation. The two isothermal boundaries were and kept either at equal or at different temperatures. Dimensionless mean velocity, dimensionless bulk temperature and Nusselt number were determined. They pointed out that the temperature distribution in the fluid was uniform when both boundaries were at the same temperature (symmetric heating) and was a linear function of the transverse coordinate when the boundaries were kept at different temperature (asymmetric heating). Therefore, in the case of asymmetric heating, heat transfer between the

two boundaries of the channels occurred by pure conduction (conduction regime). Moreover, the buoyancy force influenced the velocity profile and made the flow reversal both for upward and downward flow. Moreover effect was expected to be relevant for fluids with high values of dynamic viscosity as well for high – velocity flows. When viscous dissipation cannot be neglected; the temperature field is dependent on the velocity field through nonlinear term in the energy balance equation. This coupling term is absent when viscous dissipation is neglected. Finally they concluded that the effect of viscous dissipation could be important especially in the case of upward flow. Due to the presence of viscous dissipation term in the energy equation, the heat transfer between two boundaries of the channel is not simply due to pure conduction as in case of negligible viscous dissipation Moreover, for asymmetric heating, it had been shown that viscous dissipation enhanced the effect of flow reversal in the case of downward flow, while it lowered this effect in the case of upward flow. In fact, viscous dissipation increased the buoyancy forces and, as a consequences, the fluid velocity in the upward direction.

Hamadah et al. [16] analyzed the problem of laminar fully developed mixed convection in a parallel plate channel for the case where buoyancy opposed the flow. Complete solutions for the velocity and wall heat transfer were obtained considering following cases:

1. Both walls isothermal and having different or same temperatures.
2. Both walls at constant heat flux having same or different magnitudes.
3. Right wall at constant heat flux while the left wall is at different temperature.

He considered fully developed buoyancy opposing flow between inclined, constant heat flux plates. The results obtained for Plates in the vertical orientation were same as that obtained for case 2. They studied developing and fully developed buoyancy-aided flow between parallel plates with specified plate temperature and heat fluxes. They found that buoyancy enhanced heat transfer near the heated wall, and might cause flow reversal near the cooler wall. Here solutions to the fully developed flow energy equation were used to obtain the dimensionless velocity profiles in terms of the ratio (Gr/Re). Using this ratio, flow reversal criterion was

determined, finally Nusselt number was evaluated using mean fluid temperature. For case -1 as Gr/Re was increased, adverse buoyancy was also increased and the flow adjacent to the heated wall became retarded. So, the velocity profile inflected in this region and the velocity near the opposite wall increased in order to maintain conservation of mass. For 0 <Gr/Re<270, the velocity profiles for the thermally developing flow and the fully developed flow were very similar. The thermally developing velocity profile exhibited stronger Inflection near the heated wall and somewhat less skewing of the flow away from the heated wall, due to the existence of stronger temperature gradients near the heated wall. For very large (Gr/Re), the shear stress at the hotter wall vanished, and the flow reversed.

For case- 2 as (Gr/Re) was increased, inflection occurred adjacent to both walls and the velocity profile "popped" in the center of the channel. For sufficiently large (Gr/Re), the shear stress at the wall vanished and the flow reversal took place.

For case-3 as (Gr/Re) was increased, the velocity profile became inflected near the hot wall. At (Gr/Re) = 576, flow reversal occurred. As (Gr/Re) was increased the hot wall Nusselt number decreased and the cold wall Nusselt number increased.

Shai et al. [17] analyzed mixed convection flow in a nuclear reactor. In forced convection of fluid flow over a vertical flat plate, generating uniform heat flux, due to the temperature difference between the surface and the fluid, change in fluid density occurred causing natural convection. So they found, forced convection was always coupled with natural convection. They suggested mixed convection as a dominating heat transfer mode in case of loss of cooling accident (LOCA) in a nuclear reactor. Mixed convection assisted the upward flow of fluid, but it opposed when the fluid flow was in opposite direction to the buoyant motion. In this study considering the hydrodynamic and the thermal boundary to be the same Pr = 1 (air) and the velocity profile within the boundary layer as a superposition of pure forced and pure natural convection, a simple analysis was presented to evaluate the heat transfer coefficient in assisting mixed convection (AMC) and in opposing mixed convection (OMC). For the case of AMC one simple equation covered the entire length of the plate, but for OMC two simple equations,

depending on whether the region was dominated by forced convection or by natural convection, were needed. They used dimensionless characteristic parameter, β (which is the ratio between the governing characteristic values of each pure of conduction) as a deciding factor of heat transfer mode. When $0.1<\beta<2$, mixed convection mode was dominating, for $\beta<0.1$ pure natural convection mode was dominating and for $\beta>2$ pure forced convection mode was the dominating mode. In AMC case, the heat transfer coefficient values increased, while in OMC, this value decreased in both dominating regions and approached very low values in the critical point to cause an increase of wall temperature.

Moukalled et al. [18] studied mixed convection heat transfer numerically in channels with a heated curved surface bounded by a vertical adiabatic wall. They considered two different cases: in the first case, the flow experienced a convex curvature and an increasing cross-sectional area (adverse pressure gradient), while in the second case, the flow experienced a concave curvature with a decreasing flow cross-section (favorable pressure gradient). The primary aim of the study was to analyze the influence of stream wise curvature on the surface heat transfer for a range of Pr, Re, Gr/Re^2 and surface curvature ratio (R/L).Considering the flow as two dimensional, steady and laminar, governing equations were expressed for conservation of mass, momentum, and energy. The control volume approach was adopted to solve numerically the coupled system of equations governing the flow and temperature field. For convex entry channel, it was observed that for low (Gr/Re^2), the Nusselt number reached a minimum near the onset of flow separation along the heated wall of the convex-entry channel and then decreased towards the channel exit. The effect of increasing Pr on the total heat transfer was considerably greater than the effect of increasing (Gr/Re^2). For concave entry channels, there was no flow separation. Decreasing cross sectional area considering the buoyancy effect increased the channel velocities and the near wall gradients. Therefore, surface heat transfer rates were considerably greater than in a convex-entry channel. The overall heat transfer in a concave-entry channel was always greater than a straight channel of equal height. Comparing with a straight channel of

equal heated surface area, there was a critical Gr/Re^2 value, below which heat transfer enhancement was obtained with concave-entry channel.

Barleta [19] studied fully developed and laminar mixed convection in a parallel-plate vertical channel in case of viscous heating. The channel walls were subjected to asymmetric boundary conditions: one wall was kept at a constant and uniform heat flux, while the other was kept at a uniform and constant temperature. The velocity field and the temperature field were evaluated analytically using perturbation method. The velocity field was assumed to be parallel. The governing equations were written in a dimensionless form such that the dimensionless velocity profile and the dimensionless temperature profile were uniquely determined by the heat-flux Brinkman number, Br and by the $\varepsilon=Gr/Re$. The parameter Br accounted for the effect of viscous dissipation, while the parameter ε accounted for the effect of buoyancy. The dimensionless velocity and temperature were expressed as power series with respect toε. In case of forced convection, the order of the perturbation series was zero. Analysis of the results considering the Nusselt number and the Fanning friction factor had led to the following conclusions:

(a)The effect of buoyancy was more apparent for upward flow than for downward flow.

(b) Flow reversal next to the boundary with a prescribed temperature occurred for upward flow with a sufficiently high value of ε and for positive values of Br.

© In the case of downward flow, the absolute values of the Nusselt numbers on both walls and the friction factor on the boundary with a prescribed temperature was increased by buoyancy. Opposite was the case with the upward flow.

(d) For a given value of Br, the effect of buoyancy produced, for upward flow, an increase in the temperature difference between the channel walls, while, for downward flow, buoyancy caused a decrease of this difference.

Chen [20] investigated the linear stability of mixed convection in a differentially heated vertical channel for various Pr values of 0.7, 7, 100, and 1000. The results indicated that this fully developed heated flow became unstable under appropriate conditions. Reynolds number, Prandtl number showed crucial effects

on the critical Grashof number Gr_c , critical wave speed c_r , critical wave number α_c and instability mechanism for higher Prandtl numbers. For lower Prandtl numbers, the effects from the Prandtl number and Reynold number were relatively small. For the overall trend, the Gr_c increased with increasing Re. In general, the higher the Pr, the smaller smaller was the Gr_c. For Pr = 1000, the (Gr/Re)c was smaller than 48 for Re > 625, therefore, there was no inflection point in the base laminar profile. The number of the local minimum wave numbers was found equal to eight for Pr = 1000, which were substantially larger than those (two or three local minimum wave numbers) found in natural convection or shear flow between horizontal plates heated from below. For Pr = 100 and 1000 the Gr_c , α_c , and c_r showed discontinuities and also sudden shift of instability was found. All these were due to the presence of multiple local minimum numbers. For Pr = 100, the α_c and c_r showed a large jump at Re = 1365. Before that jump, the α_c was very small (α =0.006 for Re = 1300) and the c_r was the largest among all curves, with a value of 1.6 . In addition, between Re = 50 and 1365, thermal-buoyant instability was found. After that jump, the α_c and c_r approached 1.0 and 0.5, respectively, and the instability also suddenly shifted to shear instability. For Pr = 1000 the α_c was found highest (α_c = 3.99 for Re = 1000) or the wavelength was the shortest for medium and high Reynolds numbers. This implied that the instability was caused by the local disruption of the velocity field induced by the thermal fluctuation. For Pr = 0.7, and 7 the Gr_c, α_c ,and c_r didn't have discontinuities and the thermal-shear and shear instabilities dominated in low and high Reynolds number flows respectively. It was noted for Pr = 0.7, 7, and 100 the α_c and c_r were relatively close together and the instability types were the same for Re > 1365, which was significantly different from those of Pr = 1000.

Tseng et al.[21] experimentally investigated the stabilization of buoyancy driven unstable mixed convective vortex air flow in a bottom heated rectangular duct by tapering its top plate so that its aspect ratio at the inlet was 4 and at the exit gradually it raised to 12. In this study, the secondary flow in the duct was visualized and the steady and transient thermal characteristics of the flow were

examined by measuring the spanwise distributions of the time-averaged temperature. The experiments were carried out for the Reynolds number ranging from 5 to 102 and Grashof numbers from 1.0×10^4 to 1.7×10^5. The results obtained were the following-

(1) In the rectangular duct the onset of thermal instability was found to move upstream for increasing Gr number and/or decreasing Re number. The results for the tapering duct resembled those for the rectangular duct except that the onset point moved a little downstream as compared to that for a the horizontal duct for the same Re and Gr.

(2) Due to the increase of the aspect ratio from 4 at the duct inlet to 12 at the exit, more vortex rolls were induced in the tapering duct than in the rectangular duct in the downstream region.

(3) In the tapering duct, the main forced flow accelerated so rapidly in the downstream region that the vortex intensity of the longitudinal rolls was much weaker.

(4) The unstable vortex flow at high buoyancy-to-inertia ratio in the rectangular duct can be completely stabilized by tapering the top plate over the range of the parameters covered in the study. Ultimately it was realized that although the top plate tapering resulted in the complete stabilization of the vortex flow, the weaker vortices still dominated the secondary flow in the tapering duct.

Gau et al. [22] experimentally studied the mixed convection flow and heat transfer inside a divergent channel formed by two plane walls. One of the side walls was oriented vertically and was heated uniformly, and the opposite insulated wall was tilted at an angle of 3 deg with respect to the vertical position. The ratio of the height to wall spacing at the flow inlet was 15.The Reynolds number was varied from 100 to 4000 and the buoyancy parameter Gr/Re^2, varied from 0.3 to 907. Flow reversal was found for both assisted and opposed convection. In this study, the effect of channel divergence on the reverse flow and the heat transfer has been discussed. It was found that due to the divergent section of the channel, the mainstream decelerated such that flow reversal was initiated at a much lower buoyancy parameter. The adverse pressure gradient tended to push the reversed flow upstream and thus produced a deeper penetration of the reversed flow into the

channel. The destabilization effects of the divergent channel in the downstream brokedown the vortices and made transition to turbulent flow. This significantly enhanced the heat transfer. In the upstream region, where the buoyancy parameter was relatively low such that flow reversal was absent or relatively weak, the heat transfer in the divergent channel was lower than that in the parallel-plate channel due to the deceleration of the mainstream. For assisted and opposed convection, both the local and average Nusselt numbers when divided by $Re^{0.4}$ were found to be functions only of the buoyancy parameter. This was not the case for $Gr/Re^2 <$ 100 in opposed convection. For assisted convection, the Nusselt number increased with the buoyancy parameter. For opposed convection, the increase of the Nusselt number with the buoyancy parameter made the flow reversed, which interacted strongly with the mainstream.

2.5 Miscellaneous work:

M.Behnia et al. [23] numerically investigated natural convection immersion cooling of two heat sources placed in a series of parallel interacting cavities filled with FC-72. Both low thermal conductivity (i.e. bakelite) and high thermal conductivity substrates (i.e. alumina-ceramic) were considered. Results obtained with single and double heat source configurations were compared. Non-dimensional temperatures and Nusselt numbers of the heat sources were correlated as a function of the Rayleigh number. Navier-Stokes equations in terms of vorticity-stream function were used in the fluid region considering a laminar, 2 D and incompressible fluid, with constant properties except for Boussinesq approximation. Alternating Direction Implicit (ADI) scheme was used considering pseudo-transient approach to solve the equations numerically. They showed the influence of modified Rayleigh number, Ra* and thermal conductivity ratio, K on the flow and thermal fields, and the heat transfer characteristics of the heat generating devices. Increasing Ra* produced a stronger convective flow inside the cavities for all values of K. Thin thermal and velocity boundary layers were formed along both faces of the vertical walls and the rest of the cavity was occupied by the cold fluid. For low values of K (e.g. bakelite substrate), the flow

and thermal fields were asymmetric whilst for higher conductivity substrate (e.g. alumina ceramic), symmetrical flow patterns were observed.

Jubran et al. [24] experimentally investigated the effects of the size of modules, the presence of a cylindrical module and the missing module on the heat transfer coefficient and pressure drop characteristics of array configurations composed of individual rectangular modules for three different Reynolds numbers namely; 1690, 2250, and 2625. The experiments resulted in following conclusions:

(1) Using individual rectangular modules rather than square modules in the array configuration enhanced the heat transfer significantly. In general, the implantation of odd-size modules in the array was shown to be an effective means of heat transfer enhancement with a maximum enhancement value of 40%.

(2) If in the array a missing module was placed just upstream of the module at which heat transfer coefficient was calculated, a maximum heat transfer enhancement of 37% occurred.

(3) The implantation of cylindrical module at the middle of an array configuration enhanced the heat transfer coefficient by as much as 28% at the next row downstream. However, no effect on heat transfer was observed when the cylindrical module was located side by side with the active module.

(4) The pressure drop results indicated that large size modules enhanced the pressure drop at their row locations by as much as 15%, while the cylindrical module decreased pressure drop especially at a low value of Reynolds number.

Sparrow et al. [25] experimentally investigated the heat transfer and pressure drop characteristics of arrays of heat generating, rectangular modules that are commonly encountered in electronic equipment. Experiments were performed with fully populated arrays in which there were missing modules. Arrays as barriers and arrays in which there was both a missing module and a barrier were implanted to obtain heat transfer enhancement. Air was used as a heat transfer medium in all the cases. For the fully populated array without barriers, row independent (fully developed) heat transfer coefficients were found for the 5^{th} and all subsequent rows. If there was a missing module in the array, the heat transfer coefficients at other modules placed in the neighborhood were larger than when there were no

missing modules. The greatest enhancement, on the order of 40% occurred when the missing module was just upstream of the module at which the heat transfer coefficient was being monitored. Results for the case in which there were two missing modules side by side in the given row of the array were nearly the same as that induced by a single missing module. The implantation of a barrier in the array was shown to be an effective means of heat transfer enhancement. Enhancement was further increased with further increase in barrier height. In case of a barrier and a missing module the enhancing effects of heat transfer were found to be mutually reinforcing when the missing module was upstream of the monitored module. However, there was little reinforcement when the missing module was located either to the side or downstream of the monitored module.

Parneix et al. [26] numerically studied the problem of cooling of a heated plate by an axis-symmetric isothermal fully developed turbulent jet. The axi-symmetric, incompressible, Reynolds averaged Navier Stokes equations were solved in conjunction with the k-$\in$ and v^{-2} transport equations. The computations carried out herein showed that predictions by the normal-velocity relaxation model agreed with the experiments. The k-$\in$ model did not properly represent the flow features, highly over predicted the rate of heat transfer and yielded physically unrealistic behavior.

Huang et al. [27] Performed heat transfer and flow visualization experiments to investigate and compare the heat transfer performance of new swirling jet designs with that of a conventional impinging jet having the same diameter at the same conditions. Swirling impinging jets employed a 25.4 mm long solid insert at the exit of tube to divert the air flow through four narrow channels along the surface of the insert, with the desired swirl angle (15^0,30^0, and 45^0). Flow field visualization experiments employed three flow visualization techniques. Smoke flow; smoke wires and water jet seeded with tiny air bubbles used as tracers. The smoke flow technique showed that the flow field between the exit of the jet housing tube impinged on the surface, while the smoke wires technique gave clear images showing details of the flow field at and close to the impinged surface. It was observed that swirling impinging jet induced markedly higher local and surface

average Nusselt number values and improved radial uniformity of heat transfer on the impinged surface compared to conventional impinging jet. Nusselt number for swirling impinging jets was higher than for conventional impinging jet at intermediate jet spacing.

Voke et al. [28] studied computationally the impingement of a thermally inhomogeneous turbulent jet on a solid plate, using large-eddy simulation. The case of a plane channel into an enclosed pool and impinging normally on perspex plate 1.8 jet widths was investigated. It was shown that the dynamics of the turbulence in this particular geometry resulted in temperature variations at the plate surface having very high lateral correlation, so that lateral conduction of heat within the plate failed to have any significant effect on the transmission of thermal fluctuations from the fluid into the plate.

Chapter-3

COPUTATIONAL WORK

3.1 Review of Numerical Methods:

Either of two numerical methods can be selected:

. Segregated Solution Method

. Coupled Solution Method

Using either method, the governing integral equations can be solved for the conservation of mass or momentum, and (when appropriate) for energy and other scalars such as turbulence and chemical species. In both cases a control-volume-based technique is used which consists of:

. Division of the domain into discrete control volumes using a computational grid.

. Integration of the governing equations on the individual control volumes to construct algebraic equations for the discrete dependent variables ("unknowns") such as velocities, pressure, temperature, and conserved scalars.

. Linearization of the discretized equations and solution of the resulting linear equation system to yield updated values of the dependent variables.

Segregated Solution Method:

In this approach, the governing equations are solved sequentially (i.e., segregated from each another). Because the governing equations are non-linear (and coupled), several iterations of the solution loop must be performed before a converged solution is obtained. Each iteration consists of the steps illustrated in Figure 3.1.

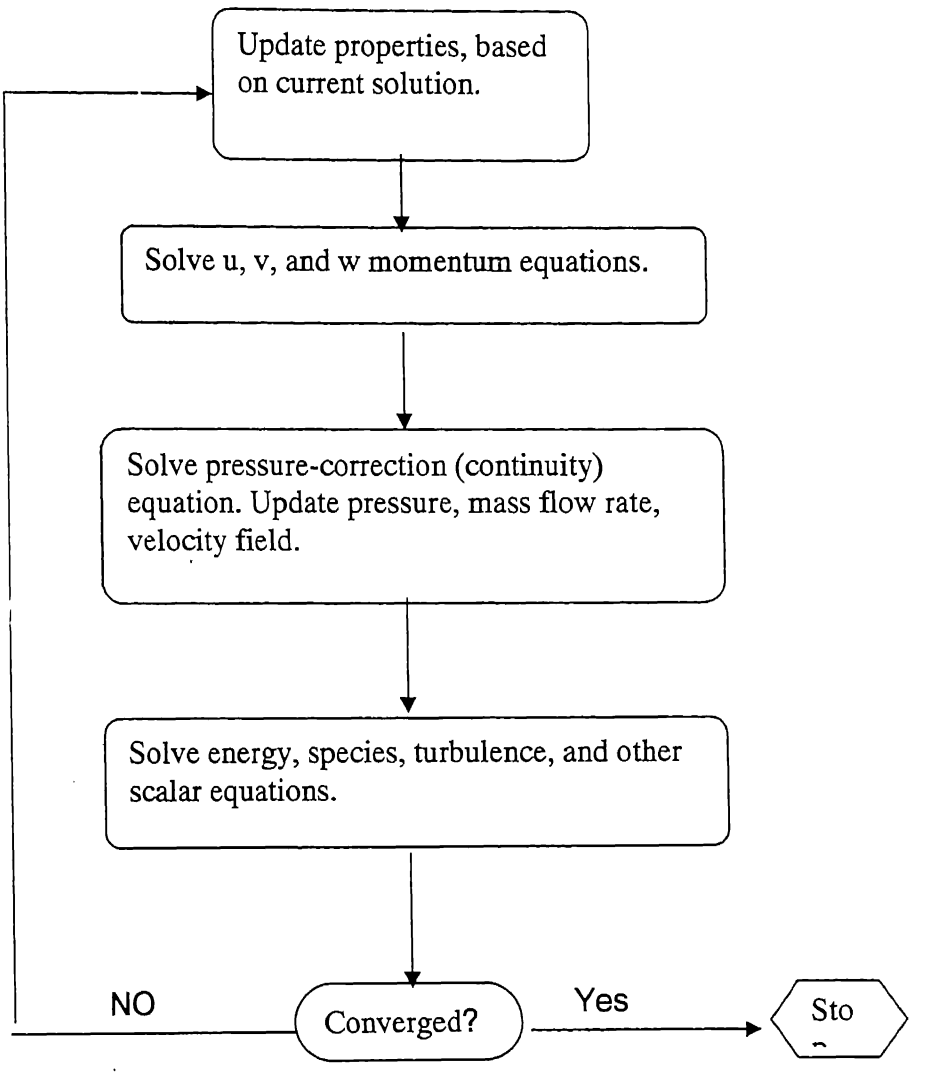

Figure-3.1: Flowchart to each iteration in Segregated Solution Method.

Coupled Solution Method:

In this approach the governing equations of continuity, momentum, and (where appropriate) energy and species transport are solved simultaneously (i.e., coupled together). Governing equations for the additional scalars are solved using the 'Segregated Solution Method' described earlier. Since the governing equations are non-linear and coupled, several iterations of the solution loop are performed before

a converged solution is obtained. Each iteration consists of the steps illustrated in Figure 3.2.

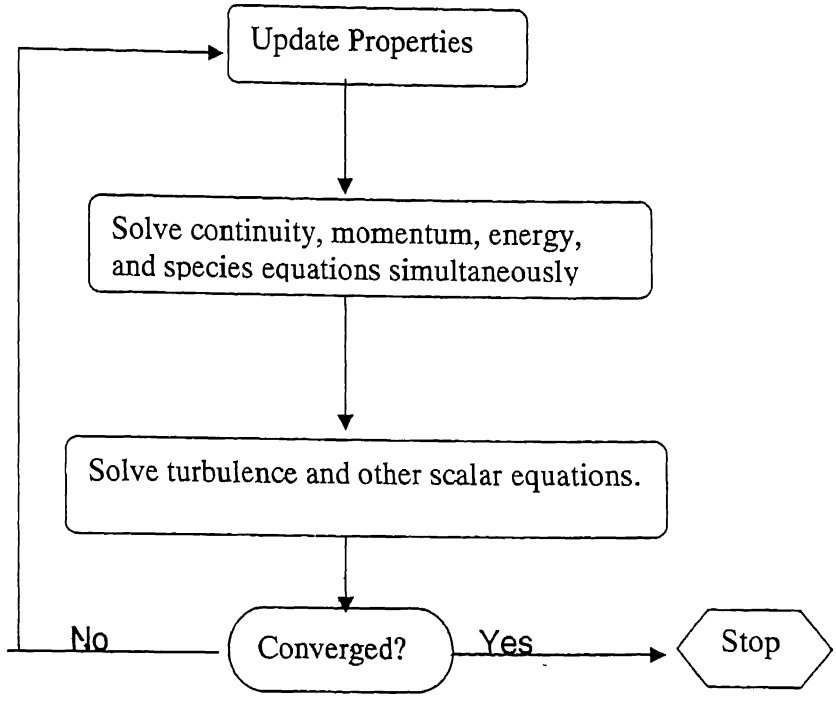

Figure-3.2: Flowchart to each iteration in Coupled Solution Method.

Linearization: Implicit vs. Explicit:

In both the segregated and coupled solution methods, the discrete, non-linear governing equations are linearized to produce a system of equations for the dependent variables in every computational cell. The resultant linear system is then solved to yield an updated flow-field solution._The manner in which the governing equations are linearized may take an "implicit" or "explicit" form with respect to the dependent variables (or set of variables) of interest. Implicit and explicit method is described below. . Implicit: For a given variable, the unknown value in each cell is computed using a relation that includes both existing and unknown values from neighboring cells. Therefore each unknown will appear in more than one equation in the system, and these equations are solved simultaneously to give the unknown quantities.

. Explicit: For a given variable, the unknown value in each cell is computed using a relation that includes only existing values. Therefore each unknown will appear in only one equation in the system and the equations for the unknown value in each cell can be solved one at a time to give the unknown quantities.

In the segregated solution method each discrete governing equation is Linearized implicitly with respect to that equation's dependent variable. This will result in system of linear equations with one equation for each cell in the domain and thus forming a "scalar" system of equations. A point implicit (Gauss-Seidel) linear equation solver is used in conjunction with an algebraic multigrid (AMG) method to solve the resulting scalar system of equations for the dependent variable in each cell. Thus, the segregated approach solves for a single variable field (e.g. p) by considering all cells at the same time. It then solves for the next variable field by again considering all cells at the same time, and so on. There is no explicit option for the segregated solver.

. In the coupled solution method, the coupled set of governing equations can be linearized either by implicit or explicit method. In implicit option of the coupled solver, each equation in the coupled set of governing equations are linearized implicitly with respect to all dependent variables in the set. This will result in a system of N linear equations for each cell in the domain, where N is the number of coupled equations in the set and thus forming a "block system of equations. A point implicit (block Gauss-Seidal) linear equation solver is used in conjunction with an algebraic multigrid (AMG) method to solve the resultant block system of equations for all dependent variables in each cell. Thus this approach solves for all variables (p, u, v, w, T) in all cells at the same time. In explicit option of the coupled solver, each equation in the coupled set of governing equations is linearized explicitly and this results in a system of N equations for each cell in the domain. And likewise, all dependent variables in the set are updated at once using a multi-stage (Runge-Kutta) solver. Thus this approach solves all variables (p, u, v, w, T) in one cell at a time.

First-Order Upwind Scheme:

When 1st-order accuracy is desired, quantities at cell faces are determined by assuming that the cell-center values of any field variable represent a cell-average value and hold throughout the entire cell; the face quantities are identical to the cell quantities. Thus when 1st-order upwinding scheme is selected, the face value ϕ_f is set equal to the cell-center value of ϕ in the upstream cell.

Second-Order Upwind Scheme:

When 2nd-order accuracy is desired, quantities at cell faces are computed using a multidimensional linear reconstruction approach. In this approach, higher-order accuracy is achieved at cell faces through a Taylor series expansion of the cell-centered solution about the cell centroid. Thus when 2nd-order upwinding scheme is selected, the face value of ϕ_f is computed using the following expression:

$$\phi_f = \phi + \nabla\phi \bullet \Delta s$$

where ϕ and $\nabla\phi$ are the cell-centered value and its gradient in the upstream cell, and Δs is the displacement vector from the upstream cell centroid. The gradient $\nabla\varphi$ is computed using the divergence theorem.

Under-Relaxation:

Because of the nonlinearity of the equation set, it is necessary to control the change of ϕ. This is typically achieved by under-relaxation, which reduces the change of ϕ produced during each iteration. In a simple form, the new value of the variable ϕ within a cell depends upon the old value, ϕ_{old}, the computed change in ϕ, $\Delta\phi$, and the under-relaxation factor,α, as follows:

$$\phi = \phi_{old} + \alpha\, \Delta\phi$$

Pressure-Velocity Coupling Method:

Extensive study has been carried out in the recent decades for developing numerical schemes to solve incompressible Navier-Stokes equations in regular and multi-dimensional complex geometries. The main difficulty with the

incompressible flow simulation is the absence of an obvious equation for pressure. Specifically the nature of coupling of velocity and pressure variables is implicit in nature. When the flow is treated as incompressible, pressure does not have the usual thermodynamic meaning. Here it has a relative value, which adjusts itself instantaneously in such a way that the condition of zero divergence is satisfied at all computational grid points. This behavior is related to the fact that the speed of sound becomes infinite in an incompressible fluid. As a consequence, the pressure field cannot be calculated by a time-advancement procedure.

Instead it requires at least one partially implicit determination, which is able to take in to account the coupling between the pressure and velocity fields, subject to the boundary conditions. The difficulties associated with the determination of pressure have led to the methods that eliminate pressure from the governing equations. Some methods are available to solve the incompressible equations. One of these methods are SIMPLE method. This procedure is based on a cyclic series of guess-and-correct operations to solve the governing equations. The velocity components are first calculated from the momentum equations using a guessed pressure field. The pressures and velocities are then corrected, so as to satisfy continuity. This procedure continues until the solution converges.

3.2 FLUENT: A Brief Description

FLUENT is a state-of-the-art computer program for modeling fluid flow and heat transfer in complex geometries. It provides complete mesh flexibility with unstructured meshes that can be generated about complex geometries with relative ease. Supported mesh types include 2D triangular/quadrilateral, 3D tetrahedral / hexahedral / pyramid / wedge, and mixed (hybrid) meshes. This solution-adaptive grid capability is particularly useful for accurately predicting flow fields in regions with large gradients, such as boundary layers. In comparison to solutions on structured or block structured grids, this feature significantly reduces the time required to generate a "good" grid. Solution-adaptive refinement makes it easier to perform grid refinement studies and reduces the computational effort required to

achieve a desired level of accuracy, since mesh refinement is limited to those regions where greater mesh resolution is needed.

Program Structure:

Following products of FLUENT package have been used here-

(1) FLUENT, the solver.

(2) GAMBIT, the preprocessor for geometry modeling and mesh (grid) generation.

Figure 3.3 shows the organizational structure of these components-

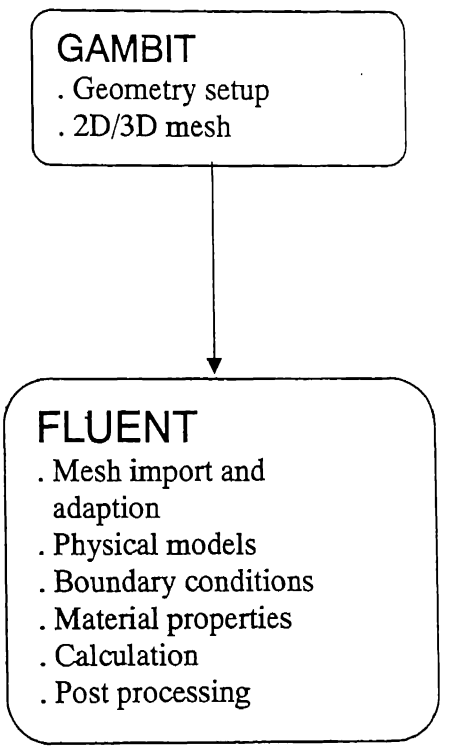

Figure -3.3: Basic Program Structure

Once a grid has been read into FLUENT, all remaining operations are performed within the solver. These include setting boundary conditions, defining fluid properties, executing the solution, refining the grid, and viewing and postprocesing the results.

Problem Solving Steps:

After determining the important features of the problem to be solved, the following basic procedural steps have to be adopted-

1. Create the model geometry and grid.
2. Start the appropriate solver for 2D or 3D modeling.
3. Import the grid.
4. Check the grid.
5. Select the solver formulation.
6. Choose the basic equations to be solved: laminar or turbulent (or inviscid), chemical species or reaction, heat transfer models, etc. Identify additional models needed: fans, heat exchangers, porous media, etc.
7. Specify material properties.
8. Specify the boundary conditions.
9. Adjust the solution control parameters.
10. Initialize the flow field.
11. Calculate a solution.
12. Examine the results.
13. Save the results.
14. If necessary, refine the grid or consider revisions to the numerical or physical model.

Choosing the Appropriate Grid Type

Fluent can use grids comprised of triangular or quadrilateral cells (or a combination of the two) in 2D, and tetrahedral, hexahedral, pyramid, or wedge cells (or a combination of these) in 3D. Depending upon the application suitable mesh type is selected considering the following issues:

. Setup time

. Computational expense

. Numerical diffusion

These points are discussed below:

Setup time:

Many flow problems solved in engineering practice involve complex geometries. In these cases structured or block-structured grids (consisting of

quadrilateral or hexahedral elements) can be extremely time-consuming. So to save the Setup time for complex geometries, unstructured grids employing triangular or tetrahedral cells are preferred. But in case of simple geometry both approach are time consuming.

Computational Expense:

When geometries are complex or the range of length scales of the flow is large, a triangular /tetrahedral mesh can often be created with far fewer cells than the equivalent mesh consisting of quadrilateral/hexahedral elements. This is because a triangular / tetrahedral mesh allows cells to be clustered in selected regions of the flow domain, whereas structured quadrilateral/hexahedral meshes wil: generally force cells to be placed in regions where they are not needed. Unstructured quadrilateral /hexahedral meshes offer many of the advantages of triangular/tetrahedral meshes for moderately-complex geometries.

In some situations quadrilateral/hexahedral elements are more economical in comparison to triangular/tetrahedral cells as they permit a much larger aspect ratio. A large aspect ratio in a triangular/tetrahedral cell will invariably affect the skew ness of the cell, which is undesirable as it may impede accuracy and convergence. Therefore, in case of simple geometry in which the flow conforms well to the shape of the geometry, such as a long thin duct, a mesh of high-aspect-ratio quadrilateral/hexahedral cells is preferable.

Single-Precision and Double-Precision Solvers:

Both single-precision and double-precision versions of FLUENT can be used. For most cases, the single-precision solvers are sufficiently accurate, but in some problems double-precision version is more useful. Several examples are listed below:

. If geometry has features of very disparate length scales (e.g., a very long, thin pipe), then single-precision calculations are not adequate to represent the node coordinates.

. For conjugate problems involving high thermal-conductivity ratios and/or high-aspect-ratio grids, due to inefficient transfer of boundary information, convergence and /or accuracy may be impaired with the single-precision solver.

Sources of Error:

Numerical Diffusion:

A dominant source of error in multidimensional situations is numerical diffusion, also termed as false diffusion. (The term "false diffusion" is used because the diffusion is not a real phenomenon, yet its effect on a flow calculation is analogous to that of increasing the real diffusion coefficient.)

The following points are important about numerical diffusion:

. Numerical diffusion is most noticeable when the real diffusion is small, that is, when the situation is convection-dominated.

. All practical numerical schemes for solving fluid flow contain a finite amount of numerical diffusion due to the presence of truncation errors in the discretized fluid flow equations.

. The second-order discretization scheme used in FLUENT reduces the effects of numerical diffusion on the solution.

. The amount of numerical diffusion is inversely related to the resolution of the mesh. therefore, to minimize the effect of numerical diffusion refined meshing should be used.

. Numerical diffusion is minimized when the flow is aligned with the mesh.

Here the last point is the most relevant during the selection of the grid. With the triangular/tetrahedral mesh, the flow can never be aligned with the grid. On the other hand, with a quadrilateral/hexahedral mesh, this situation might occur, but not for complex flows. It is only in a simple flow, such as the flow through a long duct, in which quadrilateral/hexahedral mesh can minimize the numerical diffusion.

3.3 Problem Description and Solution Methodology

3.3.1: Natural Convection

A 2D unsteady state natural convection problem considering two vertically placed model PCBs assumed to lie inside a large enclosure has been solved. Here two cases have been considered, in 1st case vertical walls have constant temperature and in 2nd case vertical walls have constant heat flux condition. In both cases temperature profile, velocity profile, Nusselt number, Grashof no., Rayleigh no., Prandtl no., Boussinesq no. have been analyzed for different spacings between vertical plates. In order to avoid assigning thermal and hydrodynamic boundary conditions at inlet, the two vertically placed model PCBs were assumed to lie in a very large enclosure with its walls having high thermal conductivity. A schematic arrangement is shown in Figure 3.4

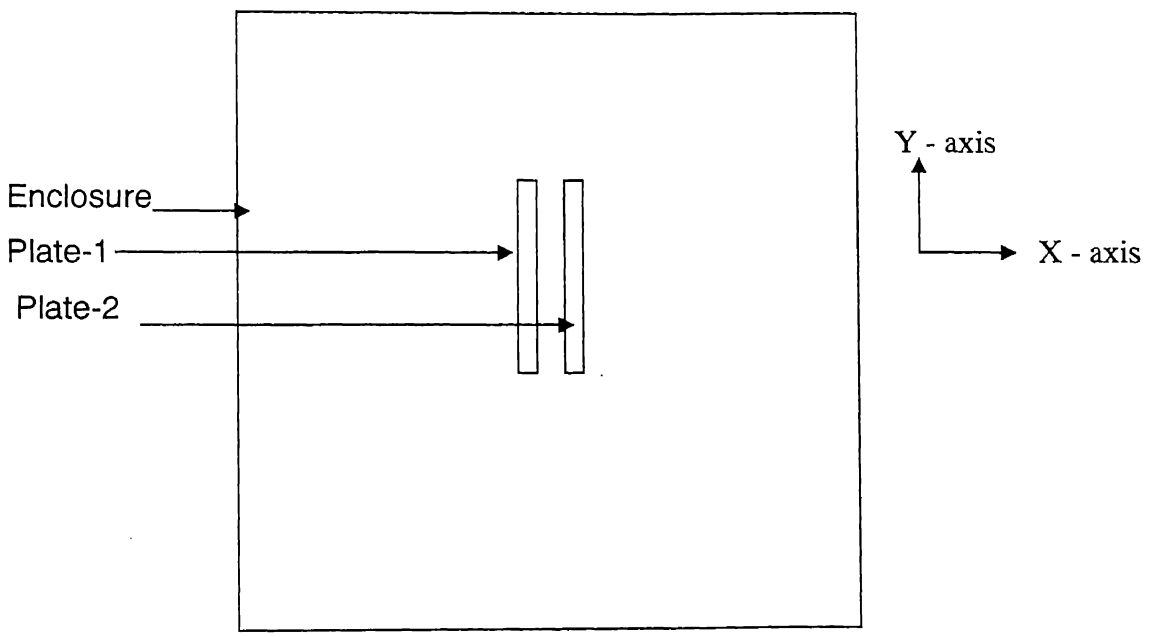

Figure 3.4: Schematic arrangements of heated plates inside computational domain

Problem Solving Steps used with FLUENT:

1. This problem is solved considering 2D, laminar, unsteady state condition.
2. Two dimensional double precision version is selected.
3. Non-uniform refined grids are generated by taking successive ratio of 0.92 for X-direction, and 0.98 for Y-direction.
4. Segregated 2^{nd} -order implicit solver is used.
5. Concerned governing equations are following:

Continuity Equation:

$$\partial u/\partial x + \partial v/\partial y = 0 \quad \text{..... (1)}$$

X-Momentum Equation:

$$u\,\partial u/\partial x + v\,\partial u/\partial y = -1/\rho(\partial P/\partial x) + \nu\,\nabla^2 u \quad \text{.....(2)}$$

Y-Momentum Equation:

$$u\,\partial v/\partial x + v\,\partial v/\partial y = -1/\rho(\partial P/\partial y) + \nu\,\nabla^2 v - g \quad \text{..... (3)}$$

Energy Equation:

$$u\,\partial T/\partial x + v\,\partial T/\partial y = \alpha\,\nabla^2 T \quad \text{.....(4)}$$

Here focus of analysis is the boundary layer region i.e. $x \sim \delta_T$, $y \sim H$, and $\delta_T << H$, then only the $\partial^2/\partial x^2$ term survives in the ∇^2 operator. And boundary layer equations for momentum and energy are then

$$u\,\partial v/\partial x + v\,\partial v/\partial y = -1/\rho\,(dP_\infty/dY) + \nu\,\partial^2 v/\partial x^2 - g \quad \text{.....(5)}$$

$$u\,\partial T/\partial x + v\,\partial T/\partial y = \alpha\,\partial^2 T/\partial x^2 \quad \text{.....(6)}$$

Considering the Boussinesq approximation for coupling between the

temperature field and flow field, the momentum equation becomes:

$$u\,\partial v/\partial x + v\,\partial v/\partial x = \nu\,\partial^2 v/\partial x^2 + g\,\beta\,(T-T_\infty) \quad \text{.....(7)}$$

(a) In case of constant wall temperature, boundary conditions are:

$$T(0,y) = T_1 \text{ and } T(b,y) = T_2 ;$$

Here $T_1 = T_2 = 100\ ^0$ C, b = 40, 50 ...100 mm. And enclosure temperature lies

between 20^0C to 25^0C.

(b) In case of constant wall heat flux boundary conditions are:

$$\partial T/\partial x = -q_1/k \quad \text{and} \quad \partial T/\partial x = -q_2/k;$$

Here value of heat flux lies in the range of 0.085 W/cm^2 – 0.2 W/cm^2.

Table 3.1: Values of heat flux for different plate spacings.

Plate Spacing (mm)	Heat Flux (W/cm^2)
40	0.116
50	0.116
60	0.170
70	0.151
80	0.197
90	0.150
100	0.190

6. Air is considered as the working fluid.
7. To increase the convergence rate suitable under – relaxation factors are considered.
8. Various discretization schemes considered are:

   For pressure ---------- Standard.

   For pressure – velocity coupling----SIMPLE.

   For momentum----------2^{nd}-order upwind.

   For energy---------- 2^{nd}-order upwind.

9. Suitable convergence criterion is selected for residuals of various parameters:

Residuals	convergence criterion
Continuity	10.0 E-03
X-velocity	10.0 E-06
Y-velocity	10.0 E-06
Energy	10.0 E-06

10. For iteration

    Time step size selected as ----------0.1 (s)

    Number of time steps selected as--------- 50

And suitable number of iterations per unit time step is selected.

3.3.2: Mixed Convection

A 2D steady state mixed convection problem considering two vertical plates with a enclosure at inlet has been solved. The aim is to analyze the effect of the plate spacing on flow field including different non-dimensional numbers. Schematic arrangement has been shown in Figure 3.5.

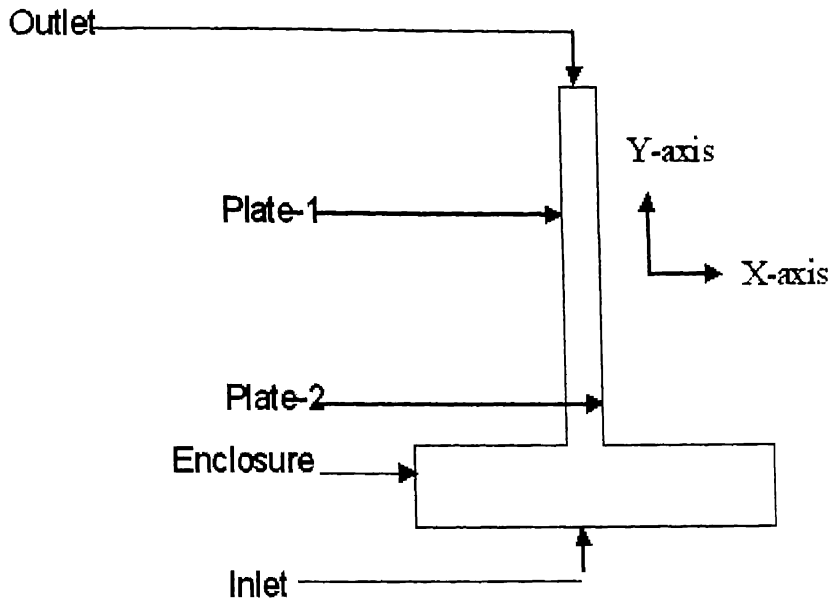

Figure 3.5: Schematic arrangements of Plates with Enclosure.

Problem Solving steps with Fluent:

Here all the steps are same as for Natural convection except the followings:

(1) Steady state with uniform grid is considered.

(2) Buoyancy force acts downwards and the forced motion is in the upward direction, i.e. buoyancy induced motion opposes the forced motion.

(3) To induce the forced motion following equation used :

$(\Delta P)_{total} = (\Delta P)_{static} + \rho g \beta \Delta T H = (1/2).\rho v_{mean}^2$;

Where ΔP_{static} = the pressure difference between the inlet and exit of the channel consisting of two vertical walls,

H = Plate height.

V_{mean} = Mean flow velocity in the channel.

(4) (a) For constant wall temperature, boundary conditions are :

$T(0, y) = 100^0C$, $T(b, y) = 100^0C$, Enclosure temp. = 20^0C.

$(\Delta P)_{static}$ = 3.4 Pa & 7.8 Pa.

H = 50 cm.

(b) For constant wall heat flux boundary conditions are:

$\partial T / \partial X = - q_1 / K$, $\partial T / \partial X = -q_2 / K$;

Here value of heat flux varies between 0.1454 and 0.4432 W/cm^2.

Table 3.2 Values of heat flux for different plate spacings

Plate Spacing (mm)	Heat Flux (W/cm^2)	
	3.4 Pa	7.8 Pa
5.0	0.2204	0.2320
10.0	0.1454	0.2151
20.0	0.2418	0.3456
30.0	0.2282	0.4432
40.0	0.2920	0.3368
50.0	0.2870	0.3503
60.0	0.2626	0.3457
70.0	0.2737	0.2814
80.0	0.2600	0.2800

3.4 Theoretical Prediction and Results:

Results for Natural Convection and Mixed Convection are given in following subsections.

3.4.1 Natural Convection:

(a) Constant wall temperature condition:

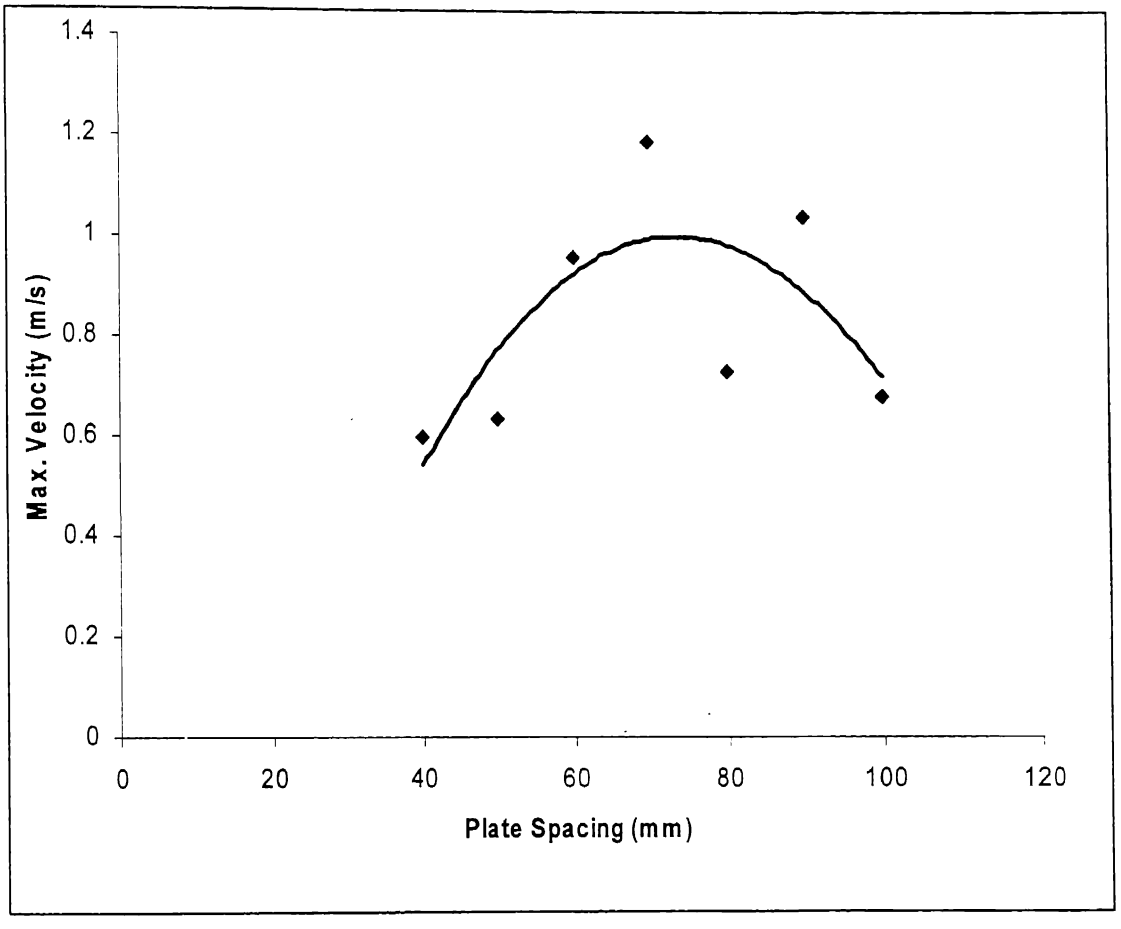

Figure 3.6: Variation of Max. velocity of fluid between the plates vs. plate spacing.

Figure 3.6 shows the variation of max. velocity of fluid passing through the spacing between the two plates. As plate spacing increases up to 70mm max. velocity of the fluid also increases, but after this spacing there is a decrease in the fluid velocity. The max. velocity corresponding to the plate spacing of 70mm is 1m/s.

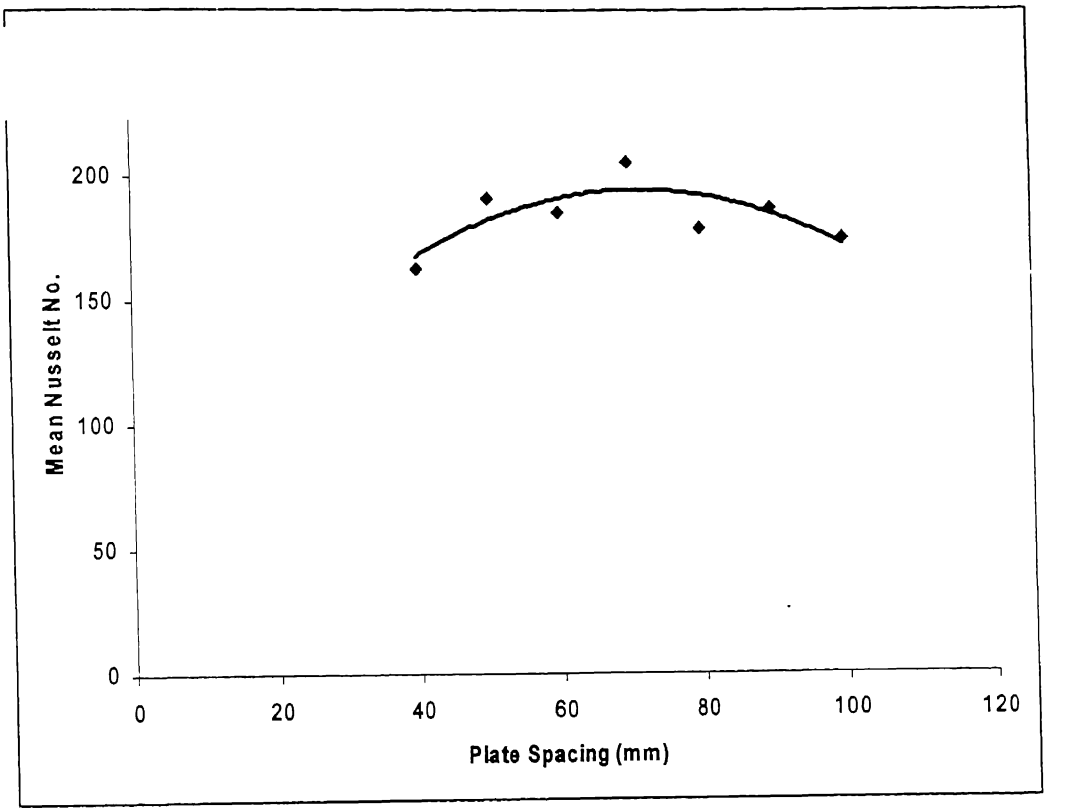

Figure 3.7: Variation of Mean Nusselt no. over the vertical plate surface vs. plate spacing.

Figure 3.7 shows the variation of mean the Mean Nusselt no. on one of the vertical plates with different plate spacings. As plate spacing increases up to 70mm, mean Nusselt no. also increases, but beyond this value it decreases. The maximum value corresponding to the plate spacing of 70mm is 200.

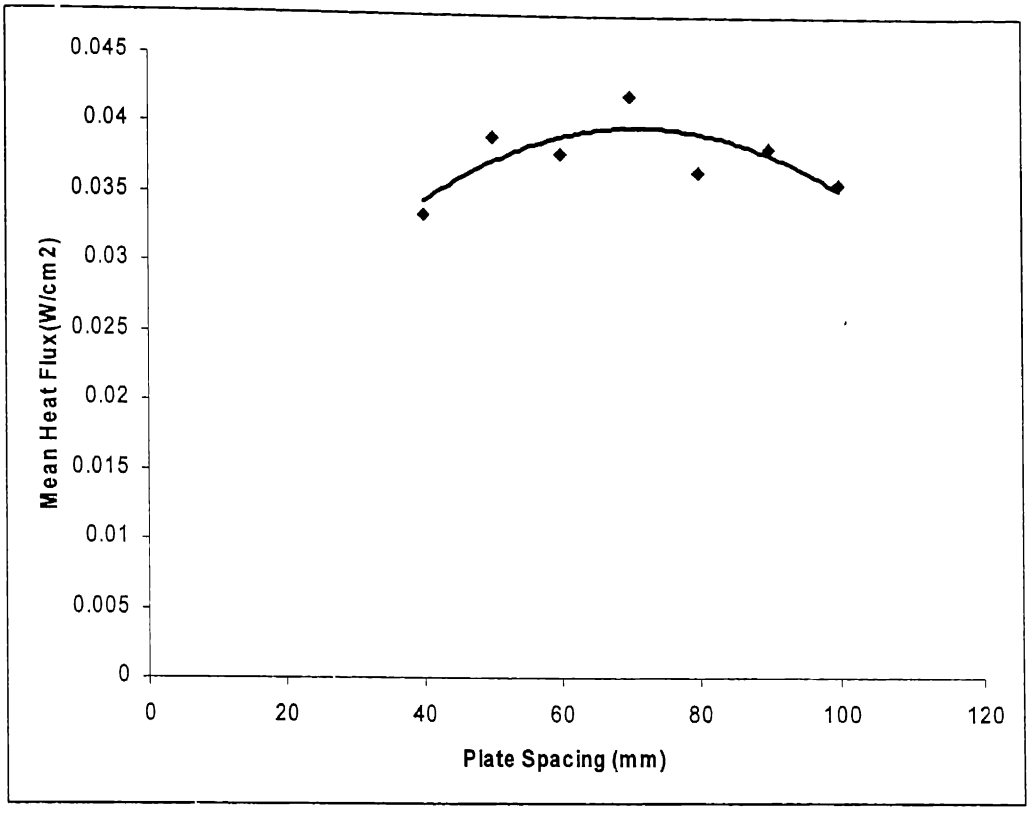

Figure 3.8: Variation of Mean Heat Flux over the vertical plate surface vs. plate spacing.

Figure 3.8 shows the variation of mean Heat Flux on one the vertical plates for various plate spacings. This mean Heat Flux increases up to the plate spacing of 70mm, beyond which it decreases. The max. value corresponding to this plate spacing of 70mm is 0.04 W/cm^2.

Here in all cases Gr_L / Re_L^2 >> 1, this indicates that buoyancy effect dominates the inertia effect, i.e. natural convection is the dominating heat transfer mode. Here also as fluid velocity increases, rate of heat transfer also increases and so does the heat flux. The case is reverse if the fluid velocity decreases.

(b) Constant Heat Flux condition:

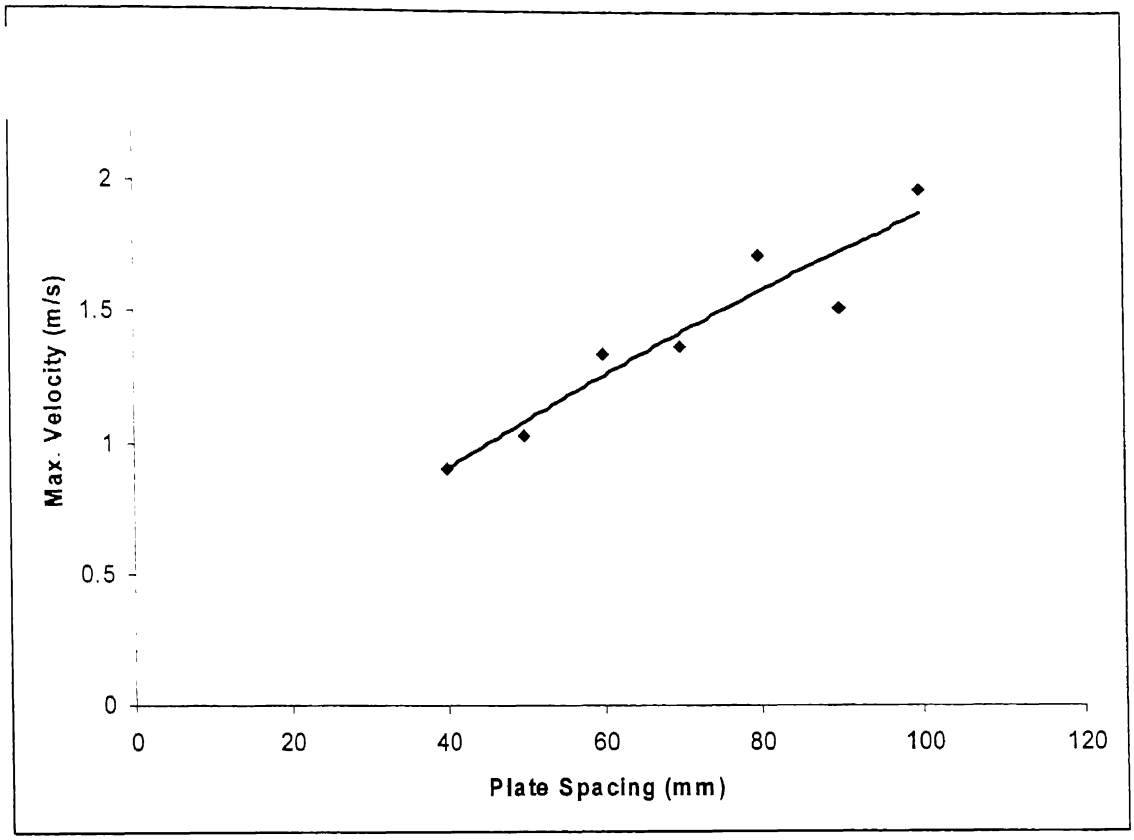

Figure 3.9: Variation of Max. velocity of fluid between the plates vs. plate spacing.

Figure 3.9 shows the variation of max. fluid velocity for different plate spacings considering the walls subjected to different values of constant heat flux. The trend line indicates max. velocity increases almost linearly to 1.8m/s at plate spacing of 100mm.

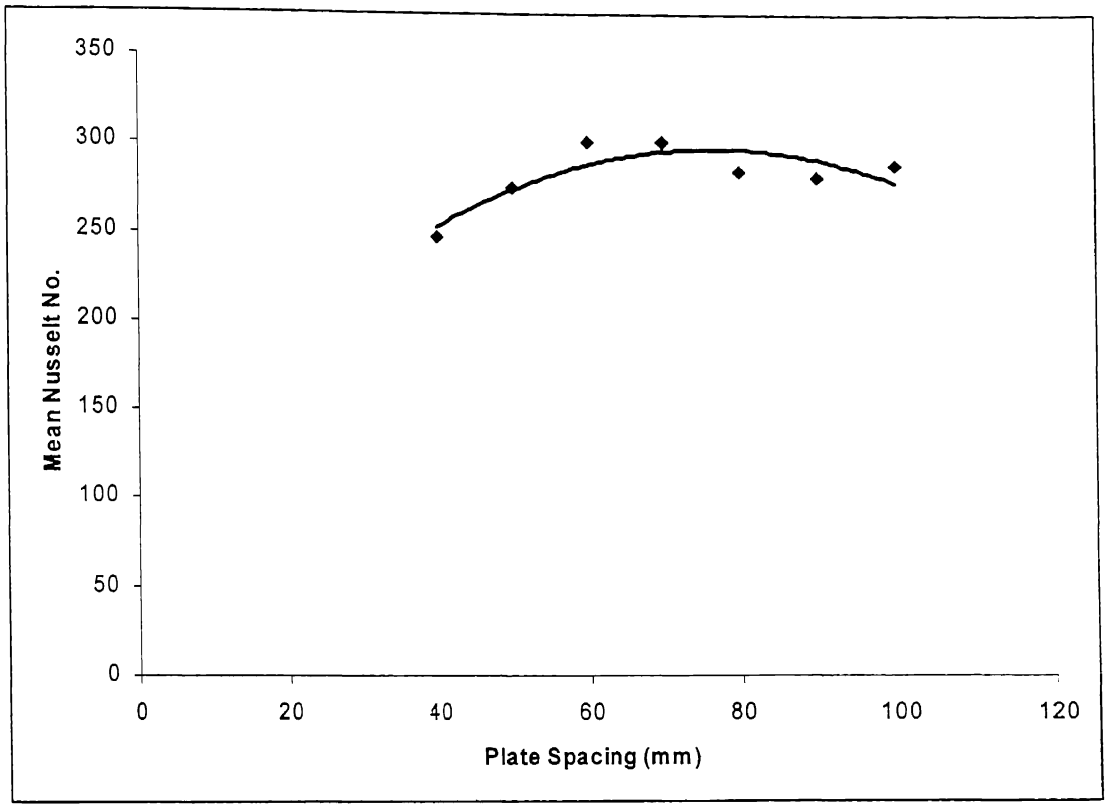

Figure 3.10: Variation of Mean Nusselt No. over the vertical plate surface vs. plate spacing.

Figure 3.10 shows the variation of mean Nusselt no. with different plate spacings. Mean Nusselt no. increases with the plate spacings upto the 60mm, then it decreases for rest of the spacings upto 100mm.

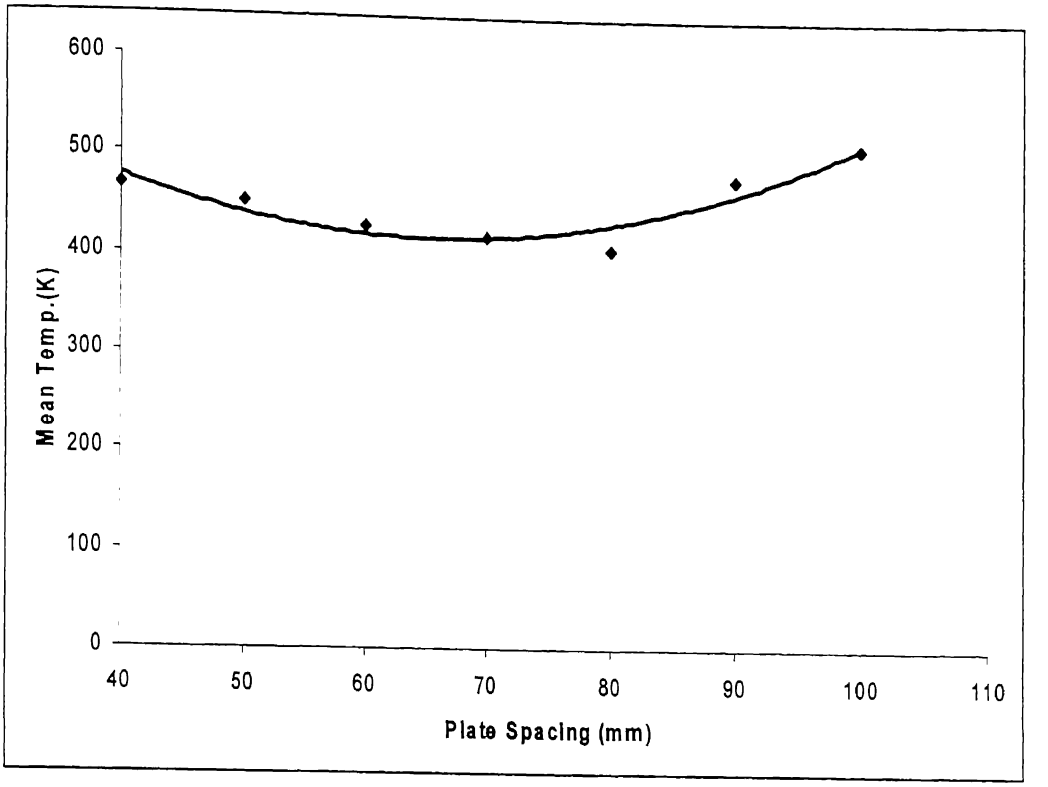

Figure 3.11: Variation of Mean Temp. over the vertical plate surface vs. plate spacing.

Figure 3.11 shows the variation of mean Temp. along the vertical wall against different plate spacings. Mean Temp. decreases as the plate spacing increases upto 60mm, then it is constant for the plate spacing between 60 & 70mm and finally for additional increase in the plate spacing it increases.

3.4.2 Mixed Convection:

The variation of temperature, heat flux and Nusselt number along the height of vertical wall is shown below:

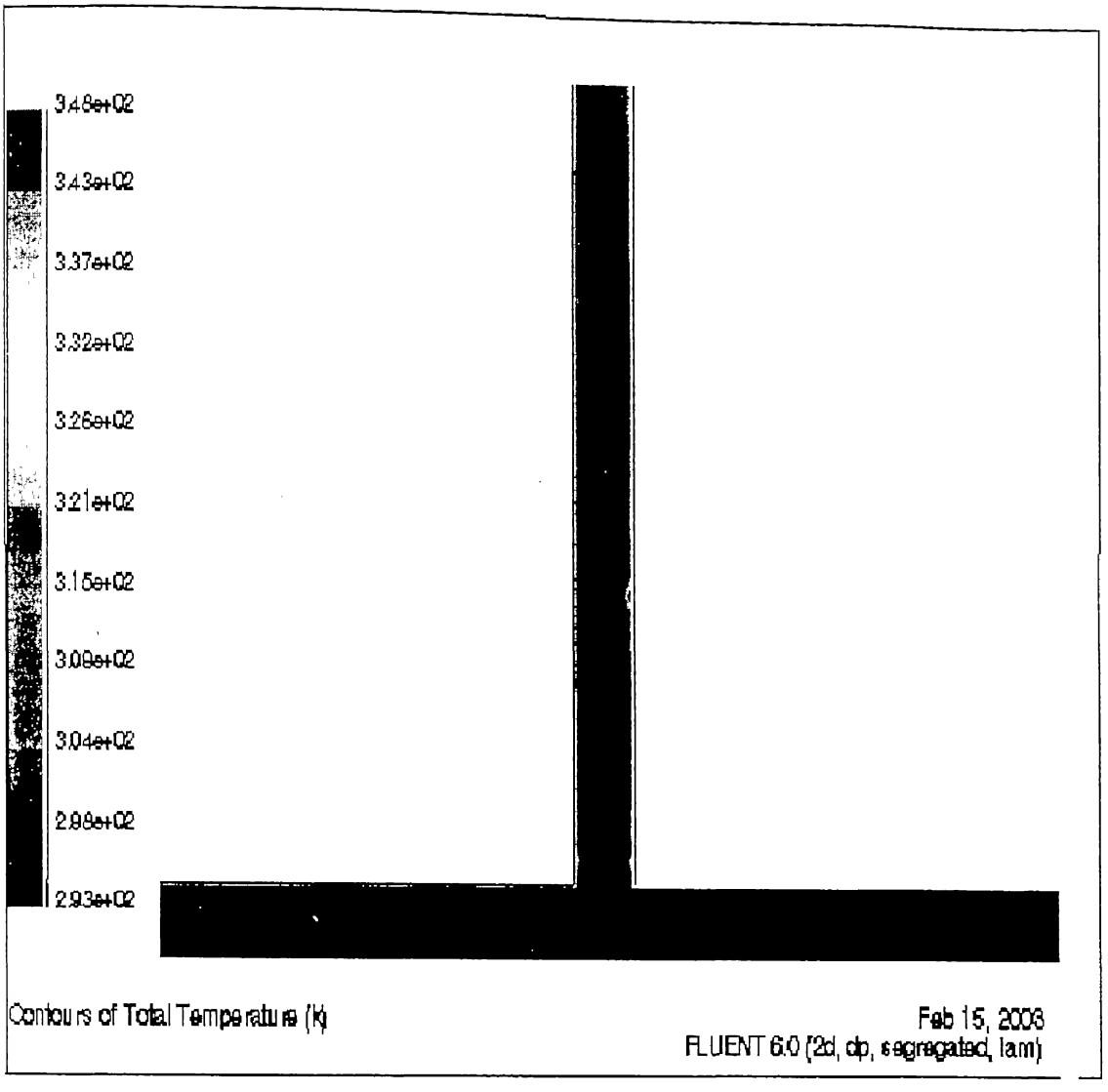

Figure 3.12: Contour of Total Temperature.

Figure 3.12 shows the contour of Temperature along the vertical wall when the wall is maintained at constant temperature of 100^0C and the wall separation is 6 cm. For this contour, variation of temperature, Nusselt no. and Heat Flux are shown in figures 3.13, 3.14 and 3.15.

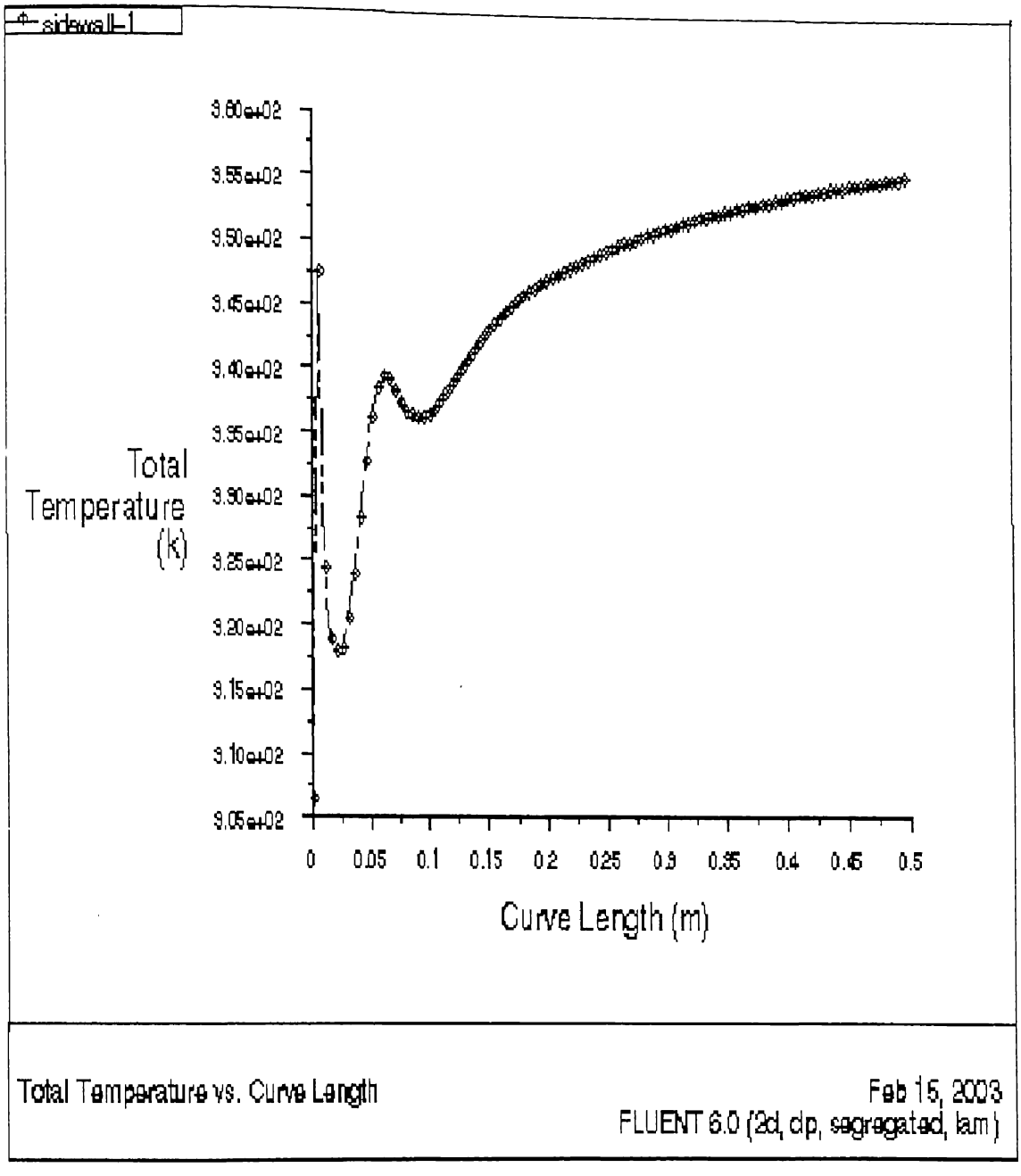

Figure 3.13: Variation of Total temperature over the vertical plate vs. plate height.

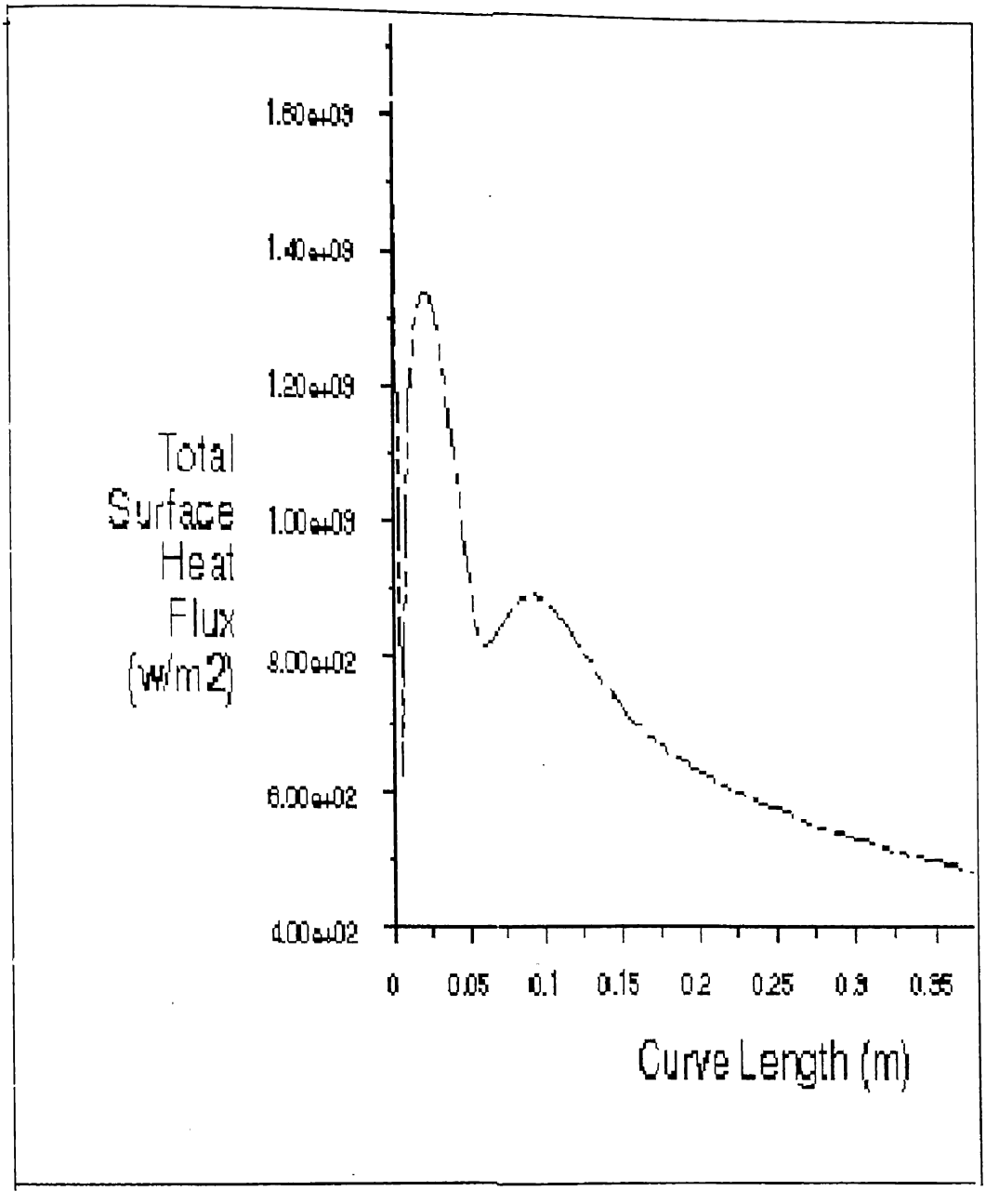

Figure 3.14: Variation of Total surface heat flux over the vertical plate vs. plate height.

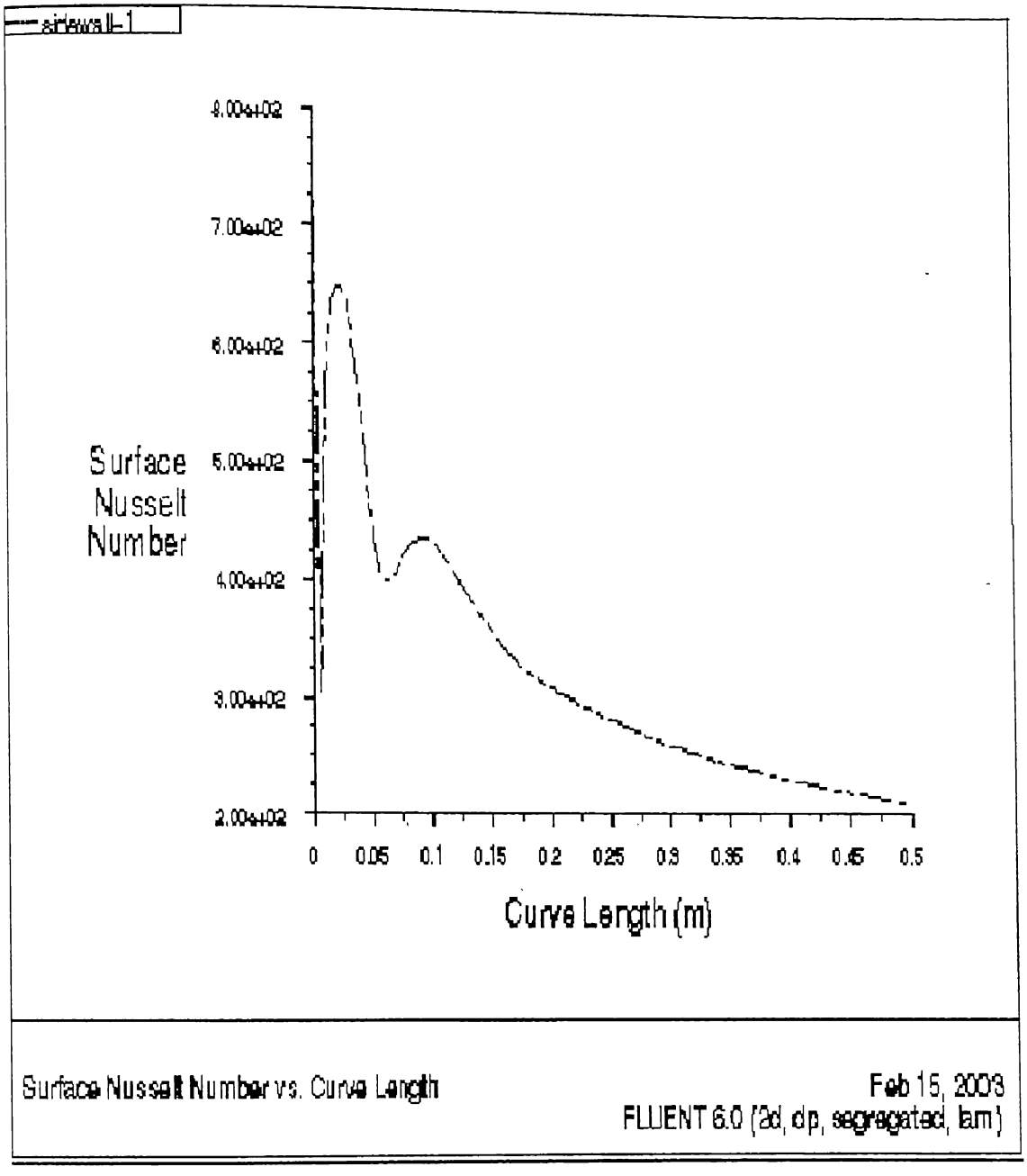

Figure 3.15: Variation of Surface Nusselt No. over the vertical plate vs. plate height.

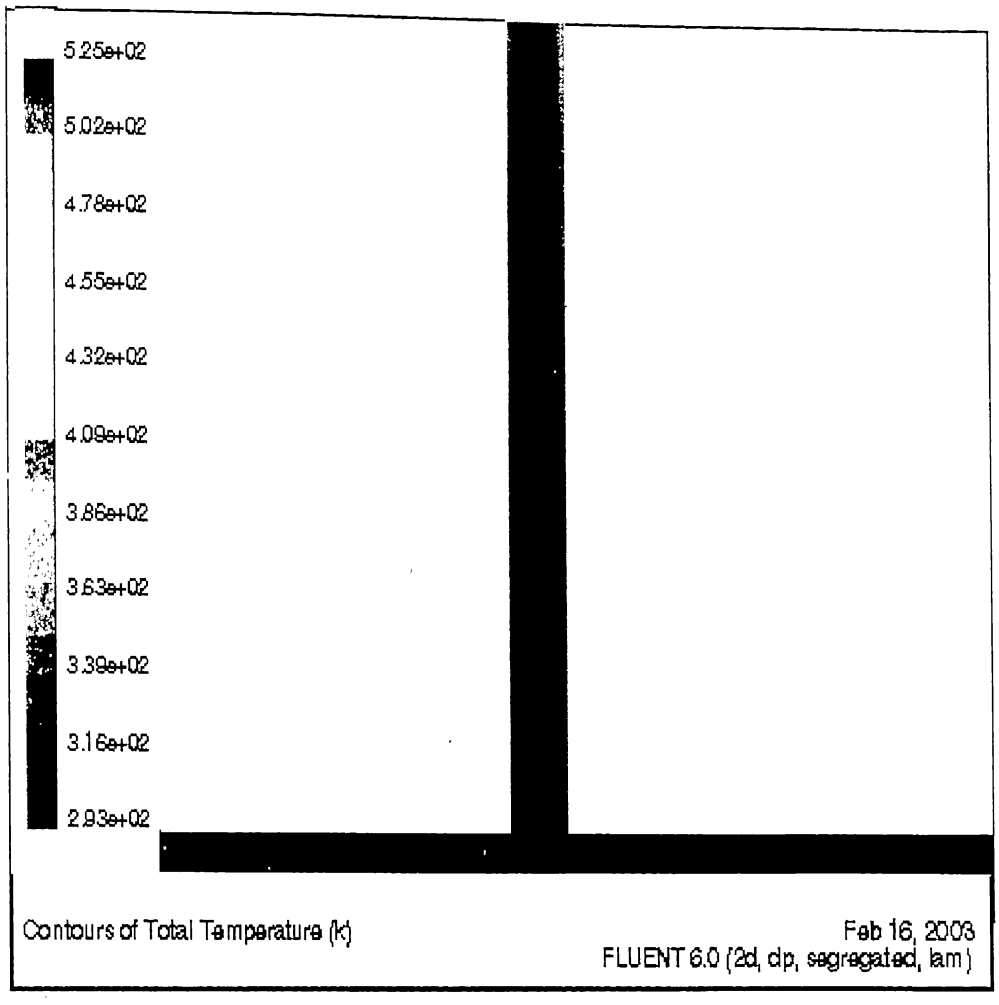

Figure 3.16: Contour of Total Temperature.

Figure 3.16 shows the Temperature contour along the vertical wall when the wall is maintained at constant temperature of 100^0 C and the wall separation is 0.5 cm. For this contour, variation of temperature, Nusselt no., Heat Flux has been shown in figures 3.17, 3.18 and 3.19.

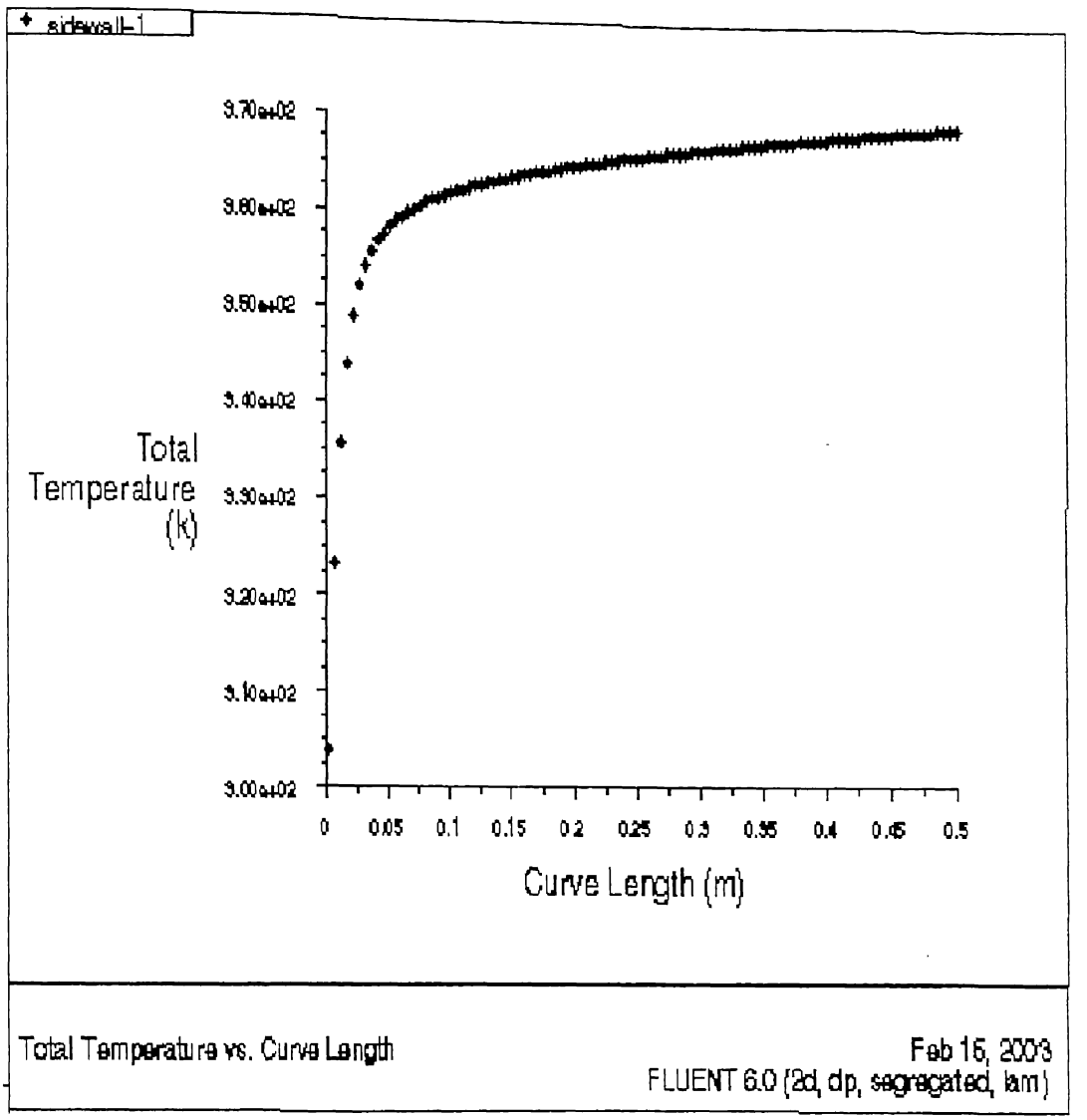

Figure 3.17: Variation of Total temperature over the vertical plate vs. plate height.

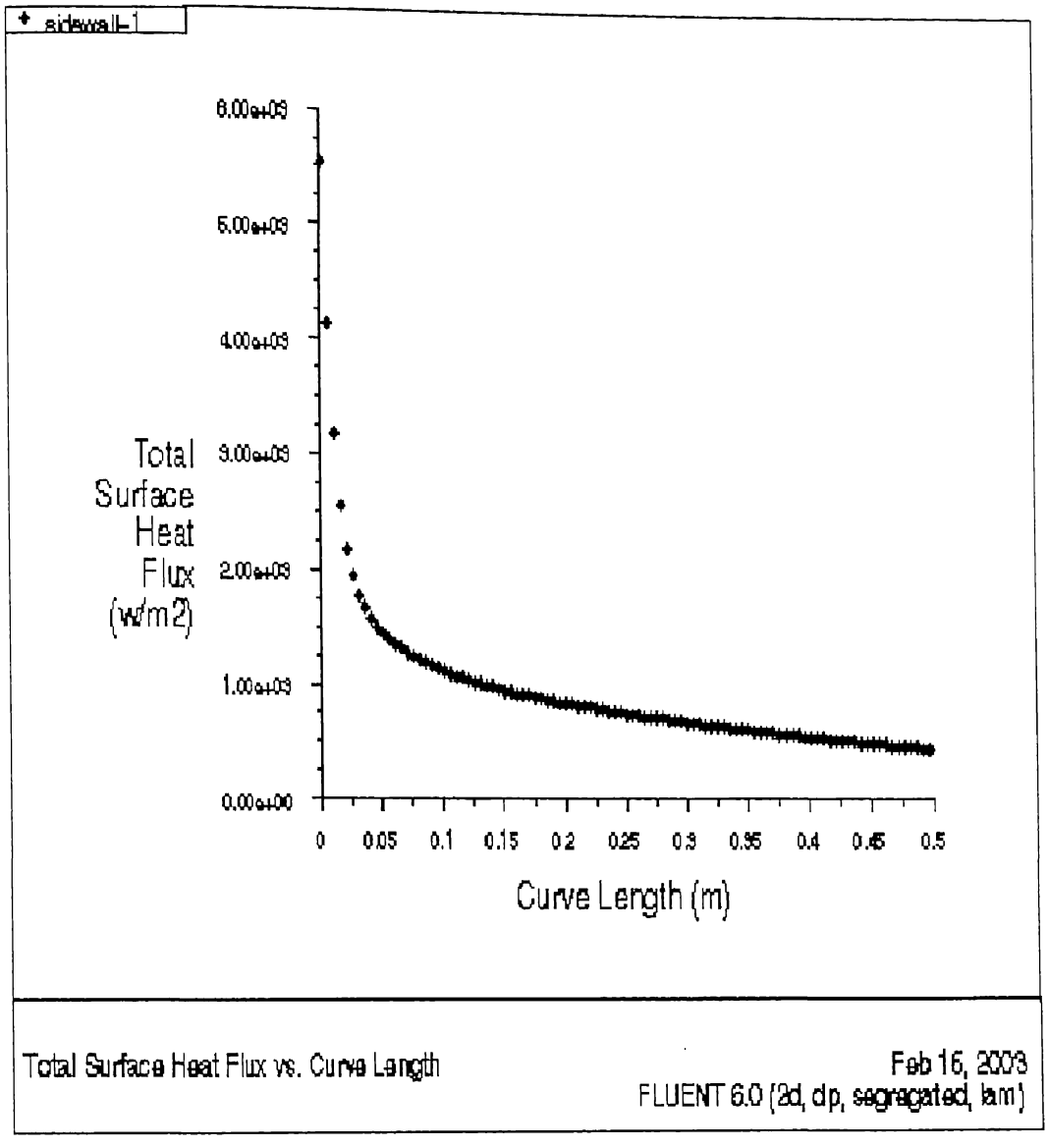

Figure 3.18: Variation of Total temperature over the vertical plate vs. plate height.

increases beyond 50 mm, whirling motion of fluid occurs in the channel due to high inlet velocity of fluid.

(a) Constant wall temperature condition:

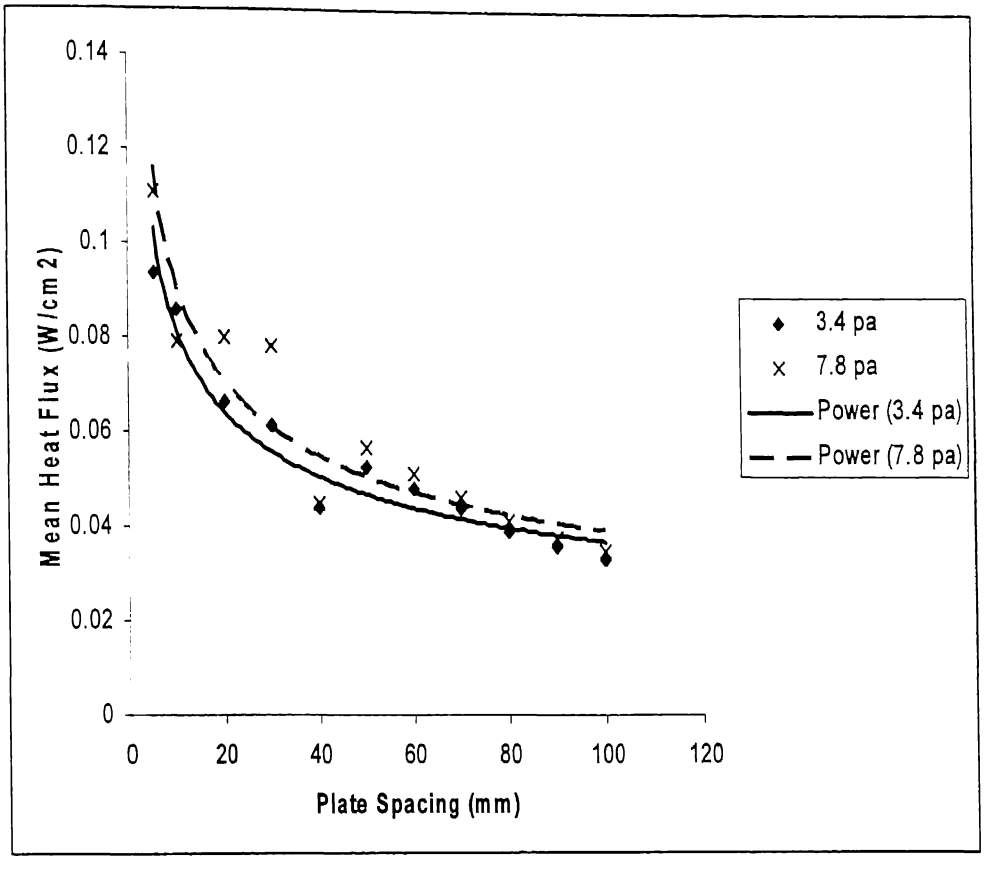

Figure 3.20: Variation of Mean Heat Flux over the vertical plate for different static pressures vs. plate spacing.

Figure 3.20 shows the variation of Mean Heat Flux on the vertical wall against different plate spacings when the pressure differences between inlet and outlet have been maintained at 3.4 Pa and 7.8 Pa. From this figure, one can observe that values of mean Heat Flux are higher at 7.8 Pa than those at 3.4 Pa for the plate spacings between 5 to 100 mm. With 3.4 pa initial value of heat flux is 0.0890

W/cm^2 at plate spacing of 5mm, which then slowly dropped to 0.0350 W/cm^2 at 100mm spacing.

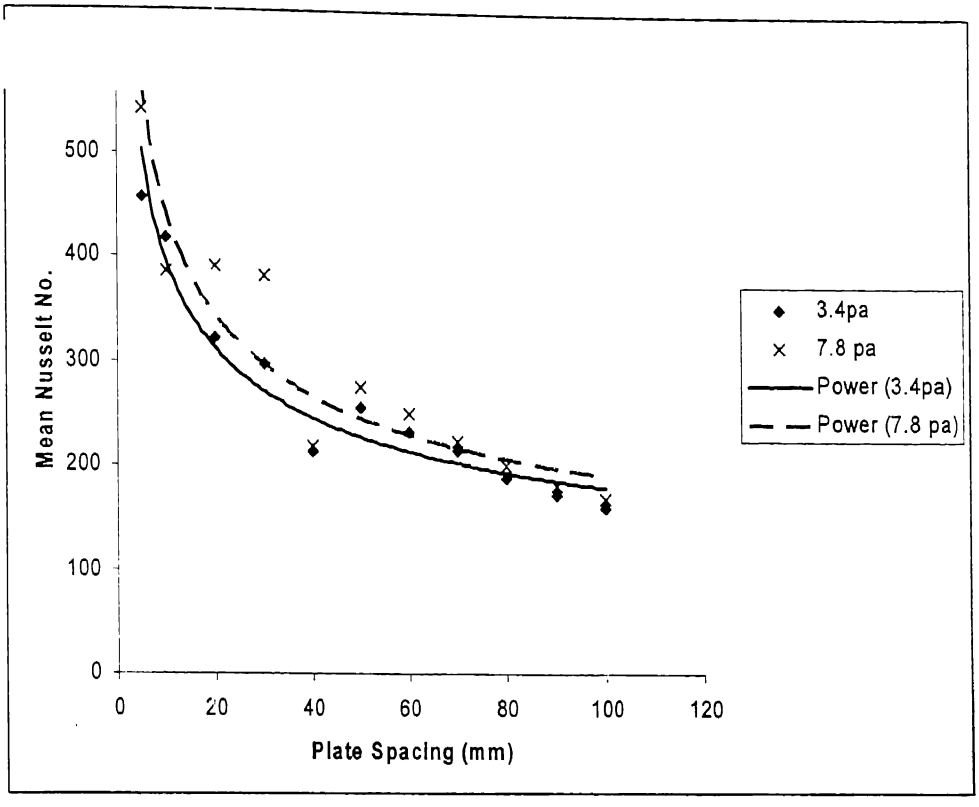

Figure 3.21: Variation of Mean Nusselt No. over the vertical plate for different static pressures vs. plate spacing.

Figure 3.21 shows the variation of Mean Nusselt No. on the vertical wall against the different plate spacings when the pressure differences between inlet and outlet have been maintained at 3.4 Pa and 7.8 Pa. From this figure one can observe that values of mean Nusselt are higher at 7.8 Pa than those 3.4 Pa for the plate spacings between 5mm to100 mm. With 3.4 pa initial value of Mean Nusselt No. is close to 500 at plate spacing of 5 mm, which then slowly dropped to 200 at 100mm spacing. But with 7.8pa the initial value of Nusselt No. is higher and close to 550 at plate spacing of 5 mm, which then gradually dropped to 225 at 100mm plate spacing.

(b) Constant Heat Flux Condition:

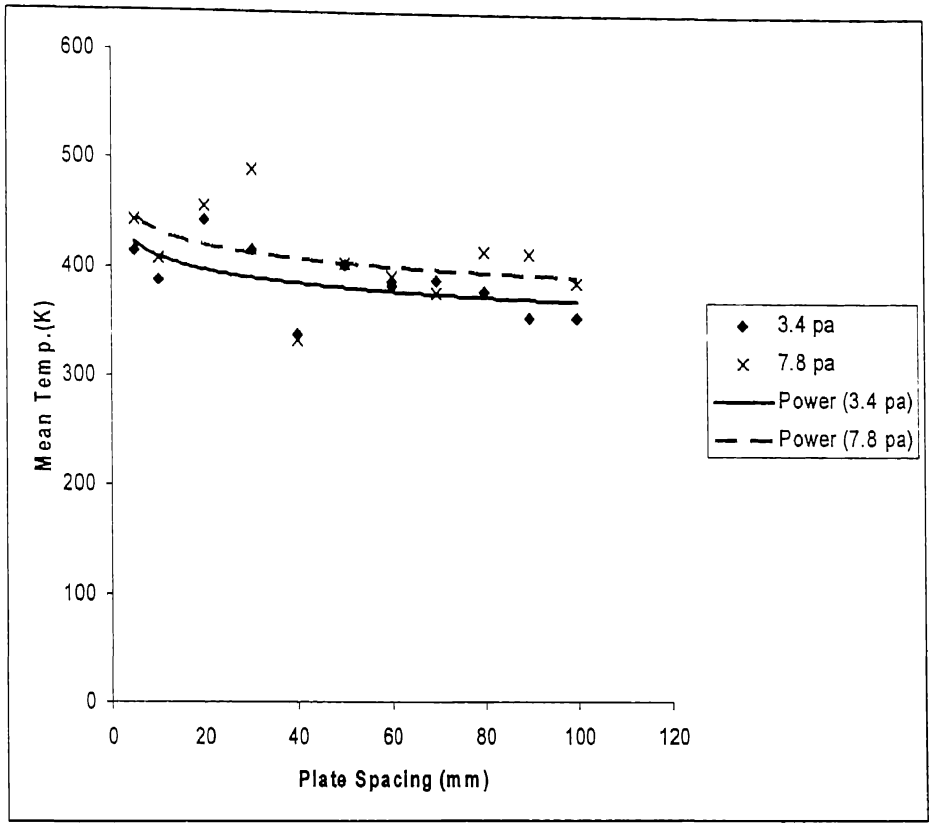

Figure 3.22: Variation of Mean Temp. over the vertical plate for different static pressures vs. plate spacing.

Figure 3.22 shows the variation of Mean Temperature on the vertical wall against the different plate spacings when the pressure differences between inlet and outlet have been maintained at 3.4 Pa and 7.8 Pa. From this figure one can observe that values of mean Temperature are higher at 7.8 Pa than those at 3.4 Pa for the plate spacings between 5mm to 10mm. With 3.4 pa initial value of Mean surface temp. is 410 K at plate spacing of 5mm, then it decreased slowly. Similar

is the trend of variation with 7.8 pa, here initial value of Mean surface temp. is 450 K at 5mm of plate spacing.

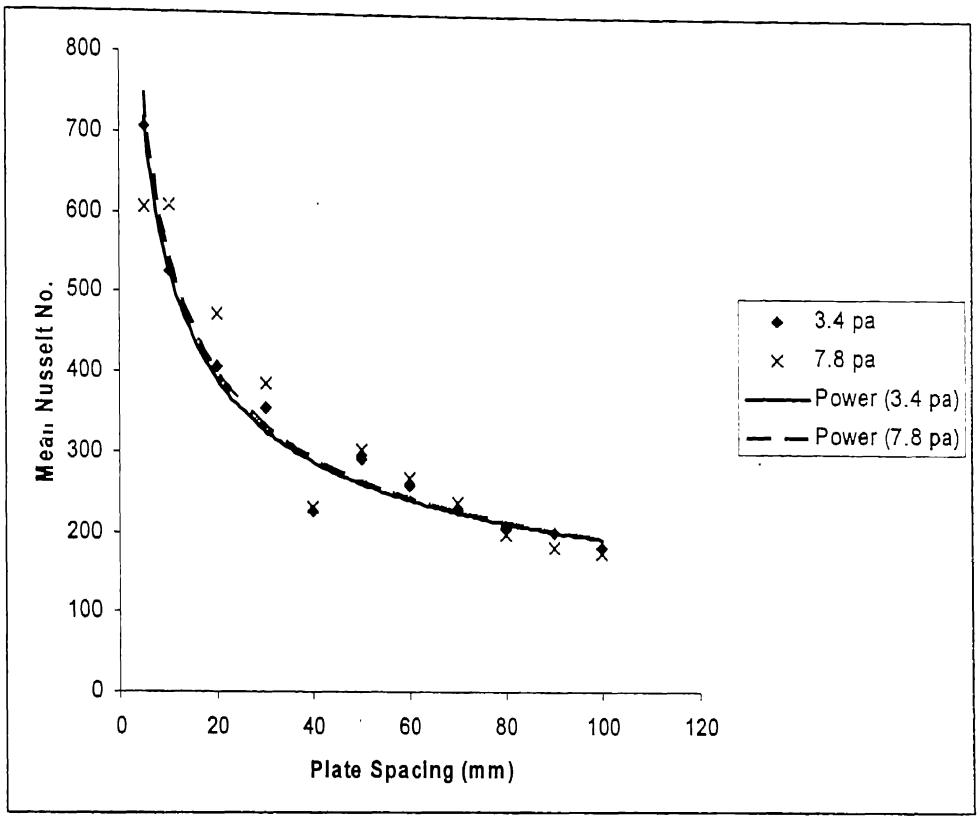

Figure 3.23: Variation of Mean Nusselt No. over the vertical plate for different static pressures vs. plate spacing.

Figure 3.23 shows the variation of Mean Nusselt on the vertical wall against the different plate spacings when the pressure differences between inlet and outlet have been maintained at 3.4 Pa and 7.8 Pa. From this figure one can observe that values of mean Nusselt No. are slightly higher at 7.8 Pa than those at 3.4 Pa for the plate spacings between 5mm and 60mm, beyond this range values of Mean Nusselt

No. are same for both pressure differences up to 100mm. With 3.4 pa initial value of Mean Nusselt No. is close to 750 at plate spacing of 5mm, which then sharply dropped to 380 at 20 mm spacing, then it decreases gradually and linearly respectively. Similar is the trend of variation with 7.8 Pa.

3.5 Closure

A ready to use software namely Fluent Version 6.0 was used to model the Natural and Mixed Convection problems. The results obtained for the heat transfer coefficient and heat flux for various spacings between the consecutive PCB type configuration and static pressures are presented. The criterion for Natural Convection & Mixed Convection in terms of Gr/Re^2 is computed and compared witn the literature values.

Chapter -4

EXPERIMENTAL WORK

4.1 Description of the Test Rig:

In the present study mixed convection cooling was simulated experimentally for PCB (Printed Circuit Board) type configurations. In this experiment one vertical channel formed by two simulated PCBs (Plates) was placed in the test section where a lead screw mechanism was used for varying the spacing between the plates. A suitable static pressure creating device (a fan unit) was provided to suck the air passing through the vertical channel. One of the plates was acting as an insulating wall while the other consisted of heating elements. Four heating elements were placed on the PCB.Vertical orientation of the channel helped in achieving the mixed convection. Since the suction device was placed at the top of the test section, the buoyancy assisted mixed convection flow was achieved. Complete assembly of the experimental setup is shown in figure 4.1. The test rig was configured to fulfil the experimental objectives. It was essential to take into account the accessibility and the flexibility of components so that there was not much difficulty in taking care of maintenance and repair problems. Provisions for rapid configurational changes were very important and these were incorporated in the design. Figure 4.3 shows the schematic diagram of the test rig designed for the purpose.

Test rig consisted of the following major parts:

(a) Air intake unit,

(b)Test Section,

(c) Diffuser unit, and

(d) Suction chamber (fan unit)

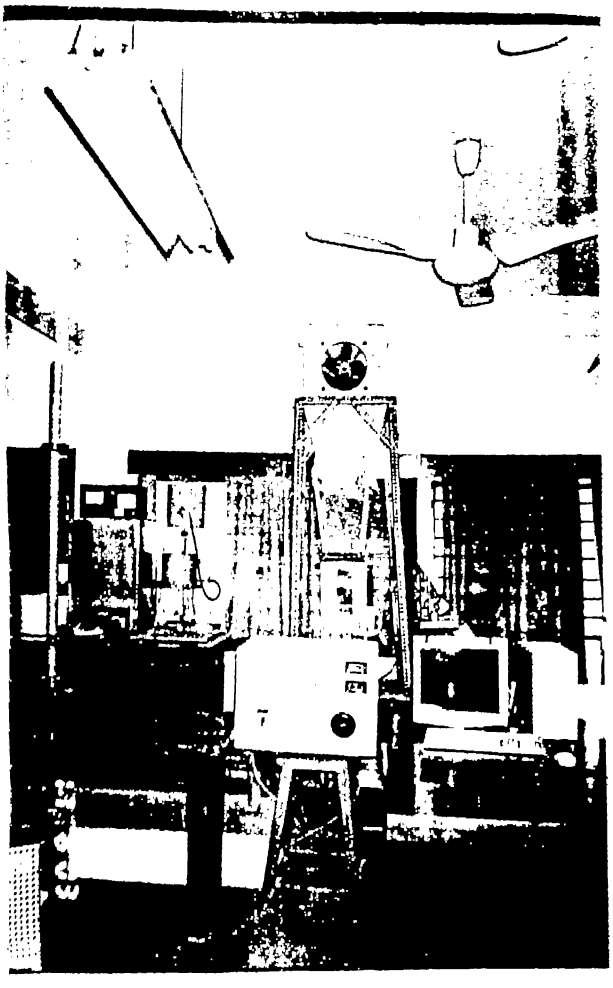

Figure 4.1: Experimental Setup

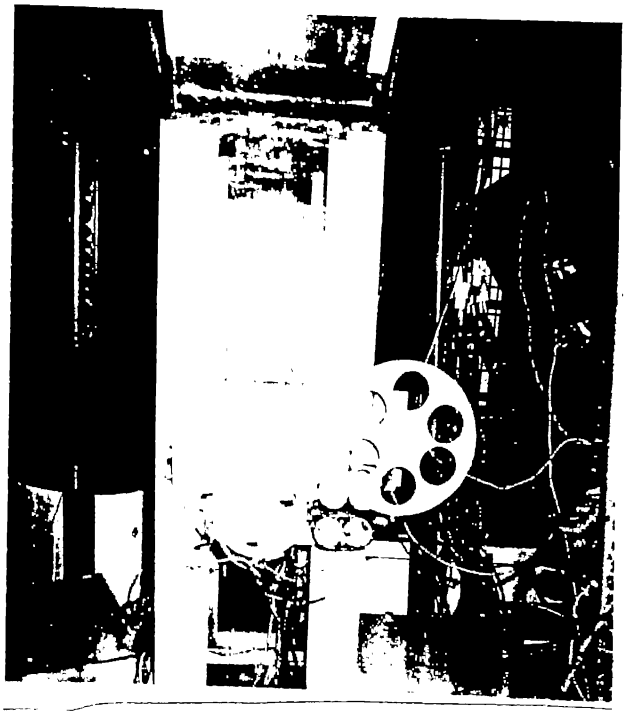

Figure 4.2: Test Section

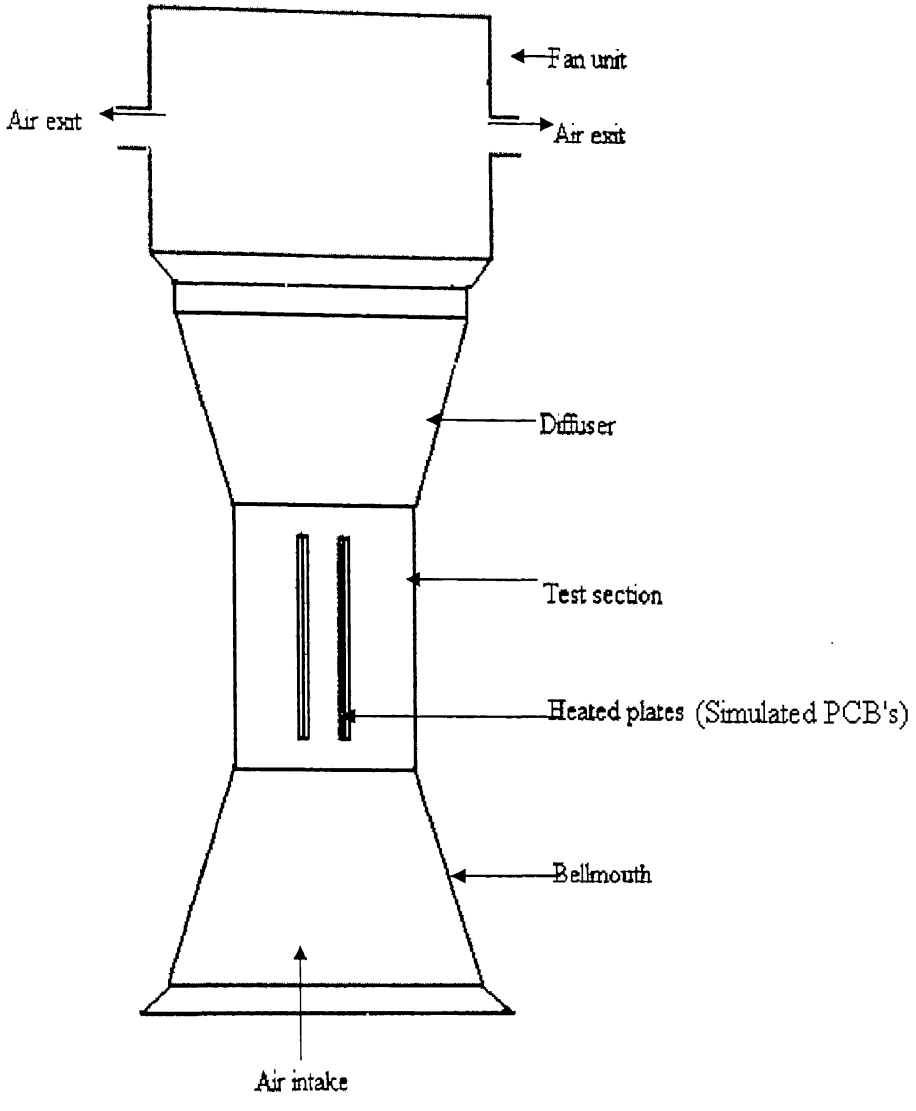

Figure 4.3: Experimental test-rig (Schematic diagram)

(a) Air Intake unit

This unit helped in achieving smooth entry of air at the test rig inlet. This unit was designed such that the flow at the inlet of test section was fully developed as far as possible. It was basically a converging duct with rectangular cross-section. The material used for intake unit was galvanized iron sheet.

(b) Test Section

The cross-sectional area of test section primarily determines overall size of the test section .Test section being the most important part was designed taking into account structural cost, power cost etc. Many shapes for the cross section of the test section are used e.g. round, elliptical, square, hexagonal and octagonal with minimal difference in losses due to its shape. But the current study used a square cross section. Length of the test section should be optimized as it affected the power consumption. It should not exceed the required length. Fifteen millimeter thick glass plate was used for making the test section. Glass being a good insulator was a right choice for this purpose; it also provided a window for viewing the whole plate assembly.

(c) Diffuser

Material chosen for the diffuser was perspex. Diffuser was designed to avoid separation of flow, which otherwise it would led to vibrations, oscillating fan-loading variation in tests section velocities. Diffuser with vane anemometer has been shown in Figure

(d) Suction Chamber

In order to create a pressure differential across the channel, suction chamber was provided with four small fans with the following rating:

Discharge Rate: 0.2 m^3/s

Rated Speed: 1440 r.p.m.

The idea behind providing four small fans was to avoid inherent vibration problems from a single fan of large discharge.

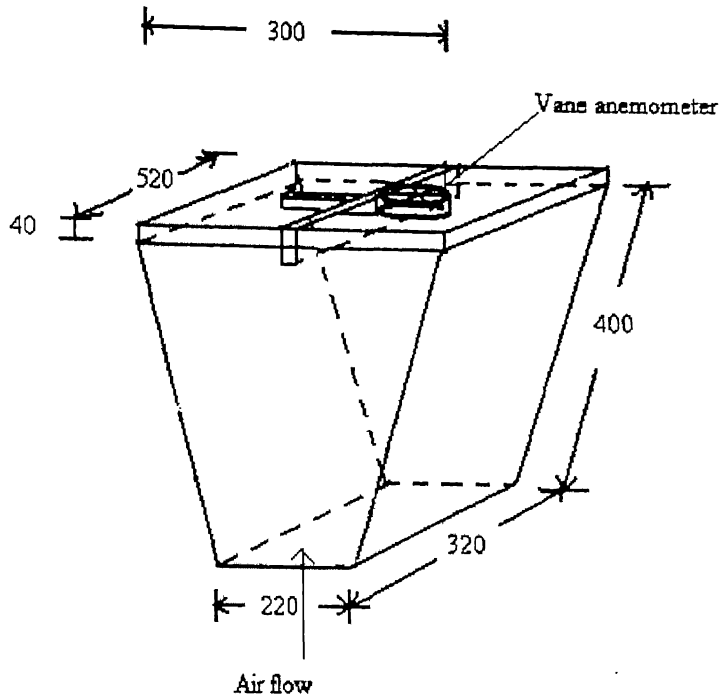

All dimensions in mm.

Figure 4.4: Diffuser

4.2 PCB Design

4.2.1 Selection of Material:

* Type of Material: Copper coated Glass Epoxy

This printed circuit Board is copper coated on one side. Here Glass Epoxy was made of glass wool and epoxy resin and annealed type copper was used as a conductor of charge.

* Material Thickness:

  Total thickness = 1.67 mm.

  Thickness of copper = 35 μm.

  Thickness of Glass Epoxy = 1.635 mm.

* Material heat resistance limit:

  Melting temperature = 250^0C.

* Thermal conductivity of Glass Wool at 23^0c = 0.038 (W/m.K)
* Thermal conductivity of epoxy resin at 27^0c = 1.6 (W/m.K)
* Limit of Electrical signal frequency passing through different electronic components mounted on the Board = 1 M Hz.
* Dimension:

  With four heaters = 295mm × 200mm

4.2.2 Selection of Heat Generating Sources:

All the commercial I.Cs are manufactured with constant parameters, so amount of heat generated by these is constant. On the other hand, the control of an I.C is also somehow a typical job. So to get rid of these limitations, commercial ICs have been simulated by artificial heat generating sources. The schematic arrangement of this artificial heat generating source is shown in Figure 4.7.

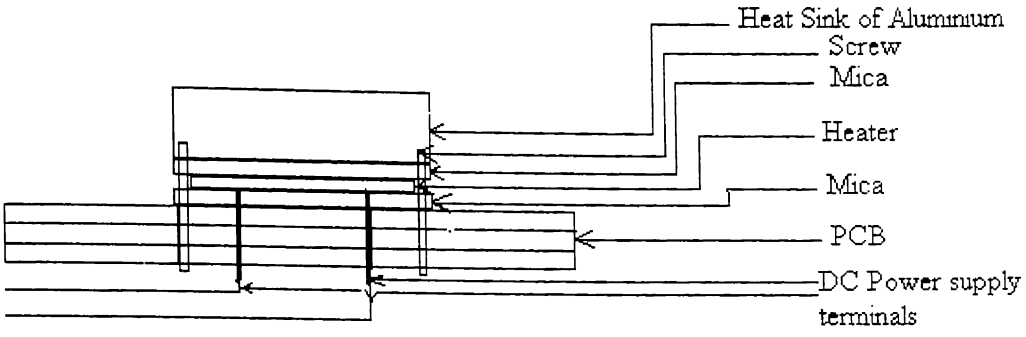

Figure 4.5: Simulation of I.C.

- Specification of Aluminium strip

  Dimension = 20mm × 20mm × 5mm

  Thermal conductivity of aluminium at 20^0C = 204 (W/m.K)

- Specification of mica

  Dimension = 20mm × 20mm × 0.15mm

  Thermal conductivity of Mica = 0.7 (W/m.K)

- Specification of oxide layer

  Overall thickness on the top and bottom of the heat sink = 200 × 2 μm

  Thermal conductivity = 8 (W/m.K)

- Specification of Teflon

  Dimension = 20mm × 5mm

  Melting point = 267^0C

  Upper service temp = 150^0C

  Thermal conductivity = 0.2 (W/m.K)

- Specification of Heater

  Material = Stainless Steel

  Dimension = 1mm × 10mm × 0.13mm

  Thermal Conductivity of Stainless Steel = 67 (W/m.K)

Resistance = 0.6 Ω

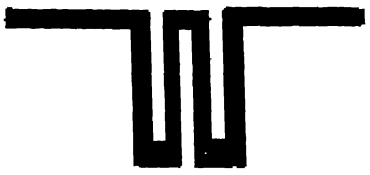

Figure 4.6: Schematic diagram of Heater.

4.2.3 Layout of Heat Generating Sources and Thermocouples placed on PCB:

For four heaters:

All the heaters were made in a identical way and placed symmetrically on the PCB. In each heater all the four side surfaces were insulated by Teflon

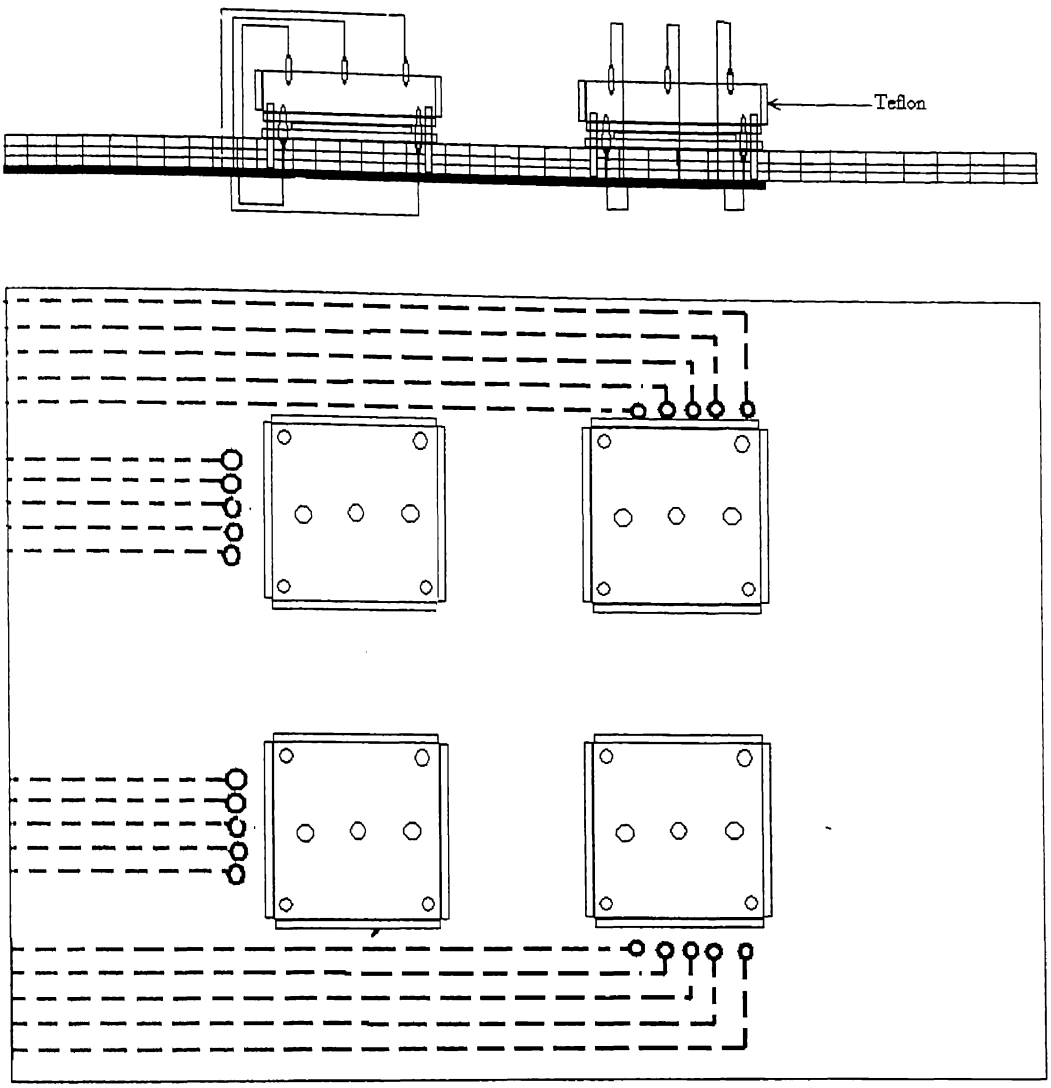

Figure 4.7: Arrangement of Heat generating sources with thermocouples on a PCB.

4.3 Selection of Thermocouple and its Mounting on Heat sink

Specification:

Type = Chromel-Alumel (K-type)

Diameter = 36 gauge

Deviation = -18.778^{0}C at 204.278^{0}C.

Calibration Chart:

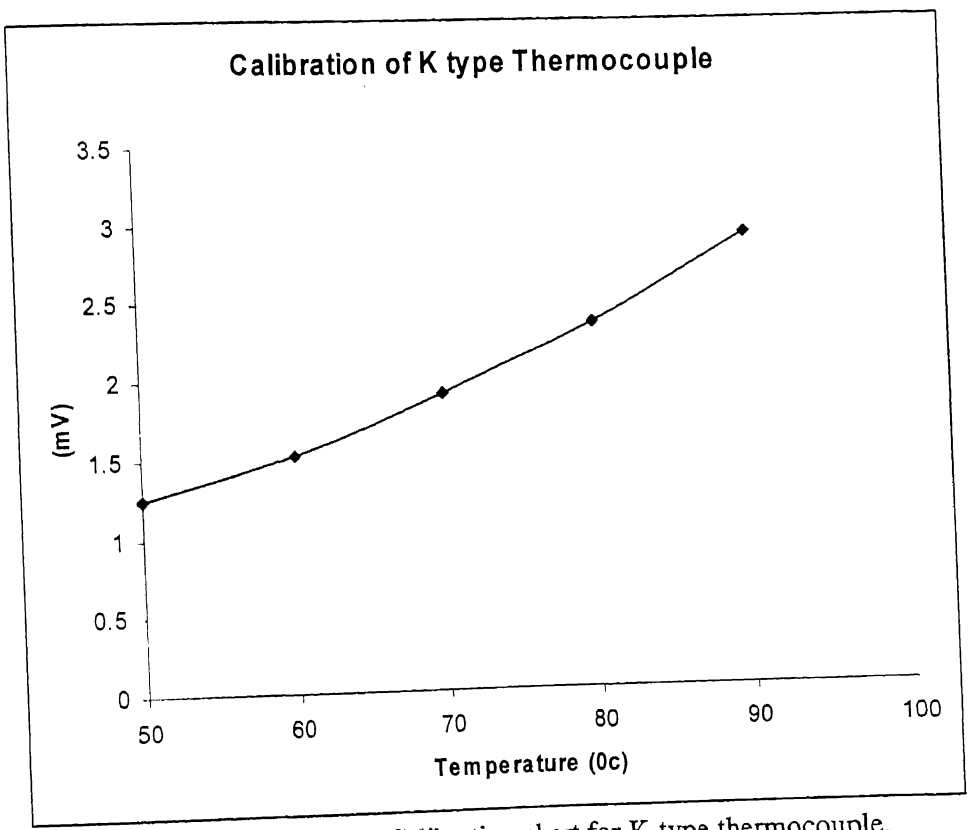

Figure -4.8: Calibration chart for K-type thermocouple.

sink were drilled. A mixture of resin, hardener and aluminium powder was prepared and applied in these holes. Thermocouples junctions were then placed in these holes and left for 24 hrs. In this way thermocouple were fixed on the heat sink. Some typical Electrical and Physical properties at room temperature with RT-7 hardeners are given below:

Characteristics	Typical Values
Specific gravity	2.35
Thermal conductivity	1.34$Wm^{-1}°C^{-1}$ (.77 Btu/hr •ft• &3176:F)
Thermal resistivity	29.4°C in/watt
Tensile strength	6.34 x 10^{7}Pa(9,2000 psi)
Compressive strength	1.44 x 10^{8}Pa(20,9000 psi)
Bond shear strength	3.17 x 10^{7}Pa(4,6000 psi)

4.4 Data-Acquisition

All the thermocouples with the help of extension wires were connected in a differential mode to the AMUX 64-T DAQ card from National Instruments. Measurements of temperatures have been done by data acquisition through DAQ card number PCI-6024E. For acquiring, storing and analysis of the data LabVIEW software was used.

A brief description of Lab VIEW is as follows:

Lab VIEW is a program development application, which uses a graphical programming language in terms of terminology, icons, and ideas familiar to scientists and engineers. Lab VIEW programs are called *virtual instruments (VIs)* because their appearance and operation imitate actual instruments. VIs contain an interactive user interface, called the *front panel* which simulates the panel of a physical instrument. VIs receive instructions from a *block diagram*. The block diagram contains the source code for the VI and supplies a pictorial solution to a programming problem.

For four heaters front panel and diagram of the Lab VIEW program is shown in Figure 4.9.

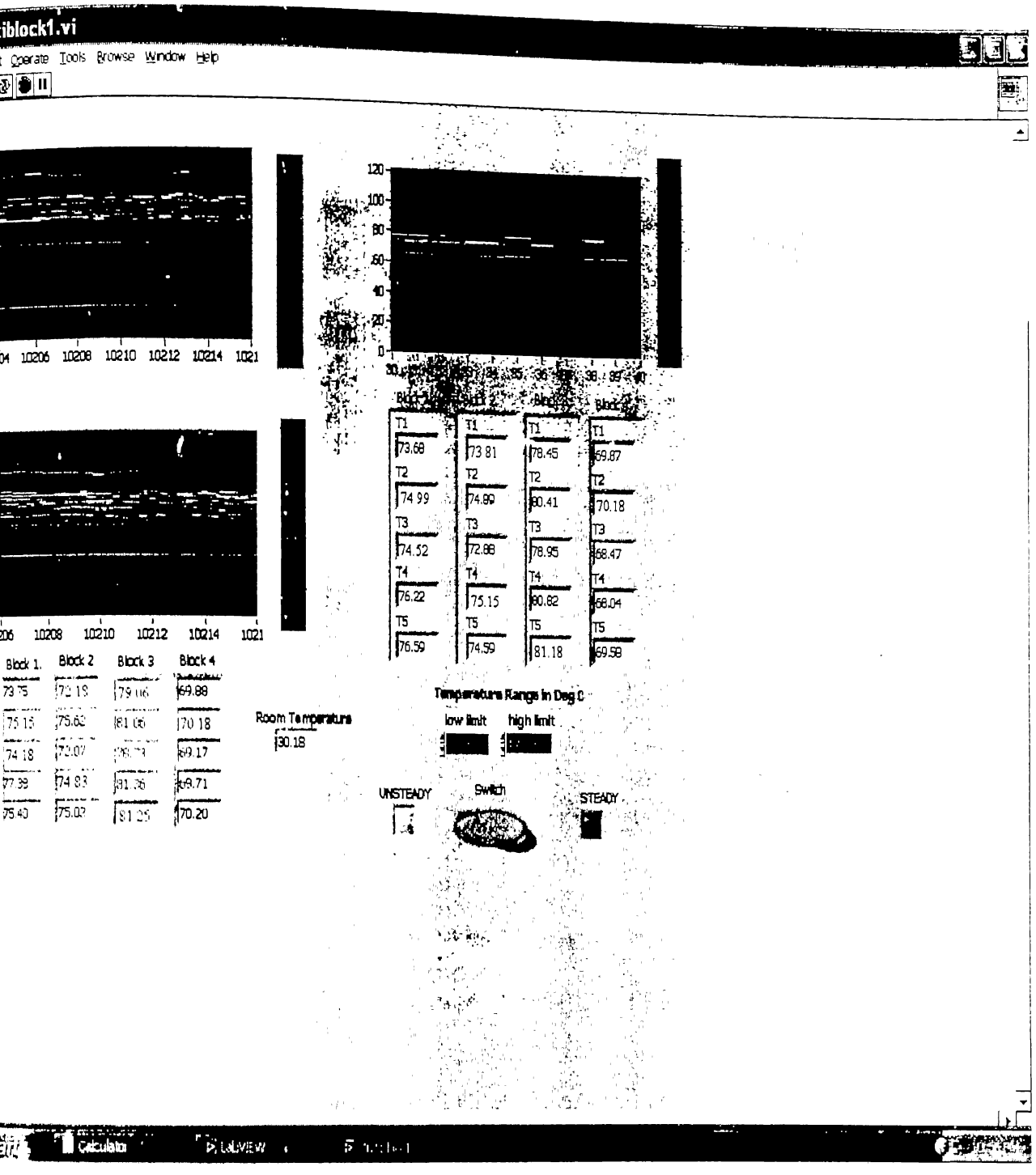

Figure 4.9: Front Panel in Lab VIEW showing variations as well as values of Standard, Calibrated and Mean temperatures on different screens.

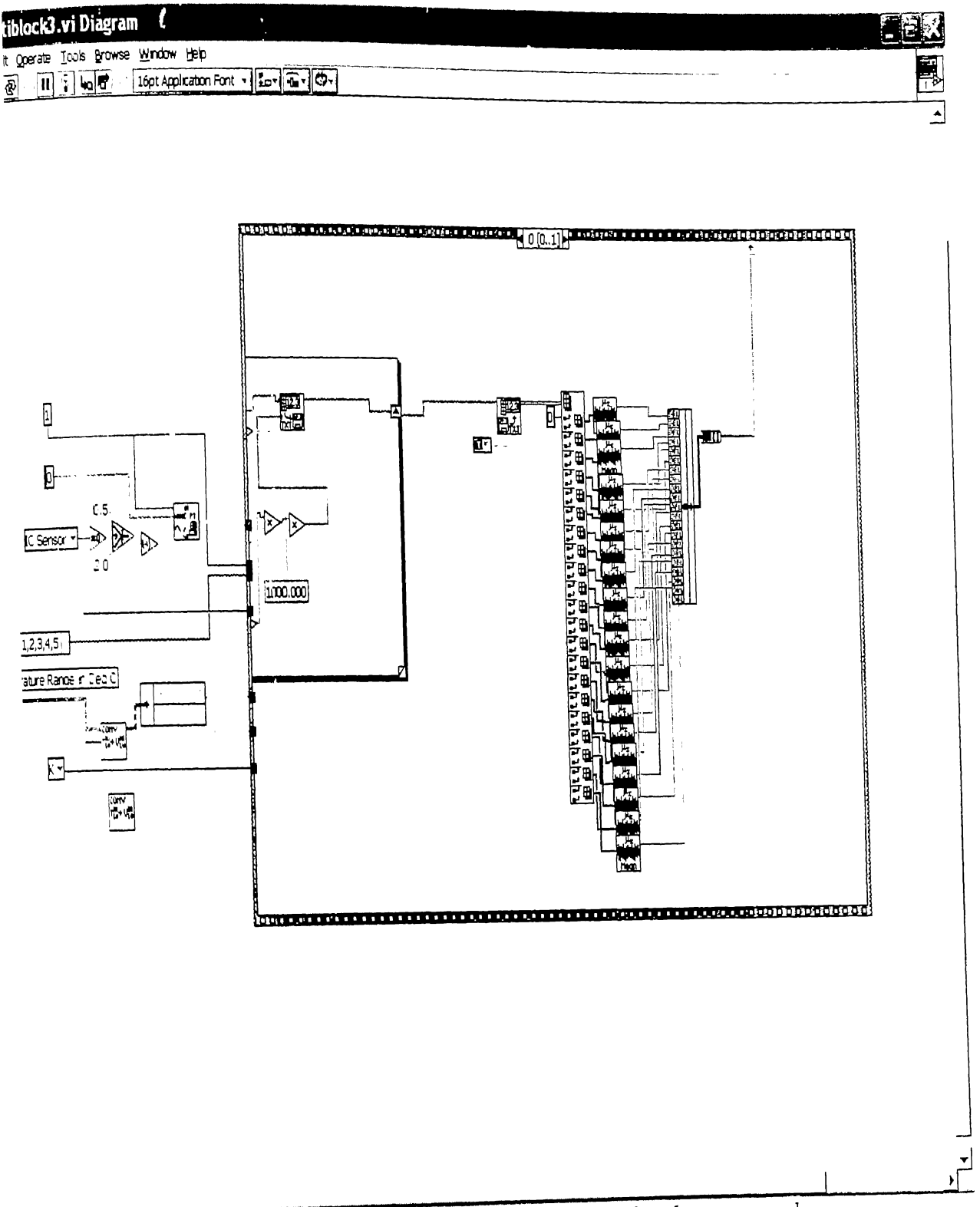

Figure 4.10: Block-diagram in Lab VIEW showing the source code.

4.5 Procedure:

The experiments were conducted to obtain heat transfer data for a vertical channel formed by a PCB like vertical configuration and a thermally insulated wall. For the modeling of a PCB having protruded heat generating sources for uniform heat flux, different approaches are possible. The approach adopted here can be described as follows.

A PCB having dimension of 295mm x 200mm with four heaters (all connected in parallel) at the center were considered and temperatures of minimum 80^0c & maximum 80^0c were maintained by the help of DC input power supply and using LABVIEW temperatures of different surfaces were recorded and values of heat flux were determined.. The experiment was run for different values of airflow rates (i.e. different static pressures) and plate spacings. Thus a typical experiment run consisted of the following steps:

1. The power was switched on.
2. The Plate spacing was fixed at required values
3. Flow velocity was adjusted by controlling the power input to the four fan mounted at the top of the apparatus to obtain the required flow rate and the static pressure.
4. Temperatures on the protruded surface were monitored using thermocouples & Lab VIEW and power to the heaters was adjusted until steady surface temperatures were obtained on each heater.

4.6 Least Count of Measured Parameters

Voltage = 0.1 V

Current = 0.1 Amp.

Air Velocity = 0.01 m/s

Temperature measured by Thermocouples = $0.1\ ^0$ C

Plate Spacing = 1 mm.

4.7 Experimental Results:

A large volume of data was collected for the uniform heat flux of the plate simulating the PCB. This section presents the analysis of these data. Some remarkable trends were observed in the heat transfer parameters like heat flux, Nusselt number profile etc.; these are being highlighted at the appropriate places. Empirical relations were also obtained and described here for the purpose.

Data Range

Parameter	Values for which data were obtained
1. Surface Temperature Limits	Min. 80^0C, Max. 80^0C
2. Surface Thermal Condition	Uniform Heat Flux Condition
3. Observed Heat Flux Range	0.258 – 2.23 (W/cm^2)
4. Plate Spacings Range	30, 40, 50, 60, 80 and 100 mm.
5. Air Velocity Range	0.5, 1.0, 1.5, 2.0, 2.5, 3.0, 3.5, 4.0, 5.0, 6.0, 7.0 (m/s).

Heat Dissipation by Mixed Convection:

4.7.1 Effect of Plate Spacing

For uniform heat flux condition figures 4.11 through 4.13 and figures 4.14 through 4.16, figures 4.20 through 4.22 show the variation of plate mean heat flux and mean Nusselt No. respectively with respect to plate spacing at different air velocities. Similar plots figures 4.17 through 4.19 and figures 4.20 and 4.22 were made when the surface temperature was limited to maximum of 80^0C. The plots clearly showed that as plate spacing was increased, heat flux value was decreased.

Plots When the Surface Temperature was limited to min.80^0C:-

In order to avoid the thermal failure, temperature was limited to min.80^0C. The temperature over the protruding surface lay in the range of 80^0C to 100^0C. For the calculation of heat flux, the effect of oxide layers and/or fouling of dust particles on the top and the bottom of the heat sink was also incorporated. Considering oxide layers, each of 200μm on the top and bottom of the heat sink overall thermal conductivity was calculated as 180 (W/m.K).

Figures 4.11 to 4.13 shows the trend lines for the variation of mean heat flux over the protruding heat sources with different plate spacings.

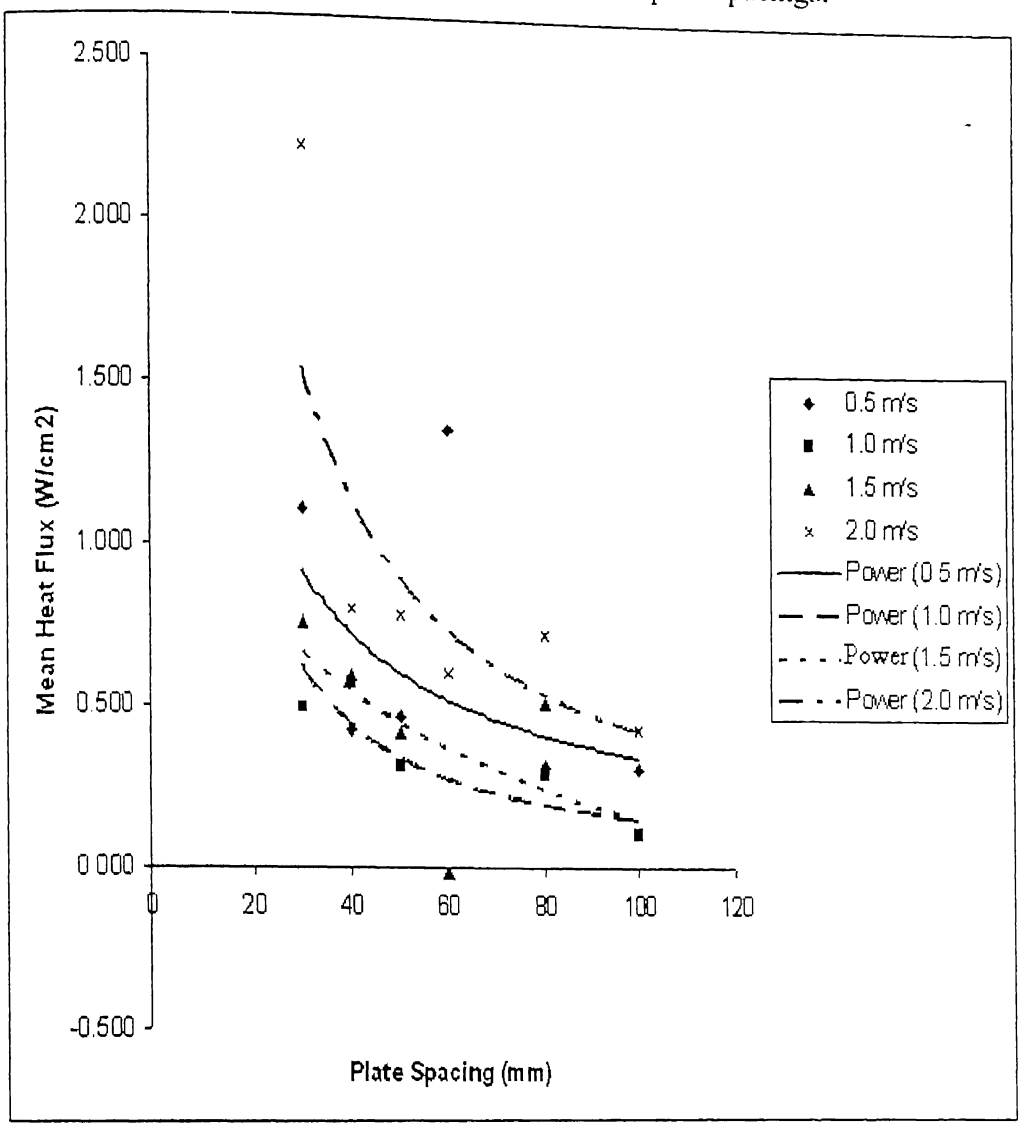

Figure 4.11: Effect of plate spacing on mean heat flux for air (velocity 0.5m/s to 2.0m/s)

Figure 4.11 shows the similar trend lines for the variation of mean heat flux. As plate spacing was increased, mean heat flux decreased gradually to a minimum value. The mean heat flux values for the entire plate spacing range decreased, as the air velocity was increased from 0.5m/s to 1.0m/s. But as soon as the air velocity increased to 1.5m/s and 2.0m/s there was gradual increase in the mean heat flux values for the same plate spacing range.

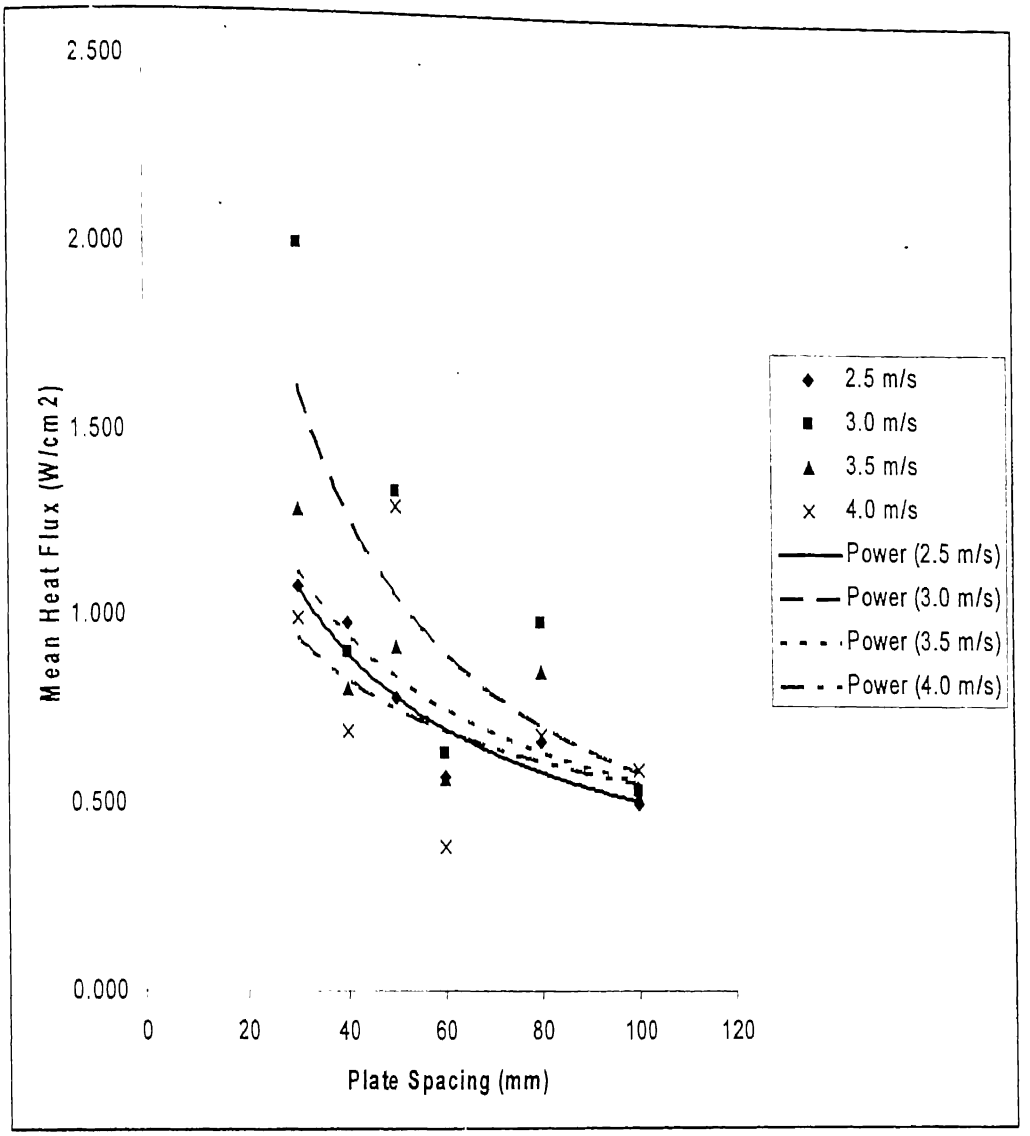

Figure 4.12: Effect of plate spacing on mean heat flux for air (velocity 2.5m/s to 4.0m/s).

Figure 4.12 shows that as plate spacing was increased all the trend lines for the different air velocities slowly converged to particular range of mean heat flux 0.52W/cm^2 to 0.62W/cm^2. When air velocity increased from 2.5m/s to 3.0m/s, the mean heat flux values for the entire range of plate spacing increased. Further increase in air velocity to 3.5m/s and 4.0m/s, mean heat flux values for the same range of plate spacing decreased.

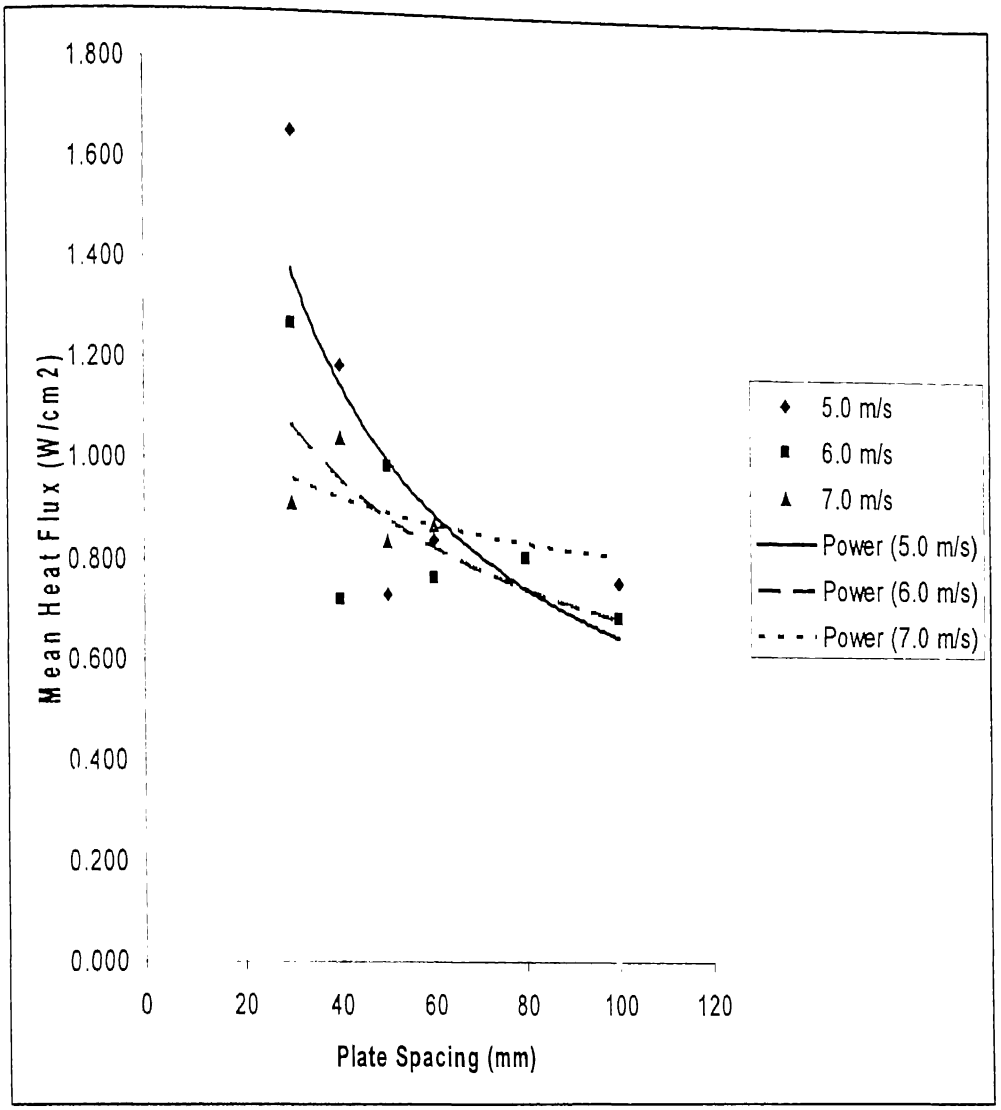

Figure 4.13: Effect of plate spacing on mean heat flux (velocity 5.0m/s to 7.0m/s).

Figure 4.13 shows similar plots for higher air velocity range. The trend lines intersect at particular plate spacing. We observe that mean heat flux values are higher at air velocity of 5.0m/s than those at the 6.0m/s for the plate spacings between 30 to 80mm, and vice-versa for the rest of the plate spacings. Similar is the trend of variation when velocity increased to 7.0m/s. Also one can observe that as air velocity increases the range of mean heat flux decreases.

Figures 4.14 to 4.16 show the trend lines for the variation of mean Nusselt no. over the protruding heat sources with different plate spacings.

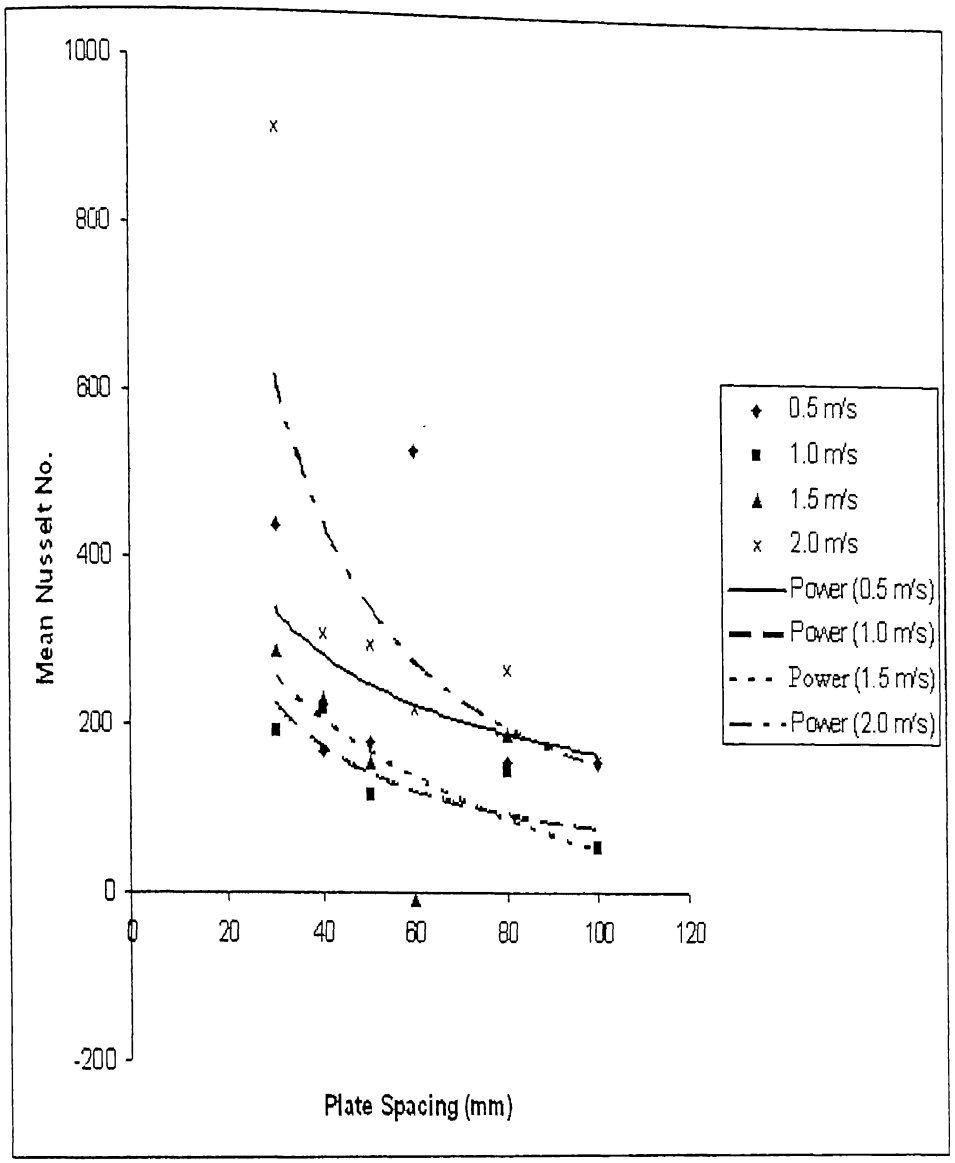

Figure 4.14: Effect of plate spacing on mean Nusselt no. (velocity 0.5m/s to 2.0m/s).

Figure 4.14 shows the similar trend lines for the variation of mean Nusselt no. As plate spacing was increased, mean Nusselt no. decreased slowly to a minimum value. Comparing the trends lines for air velocities of 0.5m/s and 1.0m/s, one can see that the mean Nusselt no. decreases for the entire range of plate spacing. Also as the air

velocity was increased to 1.5m/s and 2.0m/s there was a gradual increase in the mean Nusselt no. values for the same range of plate spacing.

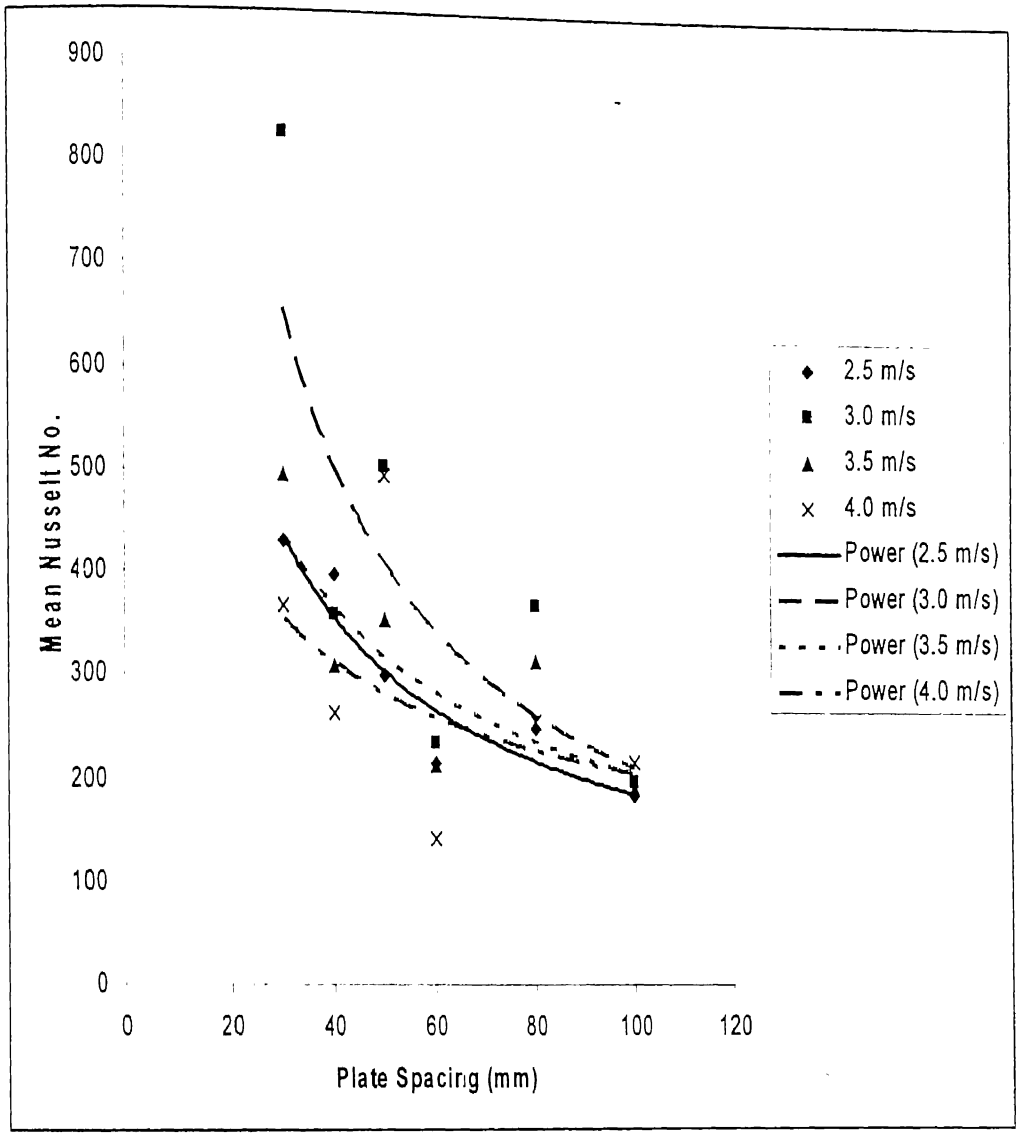

Figure 4.15: Effect of plate spacing on mean Nusselt no. (velocity range of 2.5m/s to 4.0m/s).

Figure 4.15 shows as plate spacing increased all the trend lines for the different air velocities slowly converged to particular range of mean Nusselt no. 190 to220. When air velocity was increased from 2.5m/s to 3.0m/s, the mean Nusselt no. for the entire range of plate spacing also increased. But as air velocity was further increased from 3.5m/s and 4.0m/s, mean heat flux values for the same range of plate spacing decreased.

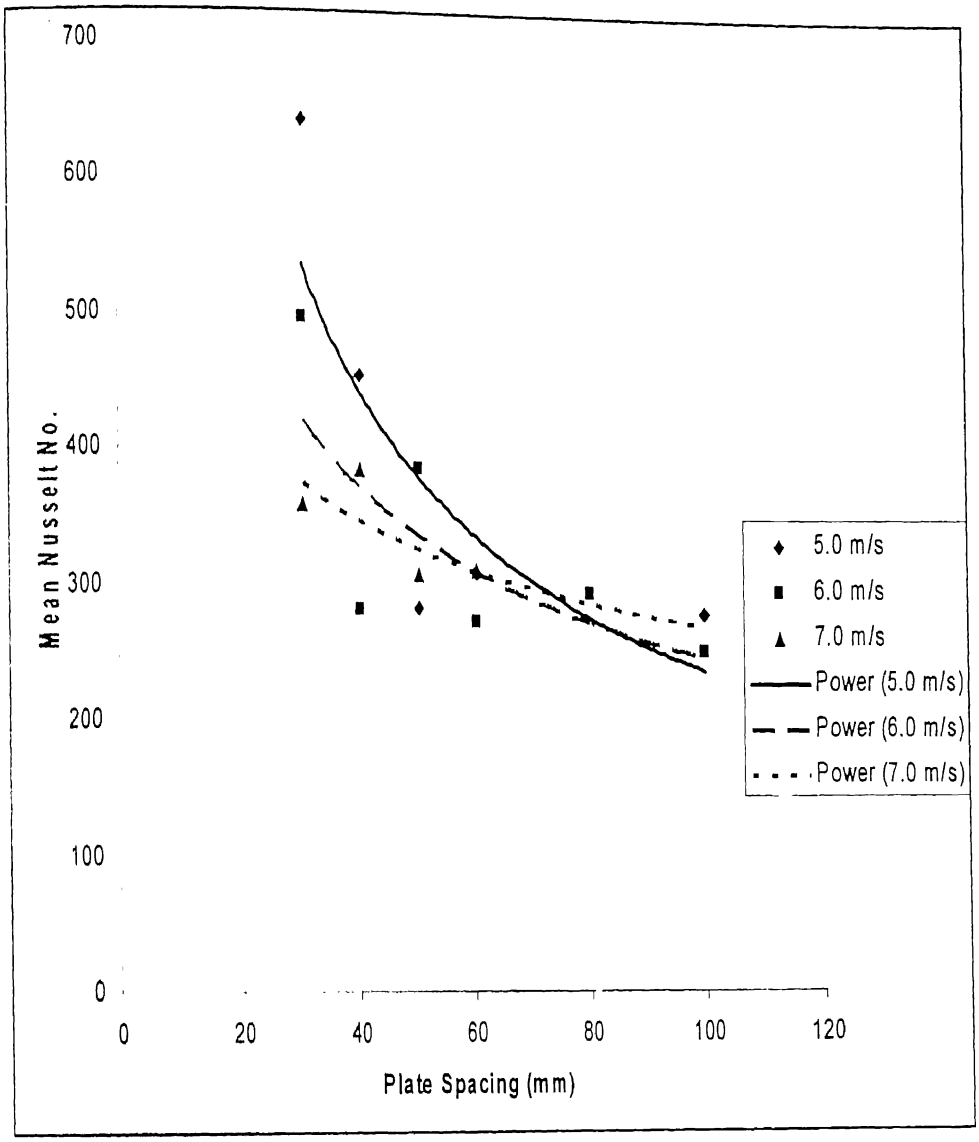

Figure 4.16: Effect of plate spacing on mean Nusselt no. (velocity range of 5.0m/s to 7.0m/s).

Figure 4.16 shows that at higher air velocity range, the trend lines intersect at particular plate spacing. We observe that mean Nusselt nos. are higher at air velocity of 5.0m/s than those at the 6.0m/s for the plate spacings between 30 to 85mm, and vice-versa for the rest of the plate spacings. Similar was the trend of variation when velocity increased to 7.0m/s. Also we can observe that as air velocity was increased the range of mean Nusselt no. decreased.

Plots When the Surface Temperature was limited to max.80^{0}C:-

In this case temperature over the protruding surface lay in the range of 65^{0}C to 80^{0}C. Figures 4.17 to 4.19 shows the trend lines for the variation of mean heat flux over the protruding heat sources with different plate spacings.

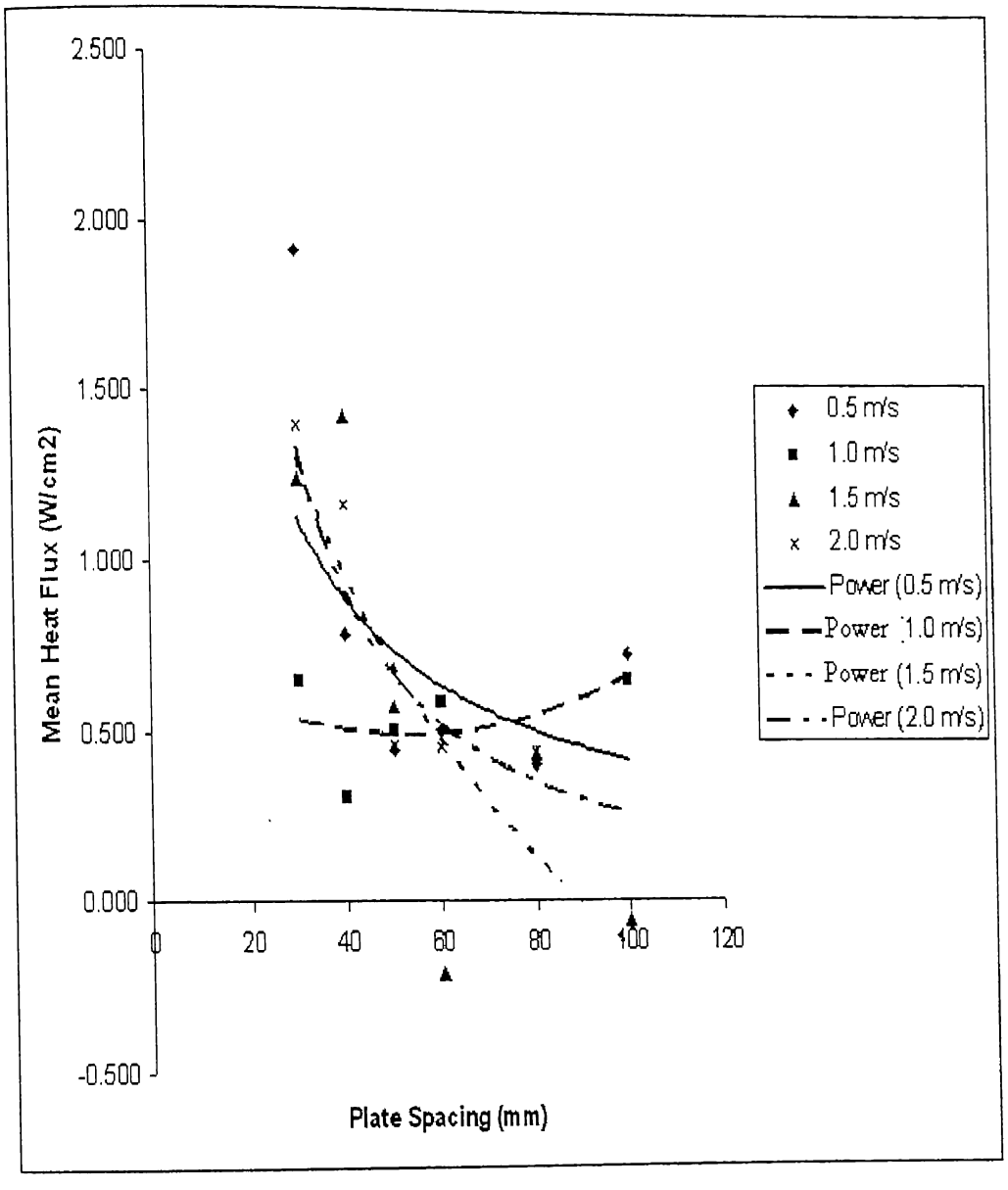

Figure 4.17: Effect of plate spacing on mean heat flux (velocity range of 0.5m/s to 2.0m/s).

Figure 4.17 shows the similar trend lines for three air velocities of 0.5m/s, 1.5m/s and 2.0m/s.But with air velocity of 1.0m/s mean heat flux values initially decreased very slowly up to the plate spacing of 60mm, beyond which it increased gradually.

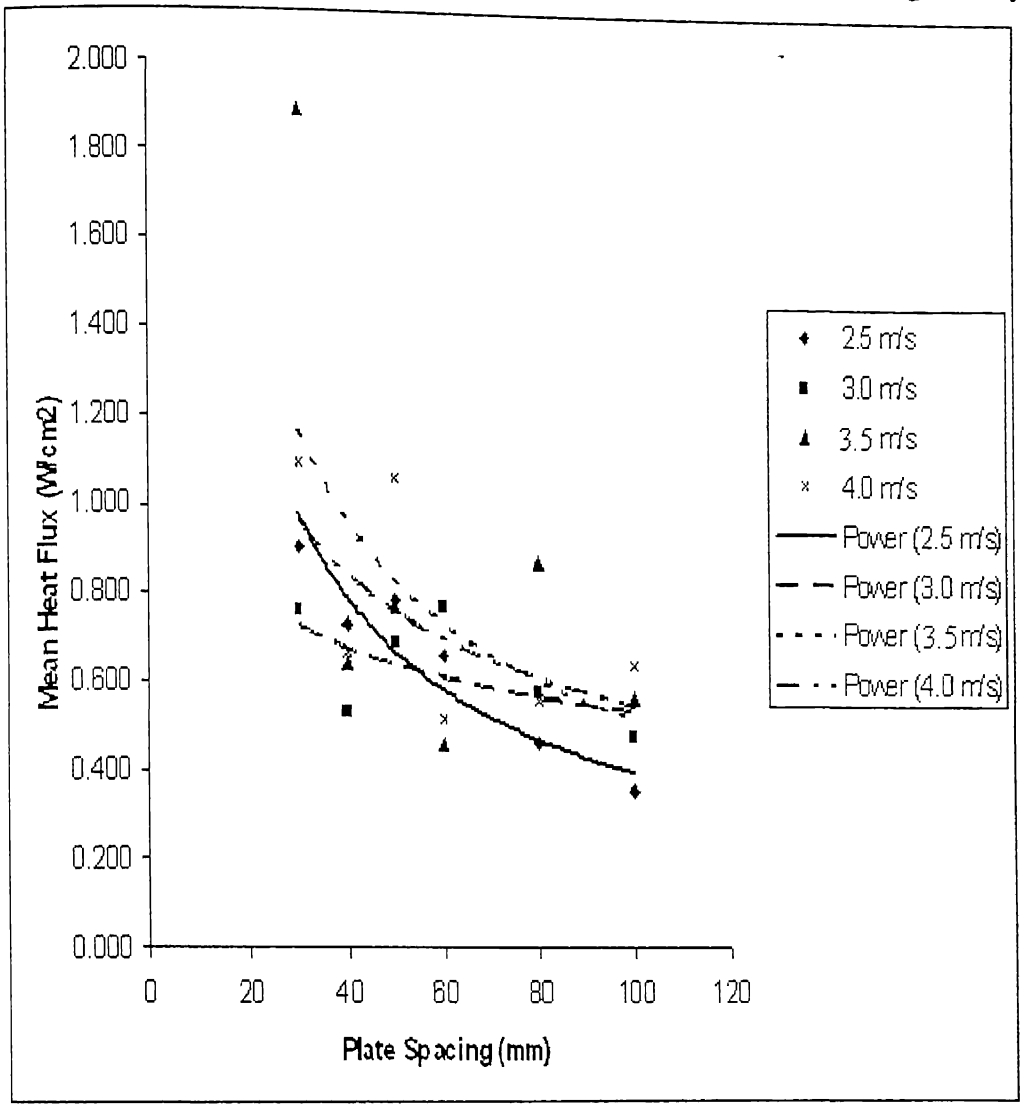

Figure 4.18: Effect of plate spacing on mean heat flux (velocity range of 2.5m/s to 4.0m/s).

Figure 4.18 shows the similar trend lines for air velocity range of 2.5m/s to 4.0m/s. But in the velocity range 3.0m/s to 4.0m/s, as plate spacing increased, mean heat flux converged to a minimum value of 0.6 W/cm^2.

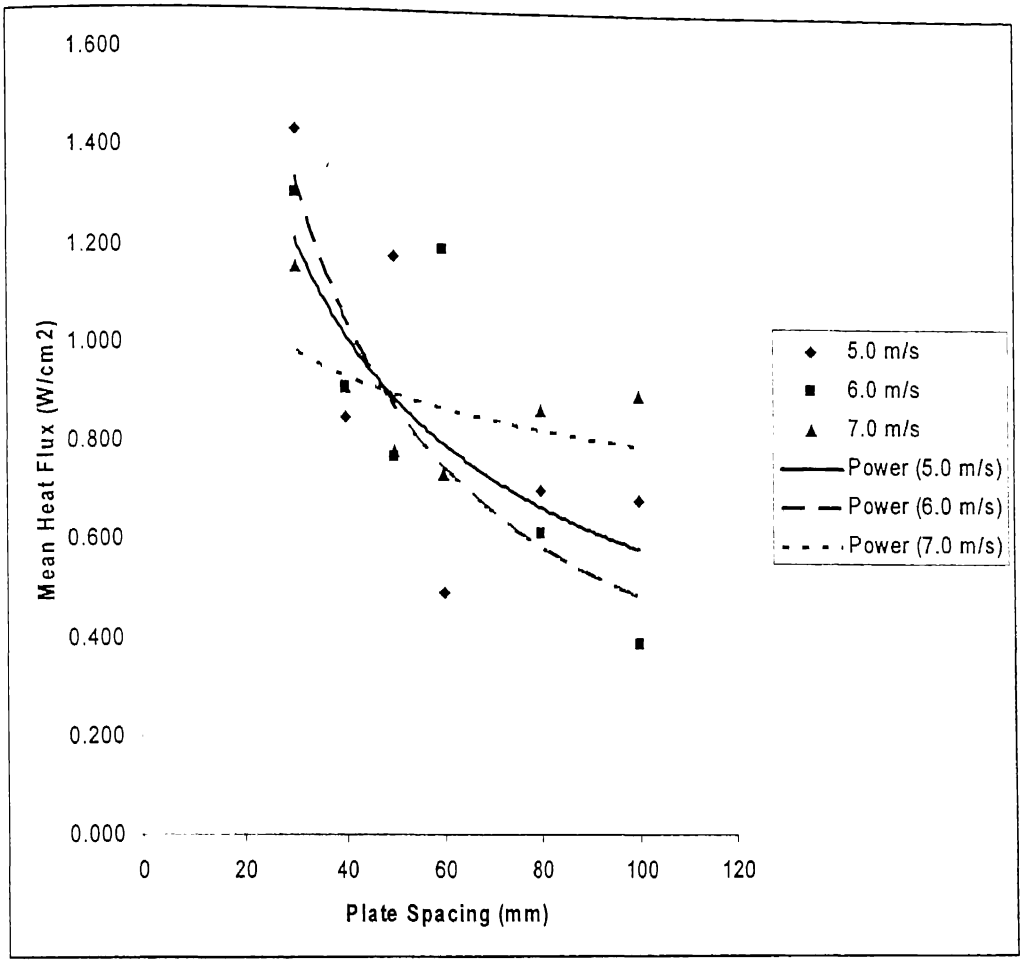

Figure 4.19: Effect of plate spacing on mean heat flux (velocity range of 5.0m/s to 7.0m/s).

Figure 4.19 shows similar trend in the variation. At plate spacing of 45mm, the mean heat flux value is same for all the velocities.

Figures 4.20 to 4.22 shows the trend lines for the variation of mean Nusselt no. over the protruding heat sources with different plate spacings.

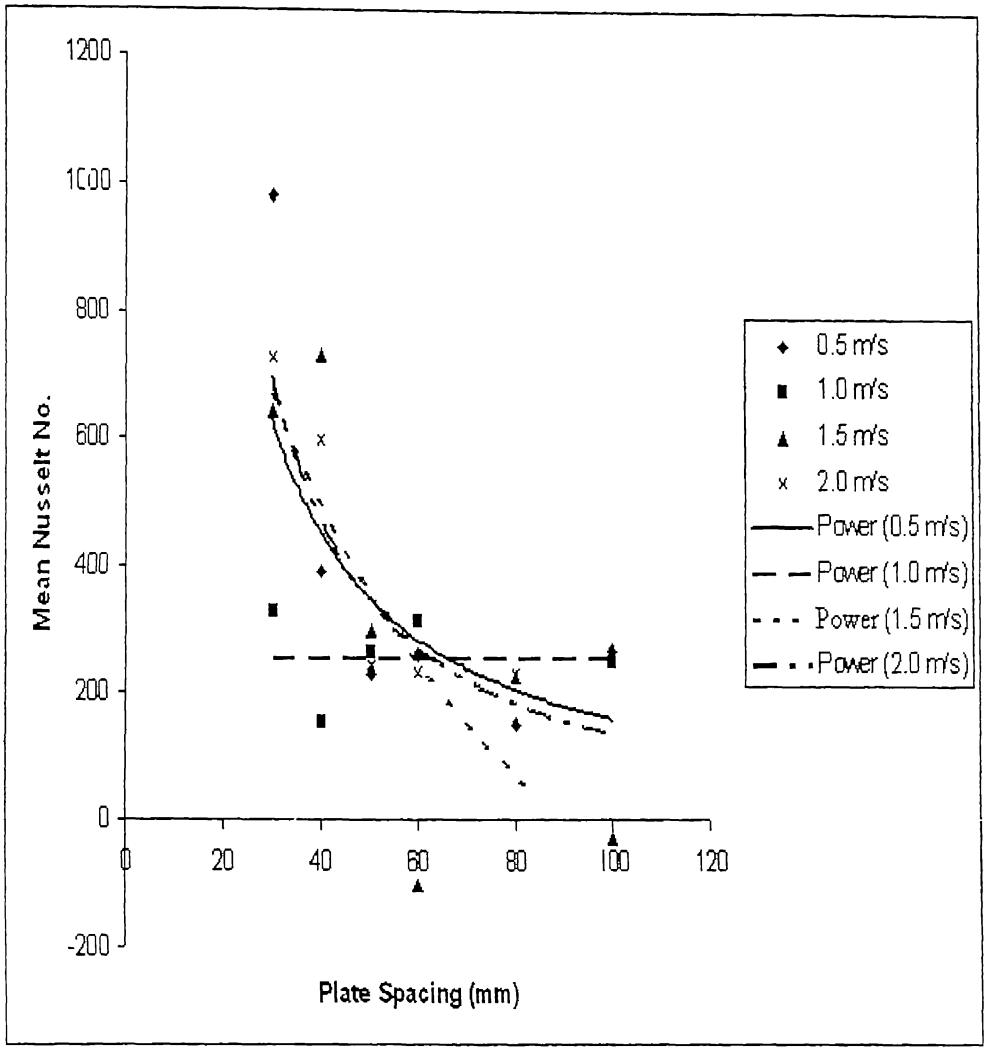

Figure 4.20: Effect of plate spacing on mean Nusselt no. (velocity range of 0.5m/s to 2.0m/s).

Figure 4.20 shows the similar trend lines for the air velocities of 0.5m/s, 1.5m/s and 2.0m/s. But with air velocity of 1.0 m/s, mean Nusselt no. increases almost linearly and gradually.

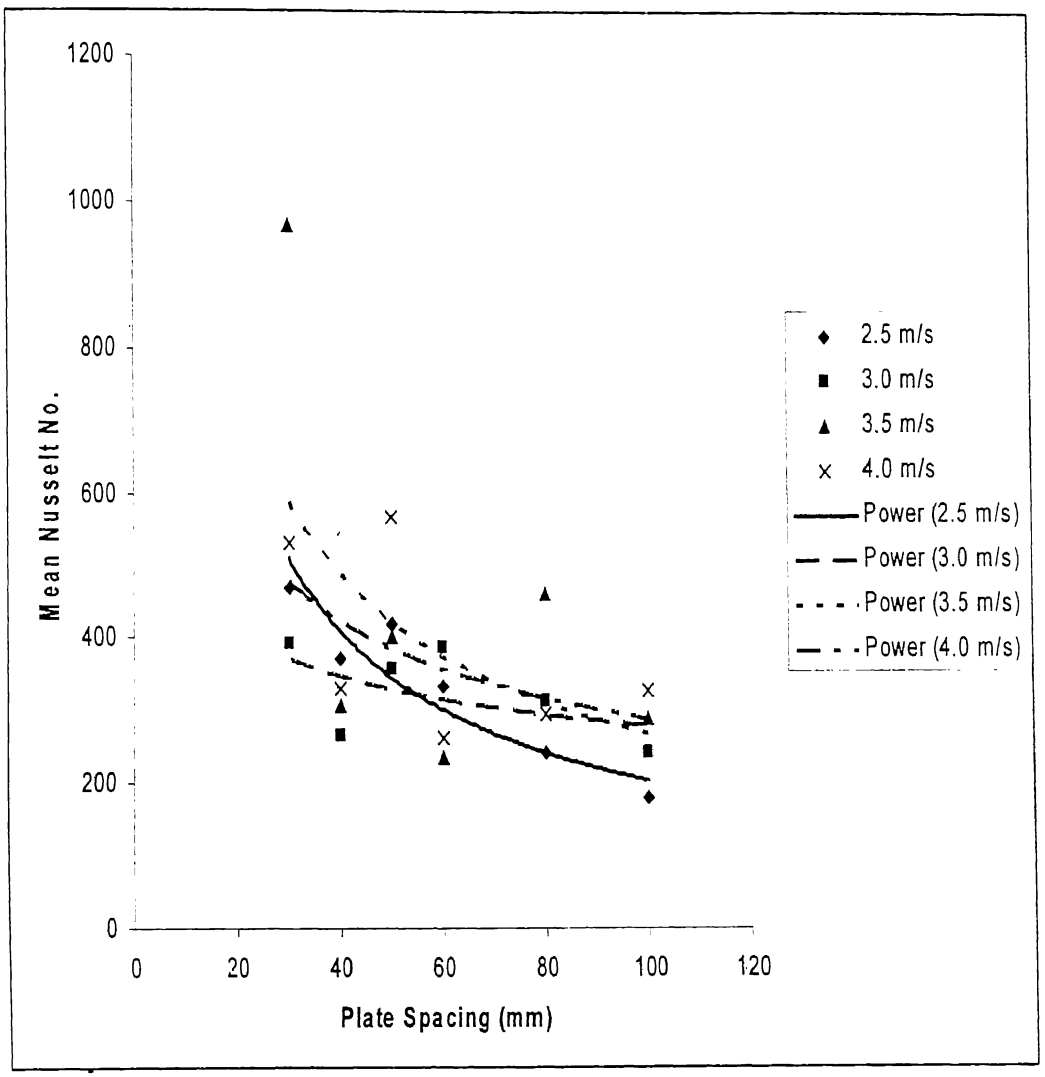

Figure 4.21: Effect of plate spacing on mean Nusselt no. (velocity range of 2.5m/s to 4.0m/s).

Figure 4.21 shows the similar trend lines for air velocity range of 2.5m/s to 4.0m/s. In the velocity range 3.0m/s to 4.0m/s, as plate spacing was increased mean Nusselt no. converged to a minimum value of 300.

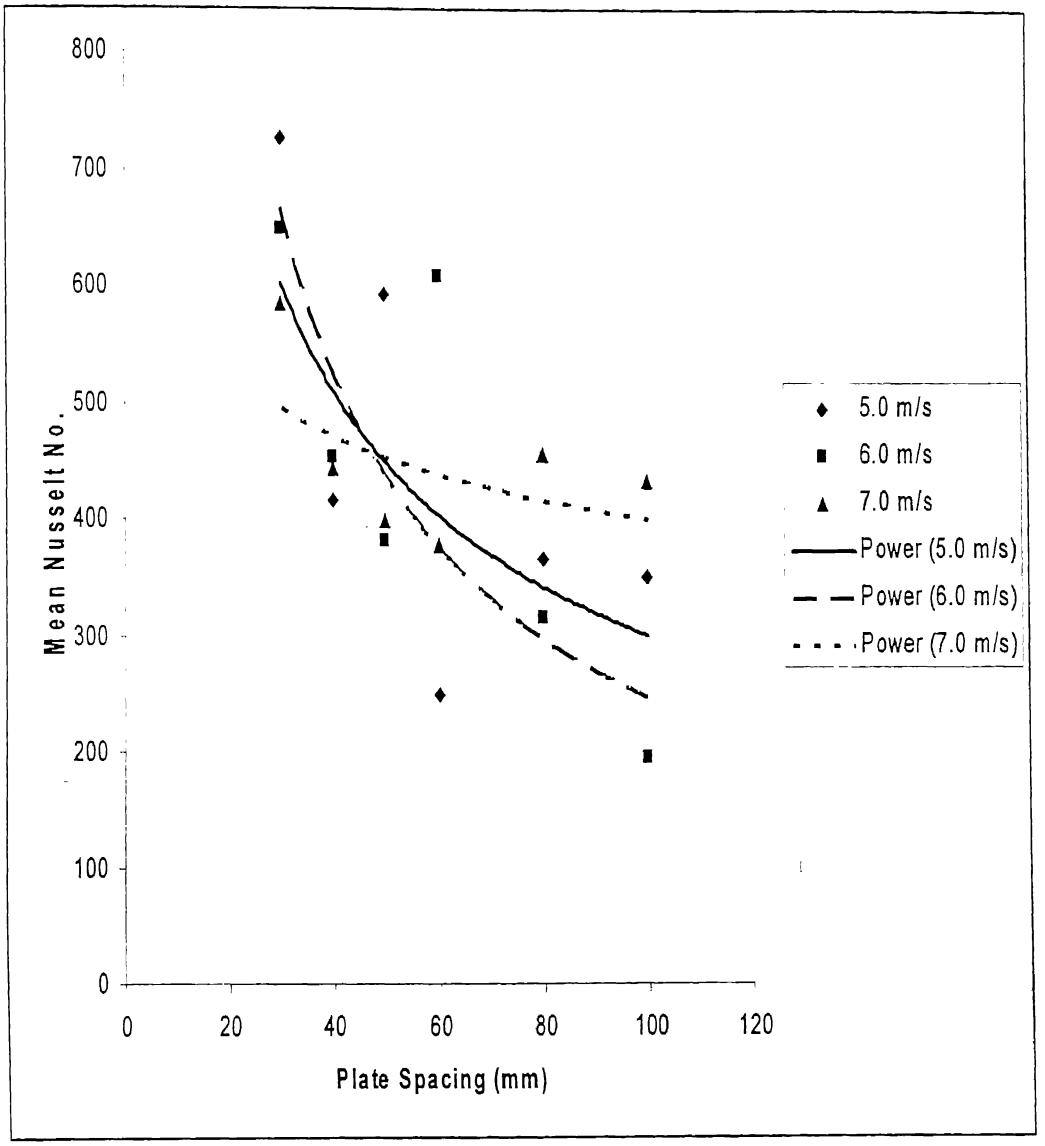

Figure 4.22: Effect of plate spacing on mean Nusselt no. (velocity range of 5.0m/s to 7.0m/s).

Figure 4.22 shows similar trend in the variation of mean Nusselt no. At plate spacing of 45mm, the mean heat flux value is same for all the velocities.

4.8 Sources of Error

The known sources of error which affect the experimental results are as follows:

1. It is difficult to produce all the thermocouple beads identical.
2. Minute differences in soldered joints of thermocouple wires with the extension wires.
3. Small differences in electrical resistance of heaters and the connecting wires and also at their joints.
4. All the thermocouple wires can not be inserted precisely to the same depth of the heat sink, so they don't show the temperature exactly of the same intended location at the heat sink.
5. Due to exposure of the heat sink to the atmosphere, some oxide layer of thickness of the order of 200 – 400μm are formed on its top and bottom surface. So, the actual $K_{overall}$ can not be calculated precisely.
6. Due to small fluctuations in the air velocity arising out of small variations in the speed of the fans driving the flow in the test rig cannot be avoided.

4.9 Uncertainty Analysis

Least count of the instruments used, method employed to measure and experimental limitations give rise to some degree of inaccuracy in the measurement of parameters. As a consequence of this, the quantity computed from these measured parameters is also likely to contain some degree of inaccuracy. The difference between the true value and the experimentally determined value of the quantity is termed as an Error.

A systematic error (bias) is quantified through careful calibration of probes and instruments in terms of a correction. During experimentation if these errors are found, then all the measured parameters can be corrected to eliminate these. This reduces error within its accuracy envelope.

A random error may be quantified statistically and may be combined by quadrature rule (pythagorian summation). It can not be corrected and eliminated

all together, but may be reduced to an extent by repeated measurement in time and space.

True value may be approached but can never be evaluated. Since the true value of the quantity is unknown, the true magnitude of the error can not be evaluated. The best possible estimate of the magnitude of the error is termed as Uncertainty. So it is unavoidable inaccuracy in the measurement. It provides a range in which the true value lies. The best estimate (most probable value) of a parameter is, therefore, associated with an uncertainty range.

Uncertainty in constants, unit conversion factors and in the physical properties are considered to be negligible as compared to uncertainties in the measured parameters. Uncertainty in the latter parameters is taken equal to least count of the instrument to ensure the mean of repeated measurements to lie within uncertainty envelope, except particle size, holdup, time and temperatures.

Uncertainty Propagation to Computed Parameters

Based on the uncertainties in the measured parameters, uncertainty in computed parameters can be determined. For a computed parameter, f, which is a function of measured parameters ($f = f(X_j)$, $j = 1, N$), the overall uncertainty in the f is obtained as Pythagorian summation of the contribution from each measured parameter. The contribution from each parameter is a product of uncertainty in the measured parameter, U_{Xj}, and sensitivity coefficient $\partial f / \partial X_j$. Thus, the summation may be described mathematically given below

$$U_f = \pm \left[\sum_{j=1} (U_{Xj} . \partial f / \partial X_j)^2\right]^{1/2}$$

Calculation of uncertainty in different parameters:

(a) Heat Flux:

$$\text{Heat Flux} = f_1 = C^* \times (T_b - T_f);$$

Where C^* is constant, T_b and T_f are back and front surface temperature of heat sink.

Sensitivity coefficient, $\partial f_1/\partial T_b = C^*$;

$$\partial f_1/\partial T_f = - C^*;$$

So uncertainty in heat flux is

$$U_{f1} = \pm \left[\left(U_{Tb}. \partial f_1/\partial T_b \right)^2 + \left(U_{Tf}. \partial f_1/\partial T_f \right)^2 \right]^{1/2}$$

Here $U_{Tb} = \pm 0.1^0$ c,

$U_{Tf} = \pm 0.1^0$ c,

$\partial f_1/\partial T_b = 0.435$ W.cm^{-2}. K^{-1},

$\partial f_1/\partial T_f = - 0.435$ W.cm^{-2}. K^{-}

So, $U_{f1} = \pm \left[\left(0.1 \times 0.435 \right)^2 + \left(0.1 \times 0.435 \right)^2 \right]^{1/2}$

$= \pm 0.0615$ W.cm^{-2}

In percentage term, the uncertainty in the heat flux lies between 2.76 to 23.84 %.

(b) Mean Surface Temperature:

Mean Surface Temperature = $f_2 = T_S = (T_{f1} + T_{f2} + T_{f3} + T_{f4}) / 4$

Where T_{f1}, T_{f2}, T_{f3} & T_{f4} are front surface temperatures of all the four sinks.

Sensitivity coefficient, $\partial f_2/\partial T_{f1} = ¼$; $U_{Tf1} = 0.1^0$ c;

$\partial f_2/\partial T_{f2} = ¼$; $U_{Tf2} = 0.1^0$ c;

$\partial f_2/\partial T_{f3} = ¼$; $U_{Tf3} = 0.1^0$ c;

$\partial f_2/\partial T_{f4} = ¼$; $U_{Tf4} = 0.1^0$ c;

So, $U_{f2} = \pm \left[\left(U_{Tf1}. \partial f_2/\partial T_{f1} \right)^2 + \left(U_{Tf2}. \partial f_2/\partial T_{f2} \right)^2 \right.$

$\left. + \left(U_{Tf3}. \partial f_2/\partial T_{f3} \right)^2 + \left(U_{Tf4}. \partial f_2/\partial T_{f4} \right)^2 \right]^{1/2}$

$= \pm 0.05^0$ c

In percentage term, the uncertainty in Mean Surface Temperature lies between 0.05 to 0.07 %.

(c) Heat Transfer Coefficient (h):

Heat Transfer Coefficient, $f_3 = f_1 / (T_S - T_R)$

Where T_R is the room temperature.

Sensitivity coefficient, $\partial f_3/\partial T_R = f_1 / (T_S - T_R)^2$; $U_{TR} = 0.1^0$c.

So, $U_{f3} = \pm U_{TR} . \partial f_3/\partial T_R$

In percentage term, the uncertainty in Heat Transfer Coefficient up to 0.16 to 2.35 %.

4.10 Closure

1. When the surface temperature was limited to min.80^0C and as the air velocity was increased from 0.5m/s to 7.0m/s, there is not a specific tendency in the variation of mean heat flux values although these lie in the range of 0.2W/cm^2 to 1.4W/cm^2.

Similar is the variation in the mean Nusselt no. and it lies in the range of 50 to 620.

2. When the surface temperature was limited to max.80^0C, then for different air velocities variation in the mean heat flux and Nusselt no. values has the same tendency and lies in the range of 0.1W/cm^2 to 1.3W/cm^2 and 50 to 700 respectively.

Chapter-5

RESULTS and DISCUSSION

Numerical data was analyzed for Natural Convection and Mixed Convection cases. In both cases Uniform Wall Temperature of 100^0C and Uniform Heat Flux conditions over the range 0.085W/cm^2 - 0.45W/cm^2 over vertical Flushed surface have been studied for the variation of Heat Flux and Nusselt No. with the plate spacing.

Experimental data was observed for uniform Heat Flux condition imposed on protruding surfaces placed on the PCB over the range 0.258W/cm^2 – 2.23W/cm^2 in order to study the variation of Heat Flux and Nusselt No. with the plate spacing in the mixed convection regime.

5.1 Comparison of Computational Data with Experimental Data

In this section computational and experimental data in Mixed Convection regime have been compared in order to study the trends in distribution of Mean Nusselt No. over vertical channel surface for different values of plate spacing. The experimental data for the air velocities of 2.5 m/s & 3.5 m/s and the computational data for the air velocities of 2.7 m/s & 3.8 m/s have been considered here.

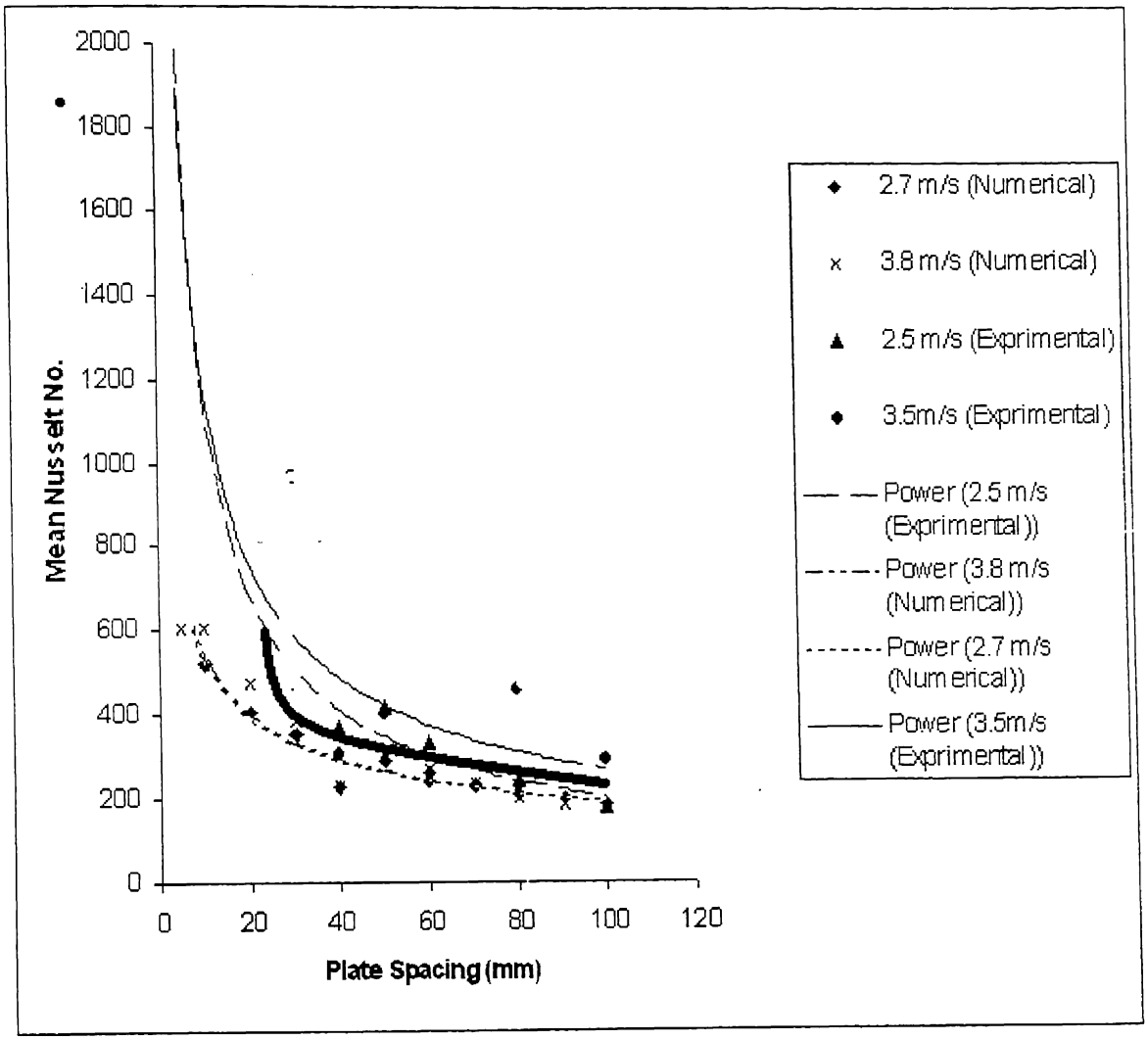

Figure- 5.1: Comparison of Mean Nusselt No. vs. Plate Spacing for different air velocities.

The trend of Computational data shows that as plate spacing is increased, mean Nusselt no. decreases gradually to a minimum. Similar trend is observed in the Experimental data, but difference lies as mean Nusselt no. decreases almost sharply to a minimum. Here Nusselt no. from numerical computations lies in the range of 175 to 608, whereas same for Experimentation lies in the range of 200 to 966. Thus the two ranges overlap considerably, since the numerical calculations are based upon certain fundamental assumptions whereas and same with the experimental is based upon certain simplifications, taking the overlap of the two ranges, one can obtain a more realistic range for the values for the Nusselt

Number. Thus the range 200 to 600 for Nusselt Number seems to be more relevant for the air velocity up to 3.5 m/s. In the figure 5.1 thick line shows the trend for the variation of Mean Nusselt No. over the common range of the experimental and numerical data.

5.2 Conclusions:

Numerical programming making use of the Fluent software version 6.0 was done successfully. Numerical data was generated for the vertical channel subjected to both UWT and UHF conditions. For the UWT case, the channel wall temperature was maintained at 100°C while for UHF case, the heat flux was maintained within a typical range 0.085 to 0.200 W/cm^2 suitable for natural and mixed convection cooling in the air. Following points may be noted:

- For the natural convection cooling under UWT condition, coolant (air) velocity was limited to 1.1 m/s; mean Nusselt number over the plate surface lay between 150 – 200 and heat flux ranged between 350 and 400 W/ m^2. Under the UHF condition, coolant velocity was raised to 2.0 m/s; mean Nusselt number ranged within 150 to 350; while the mean surface temperature surprisingly shot-up to about 500°C which is much higher then the limit prescribed for the safe operation of electronic components. This clearly means that one can not put the mentioned heat flux load under natural convection cooling of PCBs.
- Mixed convection cooling conditions were simulated for two values of externally applied static pressures viz. 3.4 and 7.8 Pa. For the UWT case, heat flux value was restricted within 0.12W/cm^2 and Nusselt number lay within 200 to 500. For the UHF case, heat flux lay with in 0.1 and 0.5 W/cm^2 resulting into maximum channel wall temperature near 127°C and peak value of surface Nusselt number resting at 650. Formation of hot spots at some places at the channel wall surface was also observed.

For the experimentation purpose already existing test rig was upgraded making use of a data acquisition hardware and Lab View software. This upgradation helped in monitoring a large number of thermocouples and adjusting power input for the heating elements with a relative ease and that too in dynamic sense. Since UWT and UHF was already been experimentally studied, this time data was taken

successfully for mounted heated blocks over the plate surface. Physical dimensions of these aluminum blocks were 20×20×0.5 mm which has a general resemblance with many of small IC packages available in the market. In an array of four symmetrically placed heated blocks upper and lower limits of temperature occurring at any of the blocks were observed and heater power input was controlled to restrict the values. Since the power input for all the heaters was practically the same, a kind of uniform UHF condition resulted over the plate surface in the region mounting these heat sources. Following points can be concluded from the experiment:

- Heat flux and heat transfer coefficient were calculated with an accuracy of 24 % and 2.3 % respectively.
- When the block temperatures were restricted to upper limit of 80°C the maximum heat flux value of 1.4W/cm^2 was found dissipating satisfactorily in the velocity range 0.5-7.0m/s. Also the values of the Nusselt number lay in the range 400-600.
- When the block temperatures were restricted on the lower side at 80°C, the heat flux dissipation fluctuated between 0.5 and 2.0 W/cm^2 depending upon the value of flow velocity, the mean Nusselt number had a peak value of 700.

Following conclusions can be drawn comparing experimental data with the numerical one:

- Nusselt numbers for the two cases were found following the same trend in variation with the values lying between 200 and 1300. Upper limit for the velocity for the comparison purpose was restricted at 3.5m/s.
- It is possible to construct a common trend line showing variation of Nusselt number with the plate spacing. Range of Nusselt number for the trend line is 200-600.

One important observation from these results is that when the value of Nusselt number decreases with the increase in channel width or plate spacing it tends to approach a limiting value of 200. This means that if the plate spacing increases beyond 100 mm (which was in the fact upper limit for both numerical and experimental data) one can predict in advance the minimum value for the Nusselt number. Thus, from thermal design point of view, in extreme case it would be safe

to assume Nusselt number value as low as 200 and then adjust the rest of the design parameters like maximum thermal load up on PCB surface, PCB dimensions, inter PCB spacing, location of IC packages at the PCB surface, mounting suitably designed heat sinks at appropriate places etc and etc. This will no doubt result in a relatively safe thermal design of a system using vertically oriented PCBs and mixed convection cooling in air.

Finally, an empirical relation is being put forward for the purpose to estimate a reliable value for Nusselt number given as follows:

$$Nu_{(mean)} = 2400 - 502 \times \log(15X + 12) + 28 \times (X - 3)^{1.3} + 180 \times X^{-1}$$

Where: X is the plate spacing subjected to the condition $X \geq 30mm$, X is in cm.

Other restrictions for the use of this relationship are:

1. Flow velocity limited in the range of 2.5 to 3.5 m/s for mixed convection cooling.
2. Wall thermal conditions: either UWT with maximum surface temperature of 100°C or UHF with heat flux values lying between 0.14 and 1.4W/cm^2.

5.3 Suggestions for Future Work

- A similar work in Turbulence regime can be carried out for uniform temperature and uniform heat flux condition.
- Hot spots on the vertical plates in computational domain can be verified experimentally.
- The effect of plate inclination on the overall performance can be investigated.
- Present study does not consider the effects of surface roughness on overall performance. The model can be extended to find the effects of surface roughness on the heat transfer characteristics.
- The relative usefulness of cooling of PCB's in a channel with air as a working fluid can be compared with other cooling techniques like cooling with Jet Impingement, Macro Channel cooling, etc.

References

1. N. K. Anand, S. H. Kim, and L. S. Fletcher, 1992, ' The Effect of Plate Spacing on Free Convection Between Heated Parallel Plates ', *Journal of Heat and Mass Transfer, Vol. 114, pp. 515-518*

2. E. K. Levy, 1971, 'Optimum Plate Spacings for Laminar Natural Convection Heat Transfer From Parallel Vertical Isothermal Flat Plates', *Journal of Heat Transfer, pp. 463-465.*

3. D. Naylor, J. M. Floryan, J. D. Tarasuk, 1991, ' A Numerical Study of Developing Free Convection Between Isothermal Vertical Plates ', *Journal of Heat Transfer, Vol. 113, pp. 620-626.*

4. F Mendez, C Trevino, 2000, 'The conjugate conduction-natural convection heat transfer along a thin vertical plate with non-uniform internal generation ', *Int. J. of Heat and Mass Transfer, Vol. 43, pp. 2739-2748.*

5. H. Y. Wang, F. Penot, and J. B. Sauliner, 1997, ' Numerical study of a buoyancy-induced flow along a vertical plate with discretely heated integrated circuit packages ', Int. J. Heat and Mass Transfer, vol. 40, No. 7, pp.1509-1520.

6. L. S. Yao, 1983, 'Free And Forced Convection in the Entry Region of A Heated Vertical Channel ', Int. J. Heat and Mass Transfer, Vol. 26, No. 1, pp. 65-72.

7. O. Manca, B. Morrone, and S. Nardini, 2000, 'Experimental Analysis of Thermal Instability in Natural Convection between Horizontal Parallel Plates Uniformly Heated ', Journal of Heat Transfer, Vol. 122, pp. 50-57.

8. Young Keun Jang, 'Convective heat transfer in a composed enclosure with a guide vane ', pp.136-702.

9. Timothy J. Young, Kambiz Vafai, 1998, 'Convective flow and heat transfer in a channel containing multiple heated obstacles ', *Int. J. Of Heat and Mass Transfer, Vol. 41, pp. 3279-3298.*

10. Timothy J. Young and Kambiz Vafai, 1998, 'Convective cooling of a heated obstacle in a channel ', *Int. J. Of Heat and Mass Transfer, Vol .41, pp.3131-3148.*

11. C. P.Tso, G. P. Xu, K. W. Tou, 1999, 'An Experimental Study on Forced Convection Heat Transfer From Flush-Mounted Discrete Heat Sources ', *Journal of Heat Transfer, Vol.* 121, *pp. 326-332.*

12. Hollworth, B. R. and Dubrin, M., 1992, 'Impingement cooling of electronics', *Journal of Heat Transfer, Vol. 115, pp. 377-387.*

13. Roeller, P. T., Stevens, J. and Webb, W. B., 1991, 'Heat Transfer and turbulent flow characteristics of isolated three-dimensional protrusions in channels', *Journal Of Heat Transfer, Vol. 113, pp. 597-603.*

14. Anderson, A. M., and Moffat, R. J., 1991, 'Direct air cooling of electronic components: Reducing temperature by controlled thermal mixing', *Journal of Heat Transfer, Vol.113, pp. 620-626.*

15. Antonio Barletta, 1998, ' Laminar mixed convection with viscous dissipation in a vertical channel ', Int. J. of Heat and Mass Transfer, Vol.41, pp. 3501-3513.

16. T. T. Hamadah and R. A. Wirtz, 1991, 'Analysis of Linear Fully Developed Mixed Convection in a Vertical Channel With Opposing Buoyancy ', Journal of Heat Transfer, Vol. 113, pp. 507-510.

17. Isaac Shai and Yacov Barnea, 1986, 'Simple analysis of mixed convection with uniform heat flux ', Int. J. Heat Mass Transfer, Vol. 29, No.8, pp.1139-1147.

18. F. Moukalled, A. Doughan, S. Acharya, 2000, 'Parametric study of mixed convection in channels with concave and convex surfaces ', Int. J. of Heat and Mass Transfer, Vol. 43, pp. 1947-1963.

19. A. Berletta , 1999, 'Analysis of Combined Forced and Free Flow in a Vertical Channel With Viscous Dissipation and Isothermal-Isoflux Boundary Conditions ', Journal of Heat Transfer, Vol. 121, pp. 349-356.

20. Y. C. Chen, J. N. Chung, 1998, ' Stability of Mixed Convection in a Differentially Heated Vertical Channel ', Journal of Heat Transfer, Vol. 120, pp. 127-132.

21. W. S. Tseng, W. L. Lin, C. P. Yin, C. L. Lin, T. F. Lin, 2000, ' Stabilization of Buoyancy-Driven Unstable Vortex Flow in Mixed Convection of Air in a Rectangular Duct by Tapering Its Top Plate ', Journal of Heat Transfer, Vol. 122, pp. 58-65.

22. C. Gau, T. M. Huang, W. Aung, 1996, ' Flow and Mixed Convection Heat transfer in a Divergent Heated Vertical Channel ', Journal of Heat Transfer, Vol. 118, pp.606-615.

22. M. Behnia, A. A. Dehghan, H. Mishima and W. Nakayama, 1998 (C) 1997, 'A numerical study of natural convection immersion cooling of multiple heat sources in parallel interacting open-top cavities ', *Int. J. of Heat and Mass Transfer, Vol.41, pp. 797-808.*

24. B. A. Jubran, S. A. Swiety and M. A. Hamdan., 1996, ' Convective heat transfer and pressure drop characteristics of various array configurations to simulate the cooling of electronic modules ', *Int. J. Heat and Mass Transfer, Vol. 39, No. 16, pp. 3519-3529.*

25. E. M. Sparrow, J. E. Niethammer and A. Chaboki., 1982, ' Heat Transfer and pressure drop characteristics of arrays of rectangular modules encountered in electronic equipment ', *Int. J. Heat and Mass Transfer, Vol. 25, No. 7, pp. 961-973.*

26. Behmia, M., Parenix, S. And Dubrin, P.A., 1997, 'Prediction of heat transfer in an axisymmetric turbulent jet impinging on a flate plate', *Int. J . of Heat and Mass Transfer, Vol. 41, pp. 1845-1855.*

27. Huang, L. And El-Genk, M.S., 1997, ' Heat transfer and flow visualization experiments of swirling, multi-channel, and conventional impinging jets, *Int. J. of Heat and Mass Transfer, Vol. 41, pp. 583-600.*

28. Voke, P. R. and Gao, S., 1998, ' Numerical study heat from an impinging jet', *Int. J. of Heat and Mass Transfer', Vol. 41, pp. 671-680.*

29. Ake Malhammar, 2001, 'The Cooling Efficiency Concept part 1', *Cooling Zone Magazine, Vol. 2 No. 9.*

APPENDIX:1

(a) Computational data:

Definitions:

$Gr_L = (g \beta \Delta T L^{3)} / \nu^2$

$Bo_L = (g \beta \Delta T L^3) / \alpha^2$

$Re_L = (u_{inlet} . L) / \nu$

$Pr = \nu / \alpha$

$Ra_L = Gr_L.Pr$

Table 1.1: Natural Convection with Constant Wall Temperature Condition:

Spacing (mm)	Max. Velocity (m/s)	Inlet Velocity (m/s)	Re_L	Gr_L	Gr_L/Re^2	Mean Nu.	Inlet Temp. (T_0) (K)	Surface Temp. (T_h)	Mean Hf. (w/cm^2)
40	0.602	0.15	5134.35	15.69×10^8	59.5	163.2	293	373	0.0335
50	0.636	0.127	4347.13	15.69×10^8	83.0	191.0	293	373	0.0392
60	0.958	0.287	9823.84	14.46×10^8	15.0	185.8	298	373	0.0381
70	1.189	0.238	8146.6	15.69×10^8	23.6	205.6	293	373	0.0422
80	0.732	0.219	7496.24	13.04×10^8	23.2	179.0	304	373	0.0360
90	1.0421	0.21	7188.17	15.69×10^8	30.4	187.0	293	373	0.0384
100	0.6823	0.136	4655.2	15.69×10^8	72.4	174.83	293	373	0.0359

Table 1.2: Mixed Convection with Constant Wall Temperature Condition $\Delta P = 3.4$ Pa. ($\Delta T = T_h - T_0 = 80^0$ C; $T_h = 100^0$ C and $T_o = 20^0$ C)

Spacing (mm)	Velocity (m/s)		$Nu_{L.}$ (mean)	$Re_{L.}$	$Gr_{L.}$	$Gr_L/Re_{L.}^2$	$Ra_{L.}$	Mean Hf. (w/cm^2)	Pr
	max	inlet							
5.0	3.94	2.68	456.0	91656	1.6×10^9	0.19	1.19×10^9	0.0936	0.744
10.0	3.81	2.69	417.3	91998	1.6×10^9	0.19	1.19×10^9	0.0856	0.744
20.0	3.12	2.11	322.29	66690	1.6×10^9	0.36	1.19×10^9	0.0662	0.744
30.0	4.21	2.74	297.94	93708	1.6×10^9	0.18	1.19×10^9	0.0612	0.744
40.0	3.45	2.60	213.86	88920	1.6×10^9	0.20	1.19×10^9	0.0439	0.744
50.0	4.05	2.63	256.40	89946	1.6×10^9	0.20	1.19×10^9	0.0526	0.744
60.0	4.31	2.80	234.27	95760	1.6×10^9	0.17	1.19×10^9	0.0481	0.744
70.0	4.34	2.81	215.73	96102	1.6×10^9	0.17	1.19×10^9	0.0443	0.744
80.0	4.37	2.80	190.00	96102	1.6×10^9	0.17	1.19×10^9	0.0390	0.744
90.0	4.39	2.89	174.38	98838	1.6×10^9	0.16	1.19×10^9	0.0358	0.744
100.0	4.49	2.91	161.00	99522	1.6×10^9	0.16	1.19×10^9	0.0331	0.744

Table 1.3: Mixed Convection with Constant Wall Temperature Condition ΔP = 7.8 Pa. ($\Delta T = T_h - T_0 = 80^0$ C ; $T_h = 100^0$ C and $T_o = 20^0$ C)

Spacing (mm)	Velocity (m/s)		Nu_L (mean)	Re_L	Gr_L	Gr_L/Re_L^2	Ra_L	Mean Hf. (w/cm^2)	Pr
	max	inlet							
5.0	5.55	3.89	541.0	133038	$1.6x10^9$	0.09	1.19×10^9	0.1110	0.744
10.0	3.13	2.19	386.0	74898	$1.6x10^9$	0.30	1.19×10^9	0.0792	0.744
20.0	5.97	4.00	391.0	136800	$1.6x10^9$	0.085	1.19×10^9	0.0802	0.744
30.0	3.81	2.55	417.3	87210	$1.6x10^9$	0.21	1.19×10^9	0.0857	0.744
40.0	4.85	3.41	300.0	116622	$1.6x10^9$	0.12	1.19×10^9	0.0605	0.744
50.0	5.74	3.45	276.4	117990	$1.6x10^9$	0.115	1.19×10^9	0.0567	0.744
60.0	6.08	3.65	251.0	124830	$1.6x10^9$	0.10	1.19×10^9	0.0515	0.744
70.0	6.18	4.02	225.4	137484	$1.6x10^9$	0.085	1.19×10^9	0.0462	0.744
80.0	6.14	4.00	412.0	136800	$1.6x10^9$	0.085	1.19×10^9	0.0201	0.744
90.0	6.17	3.86	183.4	132012	$1.6x10^9$	0.092	1.19×10^9	0.0377	0.744
100.0	6.25	4.06	169.7	138852	$1.6x10^9$	0.083	1.19×10^9	0.0348	0.744

Table 1.4: Natural Convection with Constant Heat Flux Condition. (Pr = 0.744)

Spacing (mm)	Velocity (m/s)		Re_L	Gr_L	Gr_L/Re_L^2	Mean Nu.	Inlet Temp. To (K)	Surface Temp. Th (K)	Hf. W/cm2
	max	Inlet							
40	0.9096	0.21	7188.17	$34.32x10^8$	66.42	247.0	293	468	0.116
50	1.031	0.153	5237.00	$31.00x10^8$	113.0	275.18	293	451	0.116
60	1.35	0.4	13691.7	$25.10x10^8$	13.40	301.0	298	428	0.170
70	1.38	0.276	9447.31	$24.51x10^8$	27.46	300.82	293	418	0.151
80	1.727	0.345	11809.0	$21.48x10^8$	15.40	284.14	297	408	0.197
90	1.523	0.304	10406.0	$35.53x10^8$	32.81	281.0	296	479	0.150
100	1.98	0.397	13589.0	$43.00x10^8$	23.28	288.14	293	512	0.190

Table 1.5: Mixed Convection with Constant Heat Flux Condition ΔP = 3.4 Pa.

($\Delta T = T_h - T_0 = 80^0$ C; $T_h = 100\ ^0$C and $T_o = 20\ ^0$ C)

Spacing (mm)	Velocity (m/s)		Nu_L (mean)	Mean Surface Temp. T_h (K)	Re_L	Gr_L	Gr_L/Re_L^2	Ra_L	Hf. (w/m^2)	Pr
	max	inlet								
5.0	5.52	3.32	706.4	413.22	113544	2.36 x109	0.135	1.75x109	2204	0.744
10.0	3.75	2.62	525.8	386.00	89604	$1.84x10^9$	0.229	$1.37x10^9$	1454	0.744
20.0	3.11	2.00	408.5	444.2	68400	$2.96x10^9$	0.633	$2.20x10^9$	2418	0.744
30.0	4.19	2.93	355.4	415.32	100206	$2.41x10^9$	0.240	$1.79x10^9$	2282	0.744
40.0	3.45	2.58	226.46	339.39	88236	$0.91x10^9$	0.117	$0.68x10^9$	2920	0.744
50.0	3.97	2.78	292.1	402.0	95076	$2.14x10^9$	0.237	$1.59x10^9$	2870	0.744
60.0	4.26	2.99	260.0	383.46	102258	$1.78x10^9$	0.170	$1.32x10^9$	2626	0.744
70.0	4.29	2.80	230.3	388.56	95760	$1.88x10^9$	0.205	$1.40x10^9$	2737	0.744
80.0	4.29	2.80	207.5	381.25	95760	$1.73x10^9$	0.189	$1.29x10^9$	2600	0.744
90.0	4.29	2.79	178.6	428.15	95418	$2.65x10^9$	0.291	$1.97x10^9$	2900	0.744
100.0	4.29	2.79	167.3	426.36	95418	$2.62x10^9$	0.288	$1.95x10^9$	3200	0.744

Table 1.6: Mixed Convection with Constant Heat Flux Condition ΔP = 7.8 Pa.

($\Delta T = T_h - T_0 = 80^0$ C ; $T_h = 100^0$ C and $T_o = 20^0$ C)

Spacing (mm)	Velocity (m/s) max	Velocity (m/s) inlet	Nu_L (mean)	Mean Surface Temp. T_h (K)	Re_L	Gr_L	Gr_L/Re_L^2	Ra_L	Hf. (w/m^2)	Pr
5.0	3.90	2.73	616.7	444.29	93366	$2.97x10^9$	0.341	$2.21x10^9$	2320	0.744
10.0	5.24	3.67	608.0	408.44	125514	$2.27x10^9$	0.144	$1.69x10^9$	2151	0.744
20.0	5.96	4.17	473.4	457.05	142614	$3.22x10^9$	0.158	$2.40x10^9$	3456	0.744
30.0	5.95	4.17	386.8	491.45	142614	$3.9x10^9$	0.192	$2.90x10^9$	4432	0.744
40.0	4.85	3.46	231.5	333.35	118332	$0.79x10^9$	0.056	$0.60x10^9$	3368	0.744
50.0	5.70	3.67	305.1	405.12	125514	$2.20x10^9$	0.139	$1.64x10^9$	3503	0.744
60.0	6.10	3.96	270.3	392.24	135432	$1.95x10^9$	0.106	$1.45x10^9$	3457	0.744
70.0	6.19	4.02	237.5	375.55	137484	$1.62x10^9$	0.086	$1.21x10^9$	2814	0.744
80.0	6.30	4.08	214.6	366.55	139536	$1.44x10^9$	0.074	$1.07x10^9$	2800	0.744
90.0	6.16	4.00	192.0	374.41	136800	$1.66x10^9$	0.085	$1.19x10^9$	2800	0.744
100.0	6.18	4.01	178.1	369.73	136800	$1.5x10^9$	0.08	$1.12x10^9$	3000	0.744

Experimental Data

Air	Velocity	m/s	0.5	0.5	0.5	0.5	0.5	0.5
Plate	Spacing	mm	30	40	50	60	80	100
Input	Heat Flux	(W/sq. cm	0.653	0.653	0.618	0.578	0.910	0.877
	Block1	Front face	68.8	72.9	68.9	66.5	93.3	92.6
		Back face	79.5	73.3	70.3	68.7	93.4	96.2
		ΔT1	10.7	0.5	1.4	2.3	0.1	3.6
	Block2	Front face	76.3	76.5	73.0	73.4	93.5	93.0
		Back face	77.0	77.2	73.8	74.0	94.5	93.6
		ΔT2	0.7	0.7	0.7	0.6	1.0	0.7
Thermoco	Block3	Front face	80.0	79.9	80.0	80.3	97.3	96.9
uple		Back face	84.6	84.6	81.1	81.1	99.0	98.3
		ΔT3	4.6	4.7	1.2	0.8	1.7	1.4
	Block4	Front face	71.1	71.5	69.2	69.5	82.3	82.6
		Back face	72.8	72.9	70.0	70.5	83.2	83.6
		ΔT4	1.7	1.3	0.8	1.0	0.9	1.0
Room	temp(Tr)	0 C	30.7	30.8	29.5	29.5	31.2	31.2
Surface	Temp limits	0 C	Max 80	Max 80	Max 80	Max 80	Max 80	Max 80
	c* ΔT1		4.6458	0.21315	0.59595	0.97875	0.0435	1.5747
	c* ΔT2		0.30885	0.3132	0.3219	0.27405	0.4263	0.29145
	c* ΔT3		1.99665	2.04015	0.5133	0.32625	0.7395	0.61335
	c* ΔT4		0.72645	0.57855	0.3567	0.43065	0.41325	0.43065
	Average H	(W/sq.cm)	1.919	0.786	0.447	0.502	0.406	0.728
			± 0.0615	± 0.0615	± 0.0615	± 0.0615	± 0.0615	± 0.0615
	Mean Tem	Front Face	74.03	75.20	72.76	72.42	91.59	91.26
			$\pm 0.05^0$C	$\pm 0.05^0$C	$\pm 0.05^0$C	$\pm 0.05^0$C	$\pm 0.05^0$C	$\pm 0.05^0$C
	h	W/cm^2.C	0.044336	0.017706	0.010336	0.011712	0.006712	0.012104
			±10.2E-05	±3.99E-05	±2.39E-05	±2.73E-05	±1.11E-05	±2.01E-05
	Mean Nu		979.9987	391.3591	228.4675	258.8679	148.3528	267.5525

1	1	1	1	1	1.5	1.5	1.5	1.5
30	40	50	60	100	30	40	50	60
0.681	0.660	0.660	0.618	0.861	0.787	0.703	0.675	0.675
71.6	72.6	65.6	65.5	89.7	70.6	70.5	67.9	75.7
74.9	73.3	68.0	67.7	91.5	78.8	76.5	71.1	72.6
3.3	0.7	2.4	2.2	1.8	8.2	6.0	3.2	**-3.1**
76.2	77.1	72.5	72.7	92.0	75.8	75.7	72.2	73.2
76.3	77.2	72.8	73.7	92.8	76.4	76.1	72.4	73.5
0.1	0.1	0.3	1.0	0.8	0.6	0.5	0.2	0.3
79.7	80.0	79.6	80.1	96.1	79.4	79.4	79.4	80.0
81.0	80.8	80.9	81.1	98.3	80.9	85.0	80.8	80.7
1.3	0.8	1.4	1.0	2.3	1.5	5.6	1.4	0.7
70.0	70.6	67.8	68.6	82.4	68.9	69.5	67.6	68.0
71.3	71.9	68.4	69.8	83.6	70.1	70.4	68.0	68.1
1.3	1.2	0.6	1.3	1.1	1.1	1.0	0.4	0.2
30.7	30.8	29.4	30.1	31.8	30.7	30.4	29.4	30.1
Max 80	Max 80	Max 80	Max 80	Max 80	Max 80	Max 80	Max 80	Max 80
1.43985	0.30885	1.03965	0.95265	0.77865	3.58005	2.62305	1.37895	-1.35285
0.0435	0.03915	0.12615	0.42195	0.36105	0.25665	0.21315	0.09135	0.1218
0.54375	0.34365	0.5916	0.4263	0.9918	0.63945	2.44905	0.62205	0.30885
0.5655	0.53505	0.24795	0.5481	0.48285	0.4959	0.4263	0.1914	0.08265
0.648	0.307	0.501	0.587	0.654	1.243	1.428	0.571	-0.210
± 0.0615	± 0.0615	± 0.0615	± 0.0615	± 0.0615	± 0.0615	± 0.0615	± 0.0615	± 0.0615
74.40	75.08	71.36	71.72	90.03	73.69	73.73	71.76	74.21
±0.05^{0}C	±0.05^{0}C	±0.05^{0}C	±0.05^{0}C	±0.05^{0}C	±0.05^{0}C	±0.05^{0}C	±0.05^{0}C	±0.05^{0}C
0.014847	0.006924	0.011947	0.01411	0.011233	0.028941	0.032952	0.013477	-0.004759
±3.40E-05	±1.56E-05	±2.85E-05	±3.39E-05	±1.93E-05	±6.74E-05	±7.60E-05	±3.18E-05	±1.10E-05
328.1752	153.0513	264.0628	311.8783	248.2887	639.7002	728.3572	297.8829	-105.1872

1.5	1.5	2	2	2	2	2	2.5	2.5
80	100	30	40	50	60	80	30	40
0.675	0.675	0.810	0.780	0.764	0.844	0.765	0.825	0.868
75.1	76.5	70.3	70.7	67.7	74.5	75.4	71.2	75.7
76.8	73.8	76.2	77.9	68.3	75.4	75.9	74.7	78.9
1.7	**-2.7**	5.9	7.3	0.6	0.9	0.6	3.5	3.2
76.1	74.8	75.5	75.6	71.3	72.6	76.4	75.0	76.1
77.2	74.9	76.8	76.2	72.8	73.0	77.9	76.4	76.7
1.1	0.0	1.3	0.6	1.5	0.4	1.5	1.4	0.6
79.6	79.2	79.0	79.1	79.1	79.3	79.9	78.4	78.7
80.4	80.5	83.8	81.1	80.9	80.8	81.4	81.0	81.1
0.8	1.3	4.8	2.0	1.7	1.5	1.5	2.6	2.4
68.1	67.6	70.0	69.5	67.2	67.3	67.8	70.4	70.1
68.5	68.3	70.9	70.4	67.6	68.6	68.3	71.2	70.7
0.4	0.8	0.8	0.9	0.4	1.4	0.5	0.8	0.6
32.0	31.8	31.2	30.4	29.4	30.2	32.0	31.2	31.6
Max 80	Max 80	Max 80	Max 80	Max 80	Max 80	Max 80	Max 80	Max 80
0.73515	-1.16145	2.57085	3.15375	0.2436	0.4002	0.2436	1.5312	1.3746
0.45675	0.0174	0.56115	0.24795	0.66555	0.16965	0.64815	0.6177	0.24795
0.3654	0.57855	2.0967	0.85695	0.75255	0.6525	0.64815	1.1223	1.0266
0.18705	0.3393	0.36975	0.4089	0.17835	0.58725	0.2262	0.348	0.2697
0.436	-0.057	1.400	1.167	0.460	0.452	0.442	0.905	0.730
± 0.0615	± 0.0615	± 0.0615	± 0.0615	± 0.0615	± 0.0615	± 0.0615	± 0.0615	± 0.0615
74.73	74.50	73.70	73.73	71.32	73.40	74.88	73.73	75.15
±0.05^{0}C	±0.05^{0}C	±0.05^{0}C	±0.05^{0}C	±0.05^{0}C	±0.05^{0}C	±0.05^{0}C	±0.05^{0}C	±0.05^{0}C
0.010209	-0.001326	0.032919	0.026932	0.01097	0.010469	0.010299	0.021264	0.016773
±2.39E-05	±3.10E-05	±7.74E-05	±6.22E-05	±2.62E-05	±2.42E-05	±2.40E-05	±5.00E-05	±3.86E-05
225.6615	-29.29884	727.6194	595.2913	242.484	231.3941	227.6491	470.021	370.7463

2.5	2.5	2.5	2.5	2.5	3	3	3	3
50	60	80	100	100	30	40	50	60
3.375	0.910	0.796	0.845	0.734	0.933	0.893	0.877	0.796
70.2	73.9	73.5	76.8	75.4	76.2	76.9	70.9	73.6
73.3	76.4	74.9	77.0	75.7	79.1	77.9	73.9	77.8
3.2	2.4	1.4	0.2	0.2	2.9	1.0	3.0	4.2
72.8	73.9	75.6	78.2	75.0	76.1	76.9	72.5	73.3
73.5	74.5	76.4	78.6	75.3	77.0	77.6	73.4	73.9
0.7	0.5	0.8	0.4	0.3	0.8	0.7	0.9	0.6
79.0	78.9	79.5	79.4	79.6	78.2	78.8	79.2	79.2
81.4	81.0	81.3	81.6	80.9	81.0	81.2	81.1	81.3
2.4	2.1	1.8	2.1	1.3	2.8	2.4	1.9	2.1
67.4	68.6	67.8	67.5	67.4	70.2	69.9	67.6	67.7
68.3	69.6	68.1	68.1	68.0	70.7	70.6	68.1	68.0
0.9	1.0	0.3	0.6	0.6	0.4	0.7	0.5	0.2
30.7	30.2	31.9	31.8	31.8	32.6	31.6	29.8	29.6
Max 80	Max 80	Max 80	Max 80	Max 80	Max 80	Max 80	Max 80	Max 80
1.38765	1.0614	0.609	0.08265	0.10005	1.26585	0.4524	1.3137	1.8183
0.30015	0.23055	0.35235	0.1653	0.1131	0.36105	0.3132	0.38715	0.2436
1.0527	0.90915	0.783	0.91785	0.56115	1.21365	1.044	0.83085	0.91785
0.4089	0.43935	0.10875	0.261	0.25665	0.1914	0.3132	0.2175	0.09135
0.787	0.660	0.463	0.357	0.258	0.758	0.531	0.687	0.768
± 0.0615	± 0.0615	± 0.0615	± 0.0615	± 0.0615	± 0.0615	± 0.0615	± 0.0615	± 0.0615
72.33	73.84	74.09	75.49	74.37	75.19	75.61	72.53	73.45
±0.05^{0}C	±0.05^{0}C	±0.05^{0}C	±0.05^{0}C	±0.05^{0}C	±0.05^{0}C	±0.05^{0}C	±0.05^{0}C	±0.05^{0}C
0.01891	0.015119	0.010976	0.008172	0.00606	0.017794	0.01207	0.01608	0.017497
±4.54E-05	±3.46E-05	±2.60E-05	±1.87E-05	±1.43E-05	±4.18E-05	±2.74E-05	±3.76E-05	±3.99E-05
417.9722	334.1938	242.6126	180.6272	133.959	393.3165	266.7822	355.4272	386.7511

3	3	3.5	3.5	3.5	3.5	3.5	3.5	4
80	100	30	40	50	60	80	100	30
0.844	0.829	1.039	1.031	0.928	0.861	0.928	0.894	1.150
73.7	76.7	67.9	79.7	70.2	72.3	72.0	75.8	73.2
75.8	77.6	80.8	81.8	73.8	72.4	77.1	77.6	78.9
2.1	0.9	12.9	2.1	3.5	0.1	5.1	1.8	5.7
74.5	77.7	75.8	76.2	72.4	72.2	74.3	78.8	75.7
74.9	78.2	76.2	76.4	73.2	73.4	74.9	79.3	76.3
0.4	0.6	0.4	0.2	0.8	1.2	0.7	0.5	0.6
78.8	79.0	78.0	78.3	78.7	78.8	78.4	78.9	77.6
81.1	81.2	81.5	81.6	80.9	81.1	80.8	81.5	81.0
2.3	2.1	3.5	3.3	2.2	2.2	2.5	2.6	3.4
66.8	67.1	69.7	69.7	67.3	67.3	67.1	68.3	70.1
67.3	67.9	70.2	70.0	67.9	68.0	66.9	68.6	70.4
0.6	0.8	0.6	0.3	0.6	0.7	-0.2	0.3	0.3
32.5	31.7	29.5	30.0	29.8	29.5	31.1	31.7	28.5
Max80	Max 80	Max 80	Max 80	Max 80	Max 80	Max 80	Max 80	Max 80
0.9048	0.38715	5.6289	0.91785	1.5399	0.0435	2.22285	0.79605	2.4882
0.1653	0.2436	0.16965	0.0783	0.35235	0.53505	0.29145	0.2175	0.27405
1.0005	0.9309	1.51815	1.43985	0.9483	0.97005	1.0701	1.12665	1.479
0.24795	0.34365	0.25665	0.1218	0.2436	0.2958	-0.0957	0.1392	0.1479
0.580	0.476	1.893	0.639	0.771	0.461	0.872	0.570	1.097
± 0.0615	± 0.0615	± 0.0615	± 0.0615	± 0.0615	± 0.0615	± 0.0615	± 0.0615	± 0.0615
73.43	75.13	72.84	75.96	72.18	72.65	72.94	75.45	74.13
±0.05^{0}C	±0.05^{0}C	±0.05^{0}C	±0.05^{0}C	±0.05^{0}C	±0.05^{0}C	±0.05^{0}C	±0.05^{0}C	±0.05^{0}C
0.014175	0.010961	0.043706	0.013915	0.01819	0.01068	0.02086	0.013015	0.024045
±3.47E-05	±2.52E-05	±10.1E-05	±3.03E-05	±4.29E-05	±2.47E-05	±4.99E-05	±2.97E-05	±5.27E-05
313.312	242.2857	966.0593	307.5825	402.0702	236.0625	461.0921	287.6896	531.4796

4	4	4	4	4	5	5	5	5
40	50	60	80	100	30	40	50	60
1.013	0.996	0.997	1.114	1.069	1.181	1.180	1.170	1.133
79.5	69.5	72.9	72.9	75.3	75.1	80.8	77.0	73.8
82.0	75.9	73.6	74.6	77.3	84.0	84.2	82.3	75.2
2.4	6.4	0.6	1.7	2.0	8.9	3.4	5.3	1.3
75.0	72.1	72.6	76.7	78.2	74.6	75.0	74.0	73.2
75.7	72.6	73.8	77.3	78.8	74.9	75.9	75.8	73.7
0.7	0.5	1.2	0.6	0.6	0.3	0.9	1.8	0.5
78.0	78.4	78.7	77.9	78.4	77.7	77.9	77.7	78.1
80.9	81.0	81.0	80.7	81.0	80.9	80.9	80.9	81.0
2.8	2.6	2.3	2.8	2.6	3.2	3.1	3.3	2.9
69.7	66.5	67.4	66.9	67.1	69.4	68.8	68.9	67.7
69.9	66.7	68.0	66.9	67.8	70.2	69.3	69.4	67.5
0.2	0.2	0.6	0.0	0.7	0.8	0.5	0.5	**-0.2**
30.9	30.4	29.5	31.1	31.7	30.5	30.2	30.4	29.5
Max 80	Max 80	Max 80	Max 80	Max 80	Max 80	Max 80	Max 80	Max 80
1.05705	2.7927	0.28275	0.7569	0.87435	3.8715	1.46595	2.28375	0.57855
0.28275	0.22185	0.5133	0.2697	0.2436	0.12615	0.3915	0.7743	0.19575
1.2354	1.1223	1.01355	1.21365	1.1397	1.392	1.32675	1.42245	1.27455
0.09135	0.0957	0.25665	0.0174	0.3045	0.3567	0.22185	0.23055	-0.07395
0.667	1.058	0.517	0.564	0.641	1.437	0.852	1.178	0.494
± 0.0615	± 0.0615	± 0.0615	± 0.0615	± 0.0615	± 0.0615	± 0.0615	± 0.0615	± 0.0615
75.57	71.63	72.91	73.58	74.75	74.21	75.59	74.40	73.22
±0.05^{0}C	±0.05^{0}C	±0.05^{0}C	±0.05^{0}C	±0.05^{0}C	±0.05^{0}C	±0.05^{0}C	±0.05^{0}C	±0.05^{0}C
0.014929	0.025663	0.011891	0.013295	0.014868	0.032857	0.018768	0.026769	0.011286
±3.34E-05	±6.22E-05	±2.74E-05	±3.13E-05	±3.45E-05	±7.51E-05	±4.14E-05	±6.08E-05	±2.58E-05
329.9771	567.2397	262.8284	293.8716	328.6305	726.2586	414.8456	591.6896	249.4572

5	5	6	6	6	6	6	6	7
80	100	30	40	50	60	80	100	30
1.050	1.163	1.160	1.170	1.238	1.180	1.143	1.220	1.440
72.6	74.1	78.8	79.3	79.9	71.5	72.3	74.8	81.0
75.0	75.7	86.3	82.8	82.3	78.5	73.9	75.9	86.2
2.4	1.6	7.5	3.5	2.4	7.0	1.6	1.1	5.2
72.8	78.3	74.6	74.2	74.4	74.7	76.0	79.4	73.2
73.6	79.4	75.0	74.6	75.0	75.5	76.6	79.5	73.6
0.8	1.1	0.4	0.4	0.5	0.8	0.6	0.1	0.4
78.1	78.0	77.7	77.5	77.7	78.6	78.1	79.1	76.7
81.1	81.3	81.2	81.5	81.1	81.3	81.1	81.0	80.7
3.0	3.3	3.4	4.0	3.4	2.7	3.0	2.0	4.0
66.7	68.6	69.1	69.1	68.8	66.6	66.4	67.4	67.8
67.0	68.9	69.8	69.6	69.5	67.0	66.9	67.8	68.8
0.3	0.3	0.7	0.5	0.7	0.5	0.5	0.4	1.0
29.8	31.5	30.5	30.6	30.6	29.4	29.8	30.8	30.9
Max80	Max 80	Max 80	Max 80	Max 80	Max 80	Max 80	Max 80	Max 80
1.02225	0.70035	3.2799	1.50945	1.04835	3.0363	0.69165	0.4785	2.24895
0.35235	0.47415	0.16965	0.17835	0.2349	0.35235	0.2697	0.05655	0.1827
1.3137	1.4355	1.49205	1.72695	1.479	1.17885	1.30935	0.8526	1.7487
0.13485	0.12615	0.2871	0.2262	0.31755	0.21315	0.19575	0.17835	0.44805
0.706	0.684	1.307	0.910	0.770	1.195	0.617	0.392	1.157
± 0.0615	± 0.0615	± 0.0615	± 0.0615	± 0.0615	± 0.0615	± 0.0615	± 0.0615	± 0.0615
72.55	74.77	75.04	75.05	75.18	72.81	73.19	75.15	74.66
±0.05^{0}C	±0.05^{0}C	±0.05^{0}C	±0.05^{0}C	±0.05^{0}C	±0.05^{0}C	±0.05^{0}C	±0.05^{0}C	±0.05^{0}C
0.016508	0.01579	0.029343	0.020472	0.01726	0.027499	0.014195	0.008827	0.026459
±3.86E-05	±3.65E-05	±6.59E-05	±4.60E-05	±3.87E-05	±6.33E-05	±3.27E-05	±1.99E-05	±6.05E-05
364.881	349.0243	648.5965	452.5067	381.5	607.822	313.7521	195.0983	584.8315

7	7	7	7	7
40	50	60	80	100
1.389	1.378	1.220	1.200	1.240
82.7	80.8	72.1	71.7	80.8
85.8	81.9	74.0	75.0	85.0
3.1	1.2	1.9	3.3	4.3
73.5	72.1	73.6	74.8	79 7
74.0	72.6	74.9	76.0	80.2
0.5	0.5	1.3	1.2	0.5
77.4	76.7	77.8	77.7	78.9
81.1	80.9	80.9	81.0	82.2
3.7	4.2	3.1	3.3	3.3
69.1	67.5	65.9	65.5	67.5
70.1	68.9	66.4	65.7	67.7
1.0	1.4	0.5	0.2	0.2
30.2	30.8	29.4	30.3	30.7
Max 80	Max 80	Max 80	Max 80	Max 80
1.34415	0.50025	0.81345	1.44855	1.86615
0.23925	0.2001	0.56985	0.5046	0.23055
1.6182	1.827	1.3572	1.4355	1.4268
0.435	0.59595	0.19575	0.08265	0.07395
0.909	0.781	0.734	0.868	0.899
± 0.0615	± 0.0615	± 0.0615	± 0.0615	± 0.0615
75.67	74.27	72.36	72.41	76.72
±0.05^{0}C	±0.05^{0}C	±0.05^{0}C	±0.05^{0}C	±0.05^{0}C
0.020003	0.017977	0.017069	0.020585	0.019539
±4.40E-05	±4.14E-05	±3.97E-05	±4.88E-05	±4.24E-05
442.1461	397.3544	377.2926	455.0106	431.8749

Experimental Data

Air	m/s	0.5	0.5	0.5	0.5	0.5	0.5
Plate	mm	30	40	50	60	80	100
Input	(W/sq. cm	0.827	0.795	0.844	0.893	0.633	0.618
	Front face	82.1	83.9	82.6	78.5	75.5	76.1
	Back face	89.0	84.8	83.5	88.1	76.1	77.1
	ΔT1	7.0	0.9	0.9	9.5	0.6	1.0
	Front face	88.5	88.2	87.0	87.3	77.0	74.4
	Back face	89.4	88.9	87.8	88.1	77.6	74.8
	ΔT2	1.0	0.7	0.8	0.9	0.6	0.4
Thermoco	Front face	93.1	92.2	95.6	95.9	79.7	79.4
uple	Back face	94.0	93.2	97.2	97.1	80.3	79.5
	ΔT3	0.9	1.0	1.6	1.2	0.6	0.2
	Front face	82.3	82.0	81.9	82.2	68.6	67.5
	Back face	83.6	83.3	82.8	83.1	69.6	68.7
	ΔT4	1.3	1.3	0.9	0.9	1.0	1.2
Room	^{0}C	30.7	30.8	29.5	29.5	31.2	31.2
Surface	^{0}C	Min 80	Min 80	Min 80	Min 80	Min 80	Min 80
		3.03195	0.37845	0.4002	4.13685	0.2697	0.43065
		0.4176	0.30885	0.3654	0.3741	0.26535	0.1914
		0.40455	0.435	0.70905	0.50895	0.26535	0.0696
		0.5742	0.56985	0.3828	0.3915	0.4524	0.52635
	(W/sq.cm)	1.107	0.423	0.464	1.353	0.313	0.304
		± 0.0615	± 0.0615	± 0.0615	± 0.0615	± 0.0615	± 0.0615
	Temp.T(s)	86.5	86.6	86.8	86.0	75.2	74.4
	^{0}C	±0.05^{0}C	±0.05^{0}C	±0.05^{0}C	±0.05^{0}C	±0.05^{0}C	±0.05^{0}C
	W/cm^2.C	0.019858	0.007584	0.008111	0.023961	0.007109	0.007049
		±3.56E-05	±1.36E-05	±1.42E-05	±4.24E-05	±1.61E-05	±1.63E-05
		438.9311	167.6425	179.2936	529.6305	157.1414	155.8001

Experimental Data

1	1	1	1	1	1.5	1.5	1.5	1.5
30	40	50	80	100	30	40	50	60
0.875	0.908	0.961	0.633	0.604	1.029	0.968	0.961	0.926
85.7	85.2	82.8	75.9	75.2	86.5	85.3	84.3	89.9
86.2	86.4	83.2	76.4	73.3	89.3	86.0	85.0	86.9
0.5	1.2	0.4	0.5	**-1.9**	2.8	0.7	0.7	**-3.0**
88.3	88.7	88.7	76.8	74.5	90.7	88.3	88.2	87.3
89.3	90.1	89.0	77.5	75.1	91.3	90.0	88.7	88.8
1.0	1.3	0.4	0.7	0.6	0.6	1.7	0.5	1.5
94.0	93.3	97.6	79.7	79.6	94.4	93.8	97.4	97.1
95.6	94.7	99.3	80.4	81.0	96.6	96.0	99.0	98.4
1.6	1.4	1.7	0.7	1.4	2.2	2.2	1.7	1.3
81.7	82.0	82.2	69.4	68.3	81.6	82.0	81.5	81.7
83.1	83.3	82.6	70.2	69.1	82.9	82.8	82.5	81.7
1.4	1.3	0.4	0.8	0 8	1.4	0.8	1.0	0.0
30.7	30.8	29.4	32.0	31.8	30.7	30.4	29.4	30.1
Min 80	Min 80	Min 80	Min 80	Min 80	Min 80	Min 80	Min 80	Min 80
0.22185	0.52635	0.16095	0.20445	-0.8178	1.21365	0.3219	0.2958	-1.3137
0.43065	0.56985	0.1653	0.30885	0.27405	0.26535	0.7482	0.2001	0.6438
0.696	0.60465	0.73515	0.3045	0.61335	0.9396	0.957	0.71775	0.58725
0.62205	0.56115	0.18705	0.33495	0.34365	0.58725	0.3567	0.4437	0.0087
0.493	0.566	0.312	0.288	0.103	0.751	0.596	0.414	-0.018
± 0.0615	± 0.0615	± 0.0615	± 0.0615	± 0.0615	± 0.0615	± 0.0615	± 0.0615	± 0.0615
87.4	87.3	87.8	75.5	74.4	88.3	87.3	87.8	89.0
±0.05^{0}C	±0.05^{0}C	±0.05^{0}C	±0.05^{0}C	±0.05^{0}C	±0.05^{0}C	±0.05^{0}C	±0.05^{0}C	±0.05^{0}C
0.008692	0.010002	0.005341	0.006633	0.002428	0.013055	0.01047	0.007089	-0.000314
±1.53E-05	±1.77E-05	±9.14E-05	±1.53E-05	±5.70E-05	±2.27E-05	±1.84E-05	±1.21E-05	±5.33E-07
192.1322	221.0855	118.0548	146.6053	53.6588	288.5697	231.4244	156.7007	-6.940241

Experimental Data

1.5	2	2	2	2	2	2	2.5	2.5
80	30	40	50	60	80	100	30	40
0.961	1.093	1.103	1.041	1.180	1.104	1.124	1.168	1.207
92.4	76.2	85.0	83.1	92.3	93.7	93.2	84.7	83.9
93.8	92.2	87.6	86.0	93.6	94.1	93.6	90.0	87.9
1.4	16.0	2.6	2.9	1.3	0.4	0.4	5.3	4.0
93.6	89.4	89.0	87.7	89.2	93.9	94.8	89.1	88.8
94.9	90.0	89.8	89.6	89.6	96.3	95.2	89.6	89.9
1.2	0.5	0.8	1.9	0.3	2.5	0.4	0.5	1.1
97.3	93.3	93.2	97.8	97.4	97.1	97.3	92.3	91.1
98.6	96.4	96.3	99.7	99.7	99.5	99.4	95.8	93.8
1.3	3.1	3.1	1.9	2.3	2.4	2.2	3.5	2.7
82.2	81.8	81.4	81.8	81.5	81.3	81.1	81.6	81.5
82.9	82.7	82.2	82.3	83.1	82.6	82.0	82.3	82.7
0.7	0.9	0.8	0.5	1.6	1.4	0.9	0.7	1.2
32.0	31.2	30.4	29.4	30.2	32.0	31.8	31.2	31.6
Min 80	Min 80	Min 80	Min 80	Min 80	Min 80	Min 80	Min 80	Min 80
0.6264	6.95565	1.12665	1.25715	0.5742	0.1566	0.1827	2.30115	1.74435
0.5394	0.22185	0.348	0.81345	0.1479	1.0701	0.1653	0.22185	0.48285
0.5655	1.3572	1.3485	0.8265	0.99615	1.0527	0.9483	1.52685	1.1832
0.31755	0.39585	0.36105	0.2175	0.6786	0.59595	0.4089	0.28275	0.522
0.512	2.233	0.796	0.779	0.599	0.719	0.426	1.083	0.983
± 0.0615	± 0.0615	± 0.0615	± 0.0615	± 0.0615	± 0.0615	± 0.0615	± 0.0615	± 0.0615
91.4	85.2	87.1	87.6	90.1	91.5	91.6	86.9	86.3
±0.05^{0}C	±0.05^{0}C	±0.05^{0}C	±0.05^{0}C	±0.05^{0}C	±0.05^{0}C	±0.05^{0}C	±0.05^{0}C	±0.05^{0}C
0.008626	0.041337	0.014029	0.013378	0.009997	0.012088	0.007137	0.019437	0.017983
±1.45E-05	±7.65E-05	±2.47E-05	±2.30E-05	±1.67E-05	±2.03E-05	±1.19E-05	±3.50E-05	±3.30E-05
190.6744	913.7097	310.0959	295.6965	220.9675	267.1869	157.7498	429.638	397.4959

Experimental Data

2.5	2.5	2.5	2.5	3	3	3	3	3
50	60	80	100	30	40	50	60	80
1.142	1.238	1.190	1.240	1.207	1.207	1.217	1.318	1.279
87.1	89.8	91.5	94.0	90.9	86.4	85.8	91.0	92.9
90.3	90.6	94.2	95.0	96.3	90.5	94.4	92.7	97.9
3.2	0.8	2.7	1.0	5.4	4.1	8.5	1.8	5.0
88.7	88.9	94.7	96.8	80.8	89.9	89.0	89.0	96.0
89.3	89.4	95.4	97.2	89.7	90.8	89.8	89.8	96.8
0.7	0.6	0.7	0.4	8.9	0.8	0.8	0.8	0.8
96.7	95.7	97.0	97.3	91.3	92.5	97.2	96.6	97.4
99.1	98.5	99.1	99.8	94.9	95.4	99.4	99.7	100.1
2.4	2.8	2.1	2.4	3.6	2.9	2.2	3.0	2.8
81.0	81.7	81.4	81.4	81.3	81.7	81.6	81.4	81.7
82.0	82.8	82.0	82.2	81.9	82.3	82.4	81.8	82.2
1.0	1.1	0.6	0.8	0.5	0.6	0.8	0.3	0.6
30.7	30.2	31.9	31.8	32.6	31.6	29.8	29.6	32.5
Min 80	Min 80	Min 80	Min 80	Min 80	Min 80	Min 80	Min 80	Min 80
1.37895	0.35235	1.1832	0.4437	2.32725	1.76175	3.71055	0.76125	2.175
0.2871	0.25665	0.30885	0.1914	3.88455	0.3654	0.3567	0.3306	0.3306
1.05705	1.2093	0.9135	1.0527	1.55295	1.2615	0.957	1.3137	1.2093
0.41325	0.4872	0.2784	0.34365	0.2349	0.2436	0.32625	0.14355	0.2523
0.784	0.576	0.671	0.508	2.000	0.908	1.338	0.637	0.992
± 0.0615	± 0.0615	± 0.0615	± 0.0615	± 0.0615	± 0.0615	± 0.0615	± 0.0615	± 0.0615
88.3	89.0	91.1	92.4	86.1	87.7	88.4	89.5	92.0
±0.05^{0}C	±0.05^{0}C	±0.05^{0}C	±0.05^{0}C	±0.05^{0}C	±0.05^{0}C	±0.05^{0}C	±0.05^{0}C	±0.05^{0}C
0.0136	0.009796	0.011325	0.008391	0.037389	0.01621	0.02281955	0.010631	0.016689
±2.36E-05	±1.66E-05	±1.91E-05	±1.38E-05	±6.99E-05	±2.89E-05	±3.89E-05	±1.77E-05	±2.81E-05
300.6019	216.5285	250.317	185.4785	826.4234	358.3078	504.3955851	234.9937	368.8778

Experimental Data

3	3.5	3.5	3.5	3.5	3.5	3.5	4	4
100	30	40	50	60	80	100	30	40
1.133	1.345	1.337	1.296	1.258	1.268	1.319	1.440	1.296
93.3	86.9	89.6	84.9	91.3	91.3	93.8	90.7	93.8
94.8	93.6	93.0	89.7	91.5	95.5	94.7	95.2	96.2
1.5	6.8	3.4	4.8	0.2	4.2	1.0	4.5	2.4
95.8	88.3	89.5	88.5	88.2	95.8	96.2	89.0	89.0
96.5	88.9	90.2	89.4	90.0	96.4	96.6	89.7	89.7
0.6	0.6	0.7	0.9	1.8	0.6	0.4	0.6	0.8
96.2	91.1	92.8	95.5	97.0	96.1	96.1	91.5	92.2
98.4	95.0	96.0	97.8	99.9	99.1	98.8	95.0	95.3
2.1	3.8	3.2	2.3	2.8	3.0	2.7	3.5	3.1
80.7	80.8	81.7	81.3	81.5	81.8	81.2	81.5	81.5
81.4	81.4	81.9	81.8	81.8	81.8	81.9	82.0	81.7
0.7	0.6	0.2	0.5	0.4	0.0	0.7	0.5	0.1
31.7	29.5	30.9	29.8	30.5	31.1	31.7	28.5	30.9
Min 80	Min 80	Min 80	Min 80	Min 80	Min 80	Min 80	Min 80	Min 80
0.6612	2.9406	1.47465	2.09235	0.09135	1.8357	0.42195	1.9575	1.0353
0.2697	0.25665	0.28275	0.37845	0.8004	0.28275	0.1827	0.28275	0.32625
0.9309	1.66605	1.37895	1.0005	1.23975	1.305	1.1832	1.5225	1.3659
0.3045	0.2784	0.087	0.2262	0.1566	0.0174	0.3045	0.22185	0.05655
0.542	1.285	0.806	0.924	0.572	0.860	0.523	0.996	0.696
± 0.0615	± 0.0615	± 0.0615	± 0.0615	± 0.0615	± 0.0615	± 0.0615	± 0.0615	± 0.0615
91.5	86.8	88.4	87.5	89.5	91.2	91.8	88.2	89.1
$\pm 0.05^0C$	$\pm 0.05^0C$	$\pm 0.05^0C$	$\pm 0.05^0C$	$\pm 0.05^0C$	$\pm 0.05^0C$	$\pm 0.05^0C$	$\pm 0.05^0C$	$\pm 0.05^0C$
0.00905	0.022452	0.014016	0.016004	0.009703	0.014315	0.008697	0.016687	0.011959
±1.51E-05	±3.92E-05	±2.44E-05	±2.77E-05	±1.64E-05	±2.38E-05	±1.44E-05	±2.80E-05	±2.05E-05
200.0383	496.2682	309.8001	353.7561	214.4661	316.4096	192.2299	368.851	264.3438

Experimental Data

4	4	4	4	5	5	5	5	5
50	60	80	100	30	40	50	60	100
1.358	1.339	1.573	1.508	1.547	1.627	5.977	1.530	1.541
92.2	91.5	91.9	93.0	88.7	88.0	88.6	90.9	92.8
98.6	89.5	94.1	94.1	98.8	93.0	90.7	93.5	96.0
6.4	**-2.0**	2.2	1.1	10.1	5.0	2.2	2.6	3.3
88.6	88.2	95.7	97.1	88.2	89.8	88.6	90.3	97.1
89.5	89.9	96.3	97.8	88.7	91.1	89.3	90.8	97.8
0.9	1.7	0.6	0.7	0.5	1.2	0.7	0.5	0.7
91.5	96.5	91.2	96.1	91.9	92.9	92.2	96.3	95.3
95.5	99.6	94.5	99.2	95.8	97.1	95.9	100.1	97.9
4.1	3.1	3.3	3.1	3.9	4.2	3.7	3.8	2.6
81.4	81.2	81.5	81.4	81.2	82.0	81.3	81.1	81.8
82.0	81.9	81.8	82.0	82.0	82.5	81.5	82.0	82.3
0.6	0.8	0.3	0.6	0.8	0.5	0.2	0.9	0.5
30.4	29.5	31.1	31.7	30.5	30.2	30.4	29.5	31.5
Min 80	Min 80	Min 80	Min 80	Min 80	Min 80	Min 80	Min 80	Min 80
2.79705	-0.8613	0.9657	0.49155	4.37175	2.175	0.94395	1.1136	1.41375
0.3828	0.7221	0.24795	0.30015	0.19575	0.52635	0.2958	0.22185	0.3132
1.76175	1.3485	1.4355	1.32675	1.69215	1.827	1.62255	1.63125	1.12665
0.2523	0.3393	0.10875	0.26535	0.36105	0.23055	0.0696	0.4089	0.2088
1.298	0.387	0.689	0.596	1.655	1.190	0.733	0.844	0.766
± 0.0615	± 0.0615	± 0.0615	± 0.0615	± 0.0615	± 0.0615	± 0.0615	± 0.0615	± 0.0615
88.4	89.3	90.1	91.9	87.5	88.2	87.7	89.7	91.7
±0.05^{0}C	±0.05^{0}C	±0.05^{0}C	±0.05^{0}C	±0.05^{0}C	±0.05^{0}C	±0.05^{0}C	±0.05^{0}C	±0.05^{0}C
0.02238	0.006467	0.011695	0.009893	0.029028	0.020535	0.0128	0.014023	0.012701
±3.86E-05	±1.08E-05	±1.98E-05	±1.64E-05	±5.09E-05	±3.54E-05	±2.23E-05	±2.33E-05	±2.11E-05
494.6751	142.9395	258.5009	218.679	641.6244	453.8904	282.9326	309.9581	280.7326

Experimental Data

6	6	6	6	6	6	7	7	7
30	40	50	60	80	100	30	40	50
1.603	1.538	1.639	1.779	1.663	1.734	1.956	1.969	1.922
86.7	88.2	87.7	92.3	91.3	92.2	87.8	95.2	95.8
92.9	90.7	91.1	95.2	94.1	93.7	89.7	97.8	97.3
6.3	2.5	3.5	2.9	2.8	1.5	1.9	2.6	1.5
88.5	88.1	88.0	94.9	94.0	96.7	88.0	90.7	94.3
89.0	88.7	88.6	95.4	94.6	97.6	88.5	91.8	94.5
0.5	0.6	0.6	0.5	0.5	0.9	0.5	1.2	0.2
91.8	91.6	91.7	97.1	96.4	95.1	92.6	94.0	92.9
96.0	94.6	96.0	100.2	100.0	98.6	97.7	98.8	97.9
4.3	3.0	4.2	3.1	3.6	3.5	5.1	4.8	4.9
81.0	81.7	80.9	81.2	81.2	81.3	80.9	81.9	81.1
81.7	82.2	81.6	81.8	81.7	81.7	81.9	82.9	82.2
0.7	0.5	0.7	0.6	0.6	0.5	0.9	1.0	1.1
30.5	30.6	30.6	29.4	29.8	30.8	30.9	30.2	30.8
Min 80	Min 80	Min 80	Min 80	Min 80	Min 80	Min 80	Min 80	Min 80
2.72745	1.0875	1.5138	1.26585	1.21365	0.66555	0.8178	1.1397	0.63075
0.20445	0.2784	0.2697	0.23055	0.2349	0.36975	0.2175	0.5046	0.0957
1.84875	1.29195	1.8444	1.3311	1.54425	1.52685	2.21415	2.0967	2.1489
0.3045	0.2349	0.3219	0.2436	0.24795	0.20445	0.40455	0.4437	0.4785
1.271	0.723	0.987	0.768	0.810	0.692	0.913	1.046	0.838
± 0.0615	± 0.0615	± 0.0615	± 0.0615	± 0.0615	± 0.0615	± 0.0615	± 0.0615	± 0.0615
87.0	87.4	87.1	91.4	90.7	91.3	87.3	90.4	91.0
$\pm 0.05^0C$	$\pm 0.05^0C$	$\pm 0.05^0C$	$\pm 0.05^0C$	$\pm 0.05^0C$	$\pm 0.05^0C$	$\pm 0.05^0C$	$\pm 0.05^0C$	$\pm 0.05^0C$
0.0225	0.012734	0.017479	0.012379	0.013299	0.011428	0.016192	0.017378	0.013927
±3.98E-05	±2.24E-05	±3.09E-05	±2.00E-05	±2.18E-05	±1.88E-05	±2.87E-05	±2.89E-05	±2.31E-05
497.325	281.4648	386.3397	273.6207	293.949	252.6106	357.8977	384.1245	307.8331

Experimental Data

7
60
1.850
92.1
93.9
1.8
95.41
97.0
1.6
97.5
101.6
4.1
81.5
82.0
0.5

29.4

Min 80

0.7917
0.6873
1.7835
0.2349

0.874
± 0.0615

91.6
±0.05^{0}C

0.014043
±2.26E-05

310.4009